THESIS FOR THE DEGREE OF LICENTIATE OF ENGINEERING

Sustainable Waste Flow Management: Utilization of recovered carbon black (rCB) from end-of-life tires (ELTs) pyrolysis for activated carbons (ACs) production

BARTOSZ DZIEJARSKI

Department of Space, Earth and Environment

Department of Chemistry and Chemical Engineering

CHALMERS UNIVERSITY OF TECHNOLOGY

Gothenburg, Sweden 2024

Sustainable Waste Flow Management: Utilization of recovered carbon black (rCB) from end-of-life tires (ELTs) pyrolysis for activated carbons (ACs) production

BARTOSZ DZIEJARSKI
ISBN: 978-91-8103-066-2

Doktorsavhandlingar vid Chalmers tekniska högskola
Ny serie nr: 5524
ISSN: 0346-718X

Department of Space, Earth and Environment
Department of Chemistry and Chemical Engineering
Chalmers University of Technology
SE-412 96 Gothenburg
Sweden
Telephone + 46 (0)31-772 1000

Cover:
Schematic illustration of the sustainable management of end-of-life tires via pyrolysis, resulting in the production of recovered carbon black based activated carbons for environmental applications.

Printed by Chalmers Reproservice
Gothenburg, Sweden 2024

Abstract

The escalating problem of end-of-life tires (ELTs) represents a significant challenge on environmental, economic, and health fronts globally. The issue is reconceptualized within the framework of a circular economy, advocating for a shift from a traditional linear waste management approach to a circular one. A preliminary market analysis sheds light on the current dynamics of waste tire accumulation, such as the economic impacts, environmental hazards, and the policies governing ELTs management, with a focus on the European Union's regulations. This emphasizes the necessity for recycling strategies, demonstrating the potential of ELTs not just as a waste problem, but as a valuable resource. In view of this, conversion of ELTs into activated carbons (ACs) is a promising sustainable solution. ACs are highlighted for their multifaceted applications, especially adsorption, which could be potentially useful for gas cleaning and addressing the CO_2 emissions challenge in small-scale units. The production of ACs can be effectively achieved through pyrolysis, which transforms precursor materials into carbon-rich char. The subsequent activation step, particularly alkali activation, is widely applied to further enhance textural properties. The research aims to explore how the alkali activation process can be finely tuned to optimize the performance of ACs in practical applications.

At the heart of the thesis is a characterization of rCB/ACs. This analysis is pivotal to understanding the inherent properties of the materials, such as their textural, chemical, and morphological properties, which are critical factors influencing their performance in sorption processes. Moreover, a significant portion of the thesis is dedicated to investigating the activation mechanisms of rCB using potassium-containing agents (KOH, KCl, K_2CO_3, CH_3COOK, and $K_2C_2O_4$). This process is crucial for enhancing the textural properties of the ACs, such as increasing their surface area and developing an optimal pore structure conducive. Through systematic experimental set-up, the research seeks to optimize the activation conditions and evaluate the factors influencing the development textural properties, including the physical state of KOH during the activation process, and the influence of changing KOH to NaOH to explain the distinct effects of the type of selected alkali ions. Finally, the research investigates the CO_2 adsorption mechanisms of rCB-derived ACs, along with assessing their CO_2 adsorption capacity and selectivity, as potential application. Moreover, the study examines the regeneration potential of these ACs over multiple adsorption-desorption cycles.

Firstly, KOH and air, combined with heat treatment ranging from 500 to 900 °C, were used to activate materials for CO_2 capture, as research basic line (Paper I). The materials underwent characterization through methods such as FT-IR, SEM-EDS, ultimate and proximate analysis, FT-IR, Raman spectroscopy, TGA, and N_2/CO_2 adsorption isotherms. Further investigation, based on the textural and SEM-EDS analysis of the rCB/ACs indicated that KOH was the most effective among the potassium salts tested (Paper II). It was revealed that the optimal KOH activation conditions were a temperature of 800 °C, 7 °C/min heating rate, and ration of KOH/rCB 1:5, and activation time of 4 hour (Paper II). Finally, at 0 °C and 25 °C, the best adsorption capacities of rCB/ACs (Paper I) were recorded at 30.90 cm^3/g and 20.53 cm^3/g at 1 bar, respectively. After 10 regeneration cycles, the material maintained its performance, emphasizing its durability. The selectivity for CO_2 over N_2 was equal to values of 350.91 in a CO_2/N_2 binary mix and 59.70 in a 15% CO_2/85% N_2 mixture.

Keywords: End-of-life tires valorization; Activated carbons, Circular economy; Porosity optimization; Potassium salts, CO_2 capture, Climate neutrality.

Acknowledgments

First and foremost, I would like to express my sincere gratitude to my supervisors, Professor Pavleta Knutsson and Professor Klas Andersson at Chalmers University of Technology, as well as Professor Renata Krzyżyńska at Wrocław University of Science and Technology, for their exceptional mentorship, support, and invaluable insights throughout my research journey. Their combined expertise and persistent encouragement have been crucial in shaping both my research pursuits and personal growth, instrumental in defining my path in academia. I owe much of my progress to their exemplary guidance, for which I am profoundly thankful. You have been inspirational and have consistently kept me on track. Your input in my work and knowledge in the field have been significantly vital.

Furthermore, I would like to acknowledge several of my research colleagues: Jarosław Serafin, Diego Felipe Hernandez Barreto, and Robin Faust. Our extensive and in-depth scientific discussions have not only advanced my knowledge but also greatly fueled my enthusiasm for our shared research goals.

I am also grateful to Professor Juan Carlos Moreno Piraján at Universidad de los Andes and Professor Liliana Giraldo at Universidad Nacional de Colombia for their exceptionally positive attitudes and for providing the opportunity to carry out part of my research within their esteemed laboratories.

Special thanks to everyone here at the Unit of Inorganic Environmental Chemistry and the Division of Energy Technology who have made this an excellent working environment.

Moreover, a special note of appreciation goes to my friend Maciej, whose enduring companionship has been an extremely important foundation throughout these years.

I owe a deep debt of gratitude to my family, whose moral support has been constant source of motivation.

Finally, I must extend my heartfelt thanks to Monika, a cherished friend whose continuous and invaluable support, and belief in my potential, have been instrumental over the past years. Her presence, unique enthusiasm, insightful and helpful advice, and solid reliability have been a pillar of strength and have proved indispensable during the most challenging times.

Thank you all for providing a supportive and stimulating environment that has been crucial to my academic and personal development.

Bartosz Dziejarski, Gothenburg (2024)

List of Publications

This thesis is based on the following appended papers, which are referred to in the text by their assigned Roman numerals:

Paper I
Dziejarski, B., Hernández-Barreto, D. F., Moreno-Piraján, J. C., Giraldo, L., Serafin, J., Knutsson, P., Andersson K., & Krzyżyńska, R.
Upgrading recovered carbon black (rCB) from industrial-scale end-of-life tires (ELTs) pyrolysis to activated carbons: Material characterization and CO_2 capture abilities (2024),
Environmental Research, 247, 118169.

Paper II
Dziejarski, B., Faust, R., Serafin, J., Krzyżyńska, R., Andersson K., & Knutsson, P.
Insights into activation pathways of recovered carbon black (rCB) from end-of-life tires (ELTs) by potassium-containing agents
Under review

Related peer-reviewed papers not included in the thesis

Dziejarski, B., Serafin, J., Andersson, K., & Krzyżyńska, R.
CO_2 capture materials: a review of current trends and future challenges (2023),
Materials Today Sustainability, 24, 100483.

Dziejarski, B., Krzyżyńska, R., & Andersson, K.
Current status of carbon capture, utilization, and storage technologies in the global economy: A survey of technical assessment (2023),
Fuel, 342, 127776.

Contribution report

Paper I Principal author with main responsibility for all the experimental work, conceptualization, methodology, validation, data curation, formal analysis, modeling, visualization, project administration, and writing.

Paper II Principal author with main responsibility for all the experimental work, conceptualization, methodology, validation, data curation, formal analysis, modeling, visualization, project administration, and writing.

Table of Contents

Nomenclatures

List of abbreviations

ACs	Activated carbons
BET	Brunauer-Emmett-Teller
BSE	Backscattered electrons
CBp	Pyrolytic carbon black
CCD	Charge-coupled device
CCUS	Carbon capture, utilization, and storage
DFT	Density functional theory
EABS	Sum of absolute errors
EDS	Energy-dispersive X-ray spectroscopy
ELTs	End-of-life tires
EVs	Electric vehicles
FT-IR	Fourier-transform infrared spectroscopy
GACs	Granular activated carbons
HVT	Heavy vehicle tires
IAST	Ideal adsorption solution theory
IPCC	Intergovernmental Panel on Climate Change
IUPAC	International Union of Pure and Applied Chemistry
LVT	Light vehicle tires
MVT	Medium vehicle tires
PACs	Powdered activated carbons
PSD	Pore size distribution
rCB	Recovered carbon black
SE	Secondary electrons
SEM	Scanning electron microscopy
TCD	Thermal conductivity detector
TEA	Techno-economic analysis
TGA	Thermogravimetric analysis
XRD	X-ray diffraction

List of symbols

a_{RP}	constant (bar $^{-\beta RP}$)
e_{RPr}	Radke–Prausnitz exponent (-)

I_D	D-band (-)
I_G	G-band (-)
K_{FL}	Langmuir-Freundlich constant (bar^{-nFL})
K_L	Langmuir adsorption constant (1/bar)
K_{RP}	Redlich-Peterson constant ($cm^3 \cdot g^{-1} \cdot bar^{-1}$)
K_{RPr}	Radke–Prausnitz constant (bar^{-1})
K_S	Sips constant (bar^{-1})
K_T	Toth constant (bar^{-1})
n_{FL}	Index of heterogeneity (-)
n_S	Sips exponent (-)
n_T	Heterogeneity factor (-)
P	Partial pressure of the adsorbed gas at equilibrium state (bar)
P_0	Standard pressure (bar)
$q_{e,exp}$	Experimental amount of adsorbed adsorbate at equilibrium state [cm^3/g]
$q_{e,mod}$	Predicted amount of adsorbed adsorbate at equilibrium state [cm^3/g]
q_m	Maximum adsorption capacity ($cm^3 g$)
Q_{st}	Isosteric heat of adsorption (J/mol)
R	Ideal gas constant (8.314 J/mol·K)
R^2	Coefficient of determination
T	Temperature (K or °C)
β_{RP}	Redlich–Peterson exponent (-)
$\Delta G°$	Gibbs free energy (J/mol)
$\Delta H°$	Standard enthalpy change (J/mol)
$\Delta S°$	Standard entropy change (J/mol)
θ	Specific surface coverage (-)

1. Introduction

1.1 Recovered carbon black (rCB) from end-of-life waste tires (ELTs) as a sustainable precursor for activated carbons (ACs) production

The increasing awareness of the environmental problems confronting our world has resulted in an urge to understand and address three pivotal concerns: the substantial emission of carbon dioxide into the atmosphere [1], the shortage of water by heavy metals along with organic pollutants [2], and waste accumulation [3]. In view of this, adsorption processes that would allow the CO_2 capture as well as water purification are emerging. Furthermore, adsorption processes represent an effective, easy to implement and economically and environmentally viable alternative [4,5]. Among the existing adsorbents, activated carbons (ACs) are distinguished as the most extensively studied, highly efficient, and appealing option, alongside zeolites [6]. The prominence of ACs is attributed to several key advantages: low desorption temperature, straightforward regeneration, rapid sorption kinetics, exceptional thermal and chemical stability, and, especially, the possibility to utilize wastes as their precursors, which contributes to affordability [7, 8].

The primary source for ACs production nowadays is waste biomass, which possess a moderate carbon content but is relatively low in inorganic compounds. However, the availability of specific types of waste biomass is often limited by regional availability, as biomass waste types and quantities vary geographically, depending on local agricultural or forestry outputs. In recent years, with escalating waste generation, certain industrial wastes have emerged as alternative carbon sources for ACs production. Additionally, as industries expand, the amount of non-biodegradable waste increases, posing significant environmental and public health threats. This surge emphasizes the urgent need for accelerated waste management strategies. A notable example is end-of-life tires (ELTs) that constitute a crucial challenge due to the rapid development of the automotive and transportation sectors, their chemical and mechanical resistance, or limited infrastructure for their disposal and recycling. Direct incineration is an efficient energy recovery method due to the high calorific value of waste tires, which usually exceeds 35 MJ/m^3 [9]. However, incineration emits substantial amounts of gases like carbon monoxide, dioxins, and furans [10]. Landfill, which is another prevalent method for waste tire management, occupies vast land areas, resulting in groundwater and soil pollution. The challenging degradation of discarded ELTs causes sustained impacts on future environments and land use.

Since ELTs are not properly managed in many countries, especially those with transition and emerging economies, they contribute roughly to 2% of the total waste produced around the globe [11]. It is estimated that 1.85 billion tires were manufactured and discarded worldwide in the year 2023, marking a year-on-year increase of 4.5% [12]. Among the different treatment methods (reuse of whole tires, raw material recycling, and energy recovery), pyrolysis has the potential to fulfil the requirements of the three tenets of solid waste management: reduce the amount of waste, restore resources, and prevent contaminants [13]. Given that solid products, particularly pyrolytic char, also known as pyrolytic carbon black (CBp), constitute about 35%

of pyrolysis outputs, their management is crucial for the economic viability and the commercial development of the entire process. To acquire high-value elemental carbon, the pyrolytic char must undergo further refinement to produce recovered carbon black (rCB). Moreover, there is an increasing interest in rCB due to the rising need for environmentally friendly alternatives to virgin carbon black (vCB), which is considered one of the top 50 industrial chemicals worldwide [14]. Therefore, ELTs are a compelling alternative to vCB, which is produced by heating hydrocarbon fuels and contributes to CO_2 emissions. ELTs offer significant advantages, including widespread availability, cost-effectiveness, and environmental benefits. By reducing reliance on industrial products and promoting recycling, they represent an attractive option for sustainable practices.

One of the significant potential applications of recovered carbon black (rCB) relates to the synthesis of activated carbons. rCB can be subjected to activation process to increase its surface area and porosity, aiming increase ACs adsorption capabilities. The produced ACs can be utilized across a wide range of industrial applications, such as water purification, energy storage, and, notably, the separation of flue gas streams. Considering this, the production of ACs based on rCB offers a unique opportunity for sustainable waste management, promoting the circular economy by transforming waste into a value-added product that can be further utilized for potential CO_2 capture (**Figure 1**).

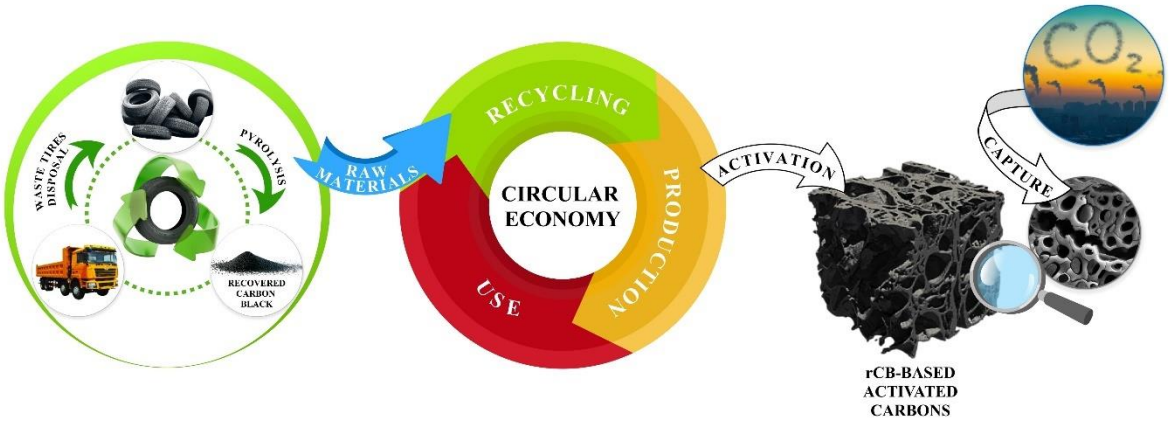

Figure 1. Conceptualized representation of rCB conversion from ELTs pyrolysis to ACs production.

1.2 Recent trends in global CO_2 emissions: the energy–climate challenge

Today, one of the most challenging and urgent environmental issues facing the world is the reduction of CO_2 concentration in the atmosphere, which is widely reported to be the main anthropogenic greenhouse gas that leads to global warming and climate changes. In 2022, the average annual CO_2 level in the atmosphere was approximately 50% higher than in the 1760s and reached its highest recorded value in history at 417.06 ppm [15, 16]. Unfortunately, the rapid development of the world's economic, and accelerating industrialization, with a soaring world population, will definitely cause a gradual growth of CO_2 emissions and will affect global warming to reach 1.5 °C in the next 30 years at the current state. According to the Intergovernmental Panel on Climate Change (IPCC) latest report from 2022, to prevent this

scenario, climate change mitigation efforts should be executed immediately. IPCC estimation indicates that the peak of greenhouse gas (GHG) emissions must take place in 2025 at the latest, so by 2030 a 43% reduction of it will possibly be achieved [17]. In view of the above, there is extensive demand for effective CO_2 capture technologies across both large industrial facilities, which are major sources of CO_2 emissions, and smaller-scale units. Effective CO_2 capture is essential for smaller units to minimize their environmental impact, while larger facilities require technologies capable of purifying the flue gas stream to separate pure CO_2 and meet stringent regulatory standards. Consequently, this widespread need has catalyzed the development and implementation of various technologies aimed at achieving net-zero emissions.

One of the technologies that is predicted to play a crucial part in the evolution toward the use of low-carbon energy, is carbon capture, utilization, and storage (CCUS) [18]. The schematic methodology to reduce the capturable and uncapturable CO_2 emissions by CCUS is presented in **Figure 2**. Over the past decade, significant research has focused on utilizing adsorption as an effective technique for CO_2 capture within the CCUS value chain. Adsorption is recognized for its considerable efficiency at low temperatures and high pressures, its ability to produce a highly pure end product, and the feasibility of full automatization of the process [19]. Among the promising CO_2 capture materials are activated carbons. ACs are notable for their effectiveness in gas separation and purification, providing necessary buffering capabilities that are essential for both capturing and cleaning CO_2. Innovatively linking this to sustainable waste management, rCB from the pyrolysis of ELTs serves as an excellent source of ACs. The rCB may undergo processing and be applied in CCUS systems to achieve efficient CO_2 adsorption. This practice directly contributes to the valorization of ELTs by reintroducing valuable materials into the industrial lifecycle and facilitating further storage or utilization of CO_2.

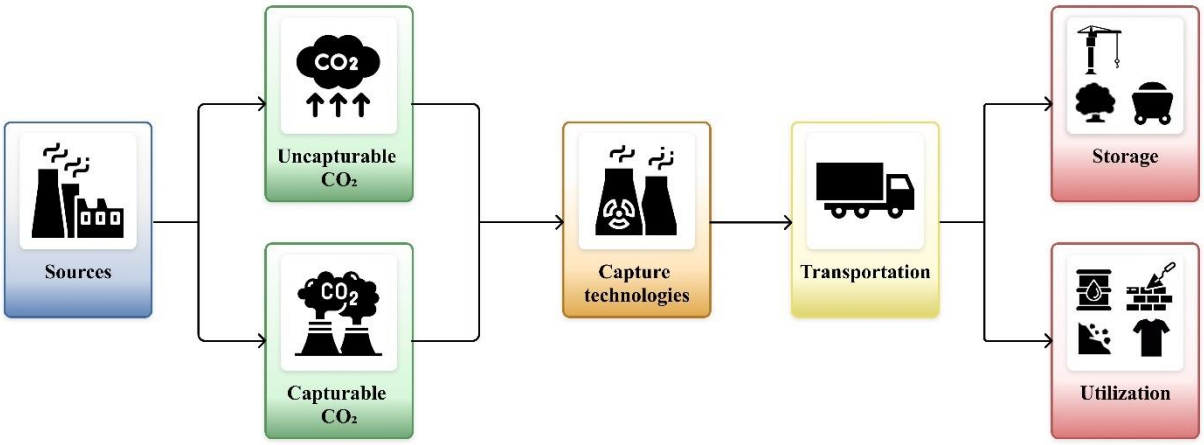

Figure 2. Generic operation methodology of CCUS technology.

1.3 Aim and scope of thesis

The focus of the present thesis is summarized in **Figure 3**. There are three main focal points, each covering different but related elements vital to advancing the understanding and application of rCB/ACs in environmental and technological fields as follows:

- **Characterization of rCB/ACs**: The thesis focuses on the importance of understanding the inherent characteristics of rCB/ACs such as their textural, chemical, and morphological properties. These properties are pivotal in determining the effectiveness in sorption applications. Material analysis is crucial for unraveling the influence of activation procedure on the conversion of rCB into activated carbons. **Paper I** sets the stage for understanding the potential of these materials in environmental remediation and industrial processes, providing a detailed baseline against which the performance of rCB/ACs can be measured.

- **Exploration of rCB/ACs activation mechanisms**: A substantial part of the research is dedicated to exploring the activation mechanisms of rCB using potassium-containing agents. This investigation is key to enhancing the textural properties of the ACs. **Paper II** presents a thorough investigation of the effect of potassium-containing salts on the surface area and pore structure of rCB/ACs. Special attention is given to optimizing activation conditions, understanding the influence of the physical state of activating agents (notably KOH), and distinguishing the roles of potassium and sodium ions in shaping the textural characteristics of the rCB/ACs. Through systematic experimentation and analysis, the research elucidates the mechanisms behind activation, paving the way for more efficient and targeted use of rCB in adsorption technologies.

- **CO_2 capture performance of rCB/ACs**: The final focus of this thesis assesses rCB-derived ACs for CO_2 adsorption as a potential application. **Paper I** studies rCB/ACs adsorption capacity, selectivity, and the CO_2 sorption mechanisms at play. Additionally, it evaluates the rCB/ACs regeneration potential over multiple cycles, which is crucial for their sustainability and effectiveness in long-term applications.

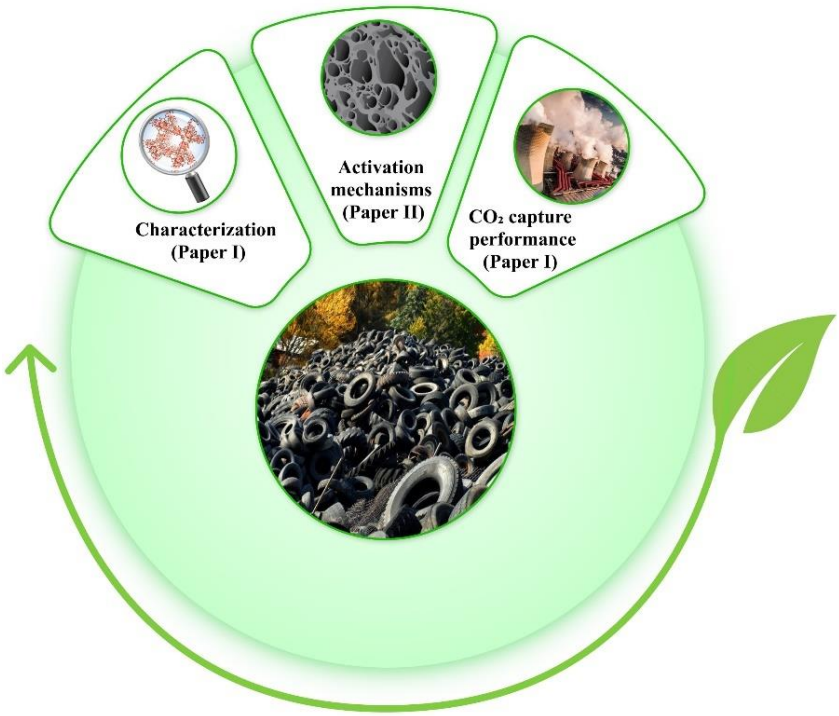

Figure 3. Overview of the appended paper and their main contribution to the investigation.

2. Overview of the field

2.1 End-of-life tires management to value-added ACs

The management of the increasing ELTs flows presents a complex challenge in modern society that necessitates the cooperation of many parties, including tire makers, buyers, collectors, recyclers, and authorities [20]. This challenge is magnified by the shift towards electric vehicles (EVs) which, due to their heavier weight and torque, contribute to accelerated tire wear. EVs are expected to exacerbate the volume of ELTs due to their higher tire wear rate compared to traditional fossil fuel-powered vehicles, necessitating advancements in recycling technologies and strategies. Specifically in the USA, which already produces approximately 315 million ELTs per year, this number could increase by 12% to a total of 352 million annually by 2030, due to the widespread adoption of EVs [21]. Nowadays, waste tire management involves established process chains that dictate how ELTs are converted into various end products, reflecting the complexity of their handling (**Figure 4**). The approach to managing ELTs varies significantly, with options that cover recycling (40-50%), energy recovery (30-40%), reuse (10-20%), and landfilling (5-10%) [22, 23]. The shares vary largely depending on local regulations, economic factors, and technological advancements.

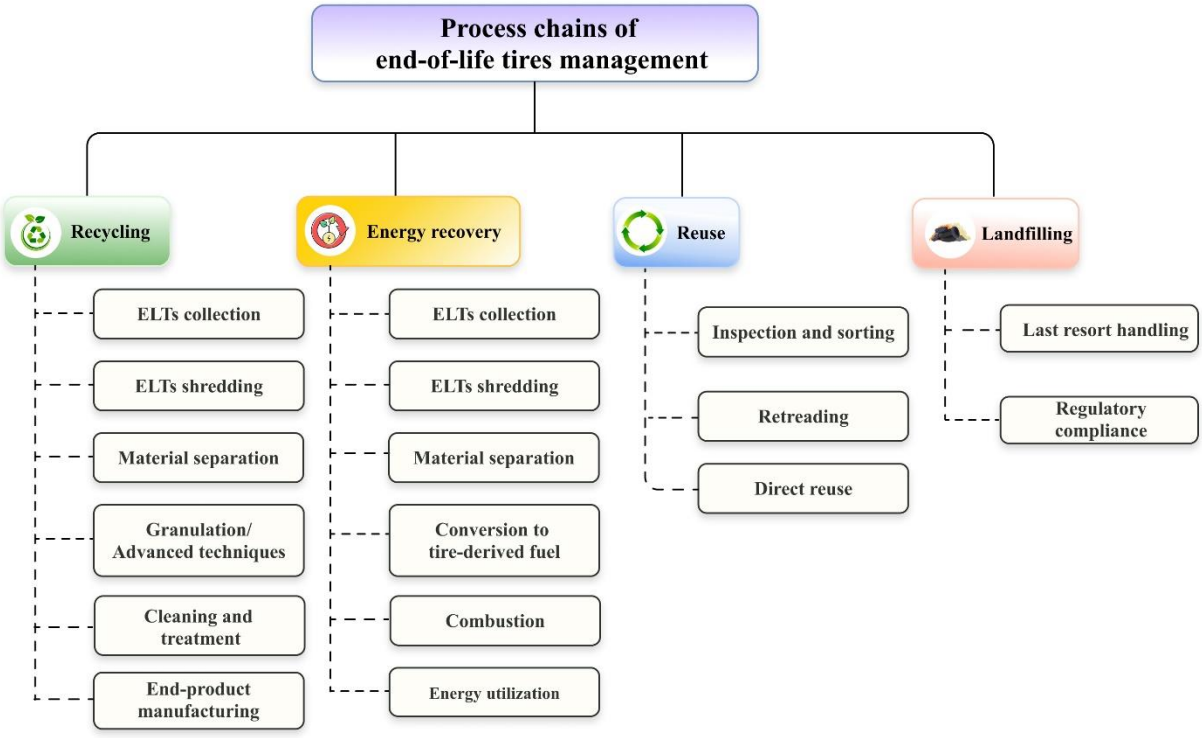

Figure 4. Overview of the existing end-of-life-tires management process chains.

Among these strategies, recycling stands out as a key method, where ELTs are processed to produce new materials. A noteworthy direction within this recycling effort involves converting recycled tires into ACs, considering a high market value and wide applicability in environmental applications [24]. The production of ACs from ELTs not only diverts waste from landfills but also capitalizes on the carbon-rich material to create a high-demand resource. The effectiveness of ACs derived from ELTs largely depends on the purity

of the CBp. A higher purity enhances adsorption characteristics, thereby improving the ability of ACs to remove contaminants and pollutants [25]. To improve the quality of the final product, it is crucial to enhance the entire process chain. This involves using specific types and brand of ELTs, optimizing pyrolysis processes, and implementing political regulations and market incentives, as shown in **Figure 5**. At every level of the process chain, optimizing pyrolysis is critical for increasing the conversion efficiency of ELTs and reducing energy consumption, while also effectively controlling the proportion of specific phases such as liquid oil, gas, and especially CBp in the production of ACs [26]. Additionally, further purification of CBp is essential as it enhances the quality of the recycled material, enabling its use in higher-value AC transformations. By removing impurities and refining the end products, the purification process ensures that rCB meets industry standards and reduces reliance on virgin resources from ELTs.

Figure 5. Graphical representation of the process chain for managing end-of-life-tires that leads to value-added activated carbons.

2.1.1. Influence of ELT type

One of the primary pathways for managing ELTs is pyrolysis, which is selected for its efficiency in breaking down the complex materials in tires for recycling. ELTs are categorized into three main types: light vehicle tires (LVT), such as bicycle tires; medium vehicle tires (MVT), which include car tires; and heavy vehicle tires (HVT), typically used on trucks. The exact composition of the materials in the tires can differ, but generally, they consist of rubber, carbon black, metals, textiles, and various additives like silica or vulcanization agents [27]. Consonantly, the yield and quality of CBp produced through pyrolysis are significantly affected by the tire type and brand. This variation is due to the different components used in tire manufacturing, which influence the pyrolysis behavior and how they impact the rubber degradation process during pyrolysis [28].

For instance, Singh et al. [29] reported that when LVT, MVT, and HVT are subjected to identical pyrolysis conditions at 700 °C, the resulting CBp yields differ. The ash content for

LVT, MVT, and HVT was 7.4, 15.32, and 5.67 wt.%, respectively. In the case of carbon content across LVT, MVT, and HVT showed minimal variation, ranging from 84.2 wt.% in LVT to 89.5 wt.% in HVT. The pyrolysis of MVTs resulted in a CBp yield of about 43 wt.%, whereas LVTs and HVTs yielded lower values of 38.0 wt.% and 43.0 wt.%. High ash content in ELT types has been positively correlated with an increased share of CBp in the pyrolysis products, that observation was proven by other studies [30]. On the other hand, the CBp yields obtained from six various brands of ELTs are very similar [31], which were reported to be 37.5 (Debica brand), 38.1 (Dunlop brand), 37.1 (Goodyear brand), 38.0 (Courier brand), 41.7 (Michelin brand), and 38.3 wt.% (Continental brand). The ash contents for these six brands were equaled 2.66, 4.81, 4.98, 3.39, 2.39, and 6.23 wt.%, respectively. Moreover, there was also emphasis on the variability of the CBp share obtained from different parts of ELTs, stemming from the diverse components used in their manufacturing, including tire tread and sidewalls [32].

In view of this, the above characteristics of ELTs will also influence the production and characteristics of the CBp. To optimize the quality of the ACs, it is crucial to sort and categorize the ELTs feedstock by type, brand, and tire structure before undergoing pyrolysis. This pre-treatment ensures a more uniform and high-quality end product.

2.1.2. Optimization of pyrolysis process

Another crucial aspect of ELTs management involves understanding the key operational parameters that influence the efficiency and outcome of the pyrolysis. Pyrolysis is a thermochemical process conducted by heating ELTs to a specific temperature in an oxygen-free environment, which prevents combustion. This process facilitates the breakdown of large molecular chains into smaller ones, resulting in three types of products, as mentioned earlier [33]. The primary parameters that control the pyrolysis include temperature, pressure, residence time, particle size, and heating rate. These factors crucially affect the composition, fractions, and product types from pyrolysis. For AC production, optimizing these conditions is vital to maximize the yield and enhance the properties of CBp.

Temperature significantly affects the pyrolysis time and yield of pyrolytic products, with an optimal range typically between 400 and 1000 °C [34, 35]. Aiming at AC manufacturing, 500 °C is ideal for maximizing CBp output (~41 wt.%), expanding its pores and increasing specific surface area, while avoiding incomplete thermal decomposition [28]. At this temperature, complete devolatilization of rubber is ensured while simultaneously minimizing secondary reactions. Below 500 °C, the pores within the tire char fail to expand, leading to incomplete pyrolysis of the ELTs. Consequently, this process results in a high yield (~86 wt.%) of CBp; however, its quality is compromised by the adhesion of pyrolysis volatiles to the surface [36]. On the other hand, higher temperatures (>500 °C) lead to sintering of CBp, its pore blockage, poor surface properties, and decreased yield (<41 wt.%) [37].

The residence duration influences secondary reactions among pyrolysis volatiles on the surface and inside the pores of CBp, as well as the extent of pyrolysis of the ELTs. To optimize the process and enhance volatile removal, the residence time in the pyrolysis reactor should be extended. However, it's important to note that longer periods can decrease the yield and carbon content of pyrolytic char compared to shorter durations [38]. As reported, 1 hour of pyrolysis

has the greatest impact on CBp yield (~38 wt.%), implying the decomposition of rubber in ELTs. Shorter durations result in higher yields of poor-quality CBp [38, 39]. In the literature, 2 hours is considered optimal for obtaining CBp yield, as effectively remove heteroatoms from the tire particles [40]. Extending pyrolysis beyond the optimal time (over 3 hours) can lead to a lower yield and no improvement in the carbon content of CBp, as the adsorption of more energy results in the complete cracking of the tire rubber. What is more, the residence time is directly related to particle size (optimal 5 mm), with larger particles requiring a longer residence time as it takes more time for heat to reach the core [41].

The heating rate is a key variable in ELTs pyrolysis as it significantly affects the rate of heat transfer, the actual effective temperature, and the thermal degradation of materials. Generally, to enhance the CBp yield, low heating rates ranging from 0.1 °C/min to 10 °C/min are beneficial [42], as they tend to increase resistance to mass or heat transfer within the ELT particles, promoting more uniform heat distribution and controlled release of volatiles [43]. When the pyrolysis temperature is below 550 °C, with around 500 °C being optimal, the char yield increases with higher heating rates [28]. Additionally, the BET surface area of the product tire char improves as the tire pyrolysis heating rate rises from 1 to 5 °C/min; however, further escalation has a negative effect [38]. Hence, a moderate heating rate of 5 °C/min is preferred to minimize the breakdown of ELTs and the formation of small molecular gases, thus preserving CBp yield and characteristic [44].

Concerning the pressure, vacuum pyrolysis may reduce energy requirements and suppress volatile carbonization [45, but its disadvantages include a low yield of tire char and a high content of heavy oil compounds in the liquid products. In contrast, pressurized pyrolysis of ELTs increases the yields of CBp and oil while reducing the gas yield. It was reported that the production of CBp can increase by 10.40% when the pressure in the pyrolysis system is adjusted from ambient to 2.0 MPa, with the process conducted at a temperature of 600 °C. However, CBp from pressurized pyrolysis, which melts and cross-links, has a smaller specific surface area compared to tire char produced at ambient pressure [28].

2.1.3. Pyrolytic carbon black (CBp) purification

The final step in the ELT waste treatment is the purification. A typical tire consists principally of three kinds of materials: rubber mixtures, metal, and textiles. Each material possesses unique properties that, when combined appropriately, impart the necessary strength and flexibility to the tire. Generally, the different types of ELTs are manufactured using a mix of carbon black (20-28%), natural rubber (22-30%), synthetic rubber (15-23%), steel (13-25%), and various additives such as fabric, fillers, accelerators, and antiozonants (10-14%) [46].

When ELTs are subjected to pyrolysis, the resulting CBp retains many of these additives, including sulfur, calcium, zinc, aluminum (1-3%) and a representative quantity of inorganics (10-15%), in addition to CB (80-90%), as presented in **Figure 6**. Hence, implementing a purification stage is critical to refining the elemental carbon content (>90%) in CBp and obtaining highly pure rCB, thereby maximizing the AC yield following the activation process (discussed in section 2.6). This step ensures the removal of unwanted contaminants, enhancing the quality of the final AC product.

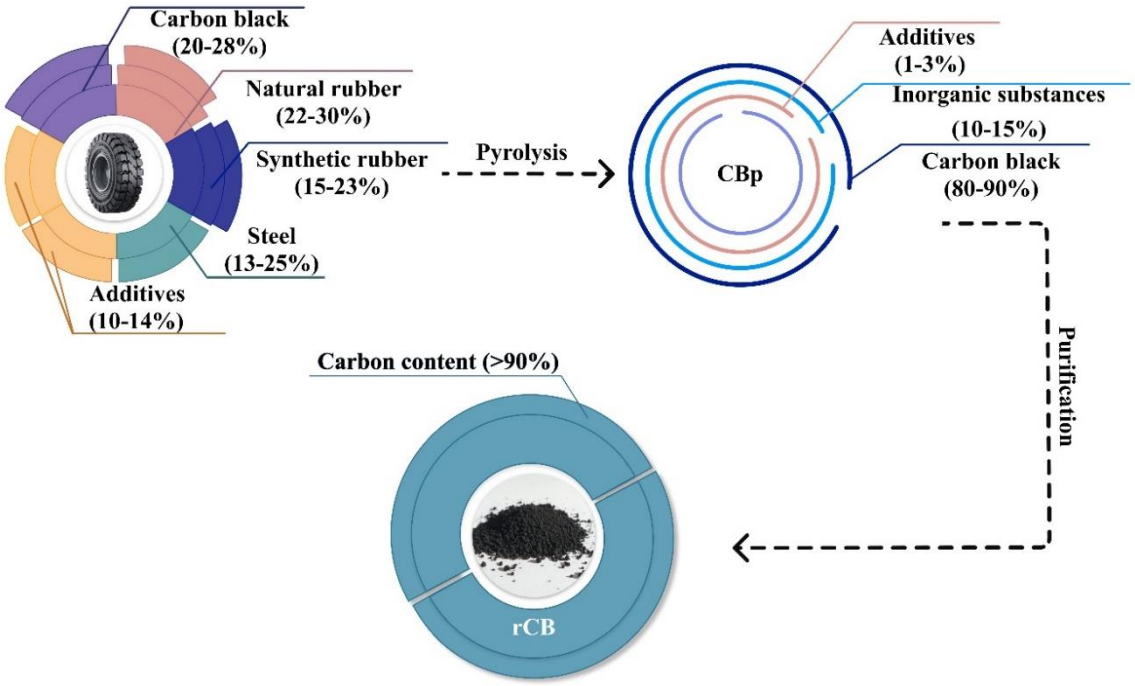

Figure 6. Schematic of the recycling stream for end-of-life-tires and pyrolytic carbon black purification to recovered carbon black, illustrating the transformation in material composition.

2.2 Activated carbons - general characteristics

The texture of ACs reflects their crystalline composition, whereas the basic structural unit is a crystallite that exhibits a graphite-like arrangement [47]. The alignment of carbon atoms within these crystallites is similar to that in graphite, where the graphitic layers (with interlayer distances of 0.3354 nm) consist of hexagonal rings and the alternate carbon atoms align vertically across adjacent layers [48]. Unlike graphite, ACs feature enlarged interlayer spacings, alongside noticeable variations in layer orientation [49]. Crystallites of ACs are also compact, multi-layered entities. The synthesis conditions of ACs, particularly the thermal treatment's duration and temperature, results in different shape and crystallite size and structure, consequently affecting the porosity [50], which is crucial for their adsorption efficiency. The disordered alignment of microcrystallites, coupled with their robust interconnections results in a porous framework.

Crystallite growth in ACs occurs through the gradual shifting of entire layer-planes or groups of them, a process evident from the earliest stages of carbonization at low temperatures. During this process, carbons differentiate into two distinct and well-defined classes: graphitizing and non-graphitizing carbons [51]. In graphitizing carbons, a pre-existing orientation facilitates the rearrangement of layer-planes, allowing this process to occur in small steps and promoting crystallite growth. The structure of these carbons is more compact, and there is a strong tendency for neighboring crystallites to align in nearly parallel orientations. Conversely, in non-graphitizing carbons, crystallite growth is hindered by strong cross-linking uniting the crystallites. This interaction leads to a random orientation of crystallites in a rigid, finely porous mass [52]. **Figure 7** illustrates the typical layered structure of crystalline graphite found in both graphitizing and non-graphitizing carbons.

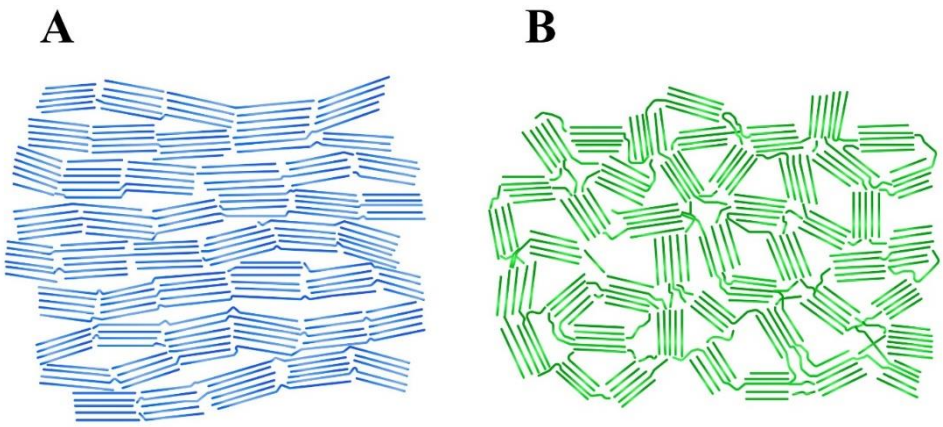

Figure 7. Schematic illustration of (A) graphitizing carbons and (B) non-graphitizing carbon structure.

2.3 Activated carbons classification

Activated carbons differ based on their production, physical attributes, and surface characteristics. ACs may be classified into two main types depending on particle size: powdered activated carbons (PACs) and granular activated carbons (GACs) [53]. PACs typically has a particle size under 0.1 mm (usually ranging from 0.015 to 0.025 mm) [54]. This small size presents challenges in fixed bed adsorption applications and during the regeneration process. In contrast, GACs exhibit larger particle size of 0.6 to 4 mm, which is more suited for continuous applications in both liquid and gas phases, offering advantages such as lower pressure drop and easier regeneration, allowing for repeated use [55].

Additionally, ACs can be categorized based on the source of the precursor, pore structure, surface chemistry, and the method of activation. These categories are explained as follows:

- The "precursor" refers to the initial raw material from which ACs are produced. A wide variety of waste biomass or industrial by-products can serve as precursors, including, but not limited to, materials like wood, olive pits, coconut shells, peat, fly ash, and coal.
- "Pore structure" is about the size and arrangement of the pores within the ACs. Based on this, ACs can be classified as microporous, mesoporous, or macroporous, each type having different implications for the material's effectiveness in various applications.
- The term "surface chemistry" relates to the chemical groups present on the AC's surface. Modifying the surface with functional groups such as -OH (hydroxyl), -NH_2 (amino), -COOH (carboxyl), and others can significantly enhance the material's adsorption properties, tailoring it for specific uses.
- Lastly, the "activation method" denotes the technique employed to convert the precursor into activated carbon. This can be achieved through physical activation or chemical activation, each method affecting the final characteristics and efficiency of the ACs.

2.4 Textural properties of ACs

Important definitions for understanding the correct adsorption characteristics and related textural properties of solid materials include the roles of the individuals involved in the process: the adsorbent, a solid that adsorbs gas molecules from the gas phase, and the adsorbate, a gas that is ultimately adsorbed onto the surface of the adsorbent. The adsorption capacity of a porous materials is often evaluated based on their specific surface area and pore size. This capacity reflects the quantity of adsorbate molecules that can be adsorbed per unit mass of the adsorbent at equilibrium.

Adsorption phenomenon occurs on surfaces, meaning carbons with larger surface areas are likely to adsorb more substrate [56]. Further, the adsorption process is enhanced by the presence of pores, which enable the transport of adsorbate molecules from the solid's surface to its interior, facilitating their accumulation. The surface of the solid materials can be classified into two categories based on its pores: internal, defined as the area comprising all the prominence, surface of all cracks, pores and cavities, which are deeper than they are wide; and external, which primarily includes the surface of all cracks, pores, and cavities that are wider than they are deep [57]. The total surface of porous materials involves mainly of the inner surface, and as a result, materials with smaller, deeper pores typically exhibit higher levels of adsorption.

Another crucial parameter is material porosity that refers to the accessibility and pore size. ACs offer a wide distribution of an extensive porous structure, with specific surface areas ranging from 500 to about 3000 m^2/g [58]. Adsorption occurs solely within open pores that communicate with the external surface (including blind and through pores), which is why it is essential to define the proportion of empty spaces and open pores relative to the total volume of the adsorbent. The classification of pores by their accessibility is presented in **Figure 8** and **Table 1.**

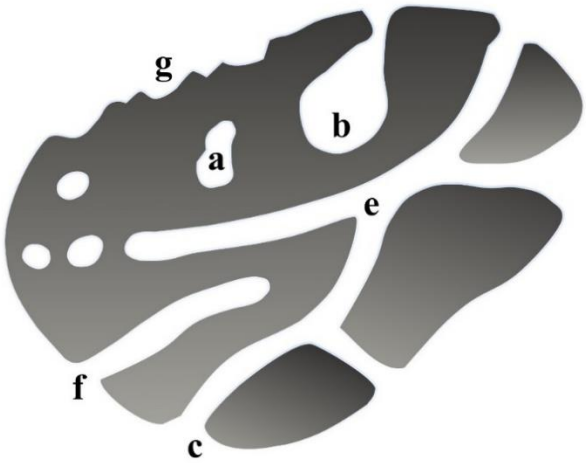

Figure 8. Schematic classification of pores according to the Union of Pure and Applied Chemistry (IUPAC) by their accessibility to surroundings (a-closed pores; b, f-blind pores; c, d-open pores; e-through pores; g-roughness).

Table 1. Pore classification by the IUPAC by their accessibility [59].

Classification of pores	Accessibility to surroundings
Closed pores	No communicating with surroundings
Open pores	Communicating with the external surface
Blind pores	Open only at one end
Through pores	Open at two ends

Considering the pore size, ACs generally possess a well-developed porous structure, containing micropores (pores with diameters less than 2 nm), mesopores (pores with diameters ranging from 2 to 50 nm), and macropores (pores with diameters greater than 50 nm). Typically, the transport of adsorbate to the interior of the activated carbon is mediated by macropores and mesopores, while micropores are primarily responsible for the adsorption process (**Figure 9**) [60]. The IUPAC officially endorses this pore classification. Additionally, Brunauer et al. [61] and Dubnin et al. [62] subsequently proposed dividing micropores into three regions: submicropores, (pores with diameters less than 0.4 nm) ultramicropores (pore with diameters less than 0.7 nm) and supermicropores (diameters ranging from 0.7 to 2 nm). This classification is particularly relevant for ACs, which often have a significant proportion of ultramicropores.

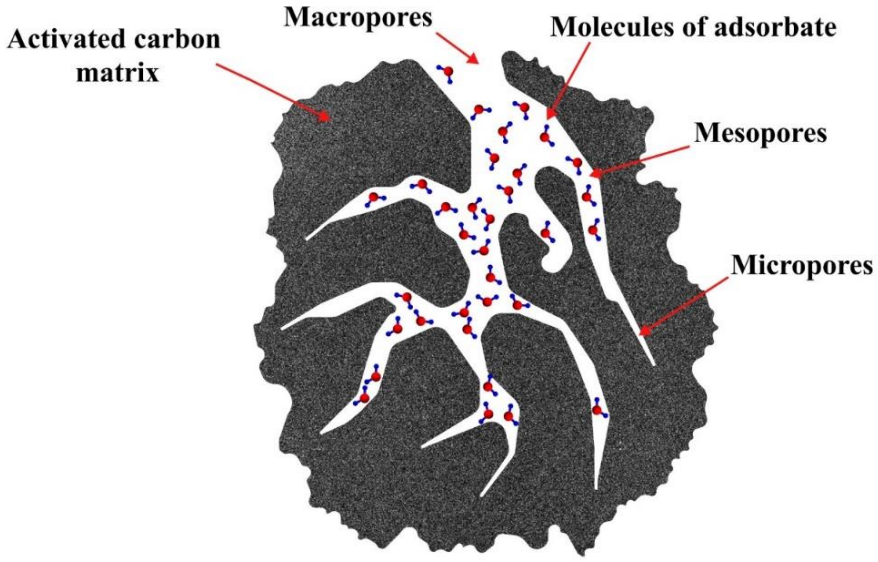

Figure 9. Diagrammatic representation of the pore structure of activated carbons (macropores, mesopores, and micropores) in the context of CO_2 adsorption.

2.5 Precursors for ACs production

Activated carbons, versatile in their applications, are primarily produced from carbon-rich materials also denoted as precursors. Ideally, ACs precursors should possess high carbon and low ash contents, low volatile matter, and low degradation tendency to keep the physiochemical characteristics (**Figure 10**) [63]. Traditionally, an array of coals, including

brown, bituminous, anthracite, peat, and even wood, are favored in the large-scale manufacturing contexts for their efficacy and availability [64]. Beyond these conventional sources, there's a growing interest in harnessing agricultural by-products, residues from forestry, or the food industry, expanding the resource base to include more sustainable options. Additional precursors are synthetic polymers and combinations like cellulose with polystyrene, discarded resins, or polyvinylidene chloride [50].

Utilizing coal and biomass as precursors for activated carbon production, while prevalent, comes with distinct drawbacks. The use of coal, despite its widespread availability and established processing techniques contribute to the overall carbon footprint [65]. On the other hand, biomass, even though renewable in nature, presents challenges in consistency and availability. The quality of activated carbon derived from biomass can therewith vary significantly depending on the source material, which might affect the product's adsorptive properties [66]. The range of use of these materials is evolving, which increases the need of finding alternatives precursors that include waste flows from landfills, including ELTs.

Figure 10. Suitable materials for the production of activated carbons.

2.6 Activation

The precursor, or char material, has underdeveloped porosity (particularly in microporosity) and a limited specific surface area, making it insufficient as an adsorbent for several practical environmental applications. To enhance the adsorption characteristics, an activation procedure, either physical or chemical, involving thermal treatment is used. This treatment is designed to increase the adsorbate storage efficiency of material by either enlarging existing pores or generating new ones at both the micro and meso scales. Specifically, chemical

activation involves the use of chemical agents that react with the material to create new pore structures, while physical activation relies on thermal processes, such as exposure to steam, air, or CO_2, to modify the existing porosity without the use of chemicals.

2.6.1 Physical activation

Physical activation involves the partial gasification of material in the presence of oxidizing gases at temperatures ranging from 800 to 1000 °C [67]. Physical activation can be categorized into two distinct approaches: the direct approach and the two-step approach. The two approaches differ by whether the thermochemical conversion is combined (direct approach) or carried out separately (two-step approach), as presented in **Figure 11.**

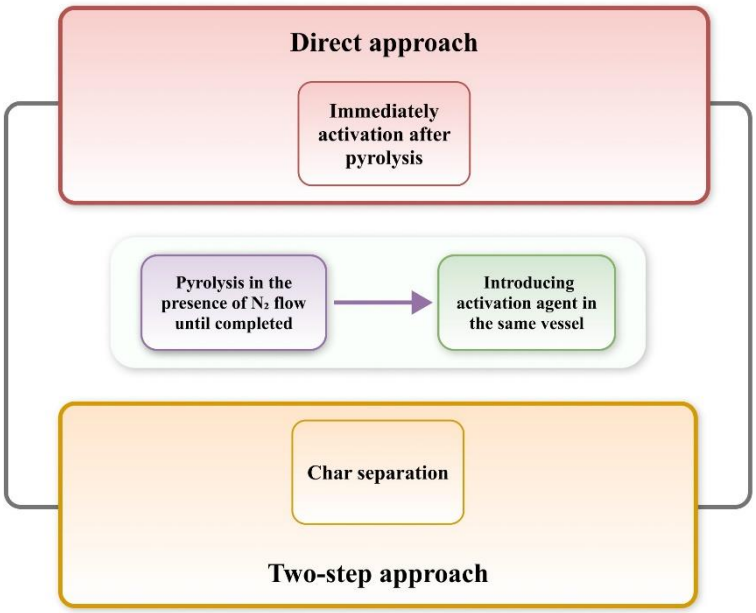

Figure 11. Schematic illustration of the two approaches of physical activation based on how thermal conversion is performed: direct and two-step approach.

Numerous comparative studies in recent years have assessed various activating agents for physical activation, with steam and CO_2 being the most commonly used methods, along with air mixtures. Reported studies show that steam activation promotes the development of high surface areas while widening microporosity. As a result, ACs prepared with steam exhibit a lower micropore volume at the expense of larger meso and macropore volumes [68]. The drawbacks of steam activation are the high necessary temperatures and long activation times, which lead to substantial energy penalties. In contrast, CO_2 activation is more energy-efficient, operates at lower temperatures, and still yields ACs with considerable surface area and a more robust growth of the microporous structure [69]. Using air as a gasifying agent is an economically attractive approach for physical activation, but it is challenging due to the risks of oxidation and combustion that can produce ACs with varied pore sizes, surface areas, and significant char loss [70]. Finally, the choice of an activator ultimately depends on the desired properties of the precursor and application.

The role of activation gases includes also chemical transformations, involving the oxidation of elemental carbon in the material. For activation with CO_2, the general reaction, also known as the Boudouard reaction, may be described as follows:

$$C + CO_2 \rightarrow 2CO \quad \Delta H = +171 \frac{kJ}{mol} \tag{1}$$

The above reaction can be divided into two separate stages. The first stage is dissociative chemisorption, where CO_2 breaks down on the carbon material's surface, leading to the formation of an oxide layer, and the second stage involving the desorption of the formed surface oxide, where the oxide is removed, and CO is produced [71].

- Dissociative chemisorption

$$C + CO_2 \rightarrow CO + C(O) \tag{2}$$

- Surface oxide desorption

$$C(O) \rightarrow CO \tag{3}$$

For activation using H_2O, the general reaction can be presented as follows [72]:

$$C + H_2O \rightarrow CO + H_2 \quad \Delta H = +117 \frac{kJ}{mol} \tag{4}$$

For activation using air, the mechanism is according to the following reactions [73, 74]:

- Chemisorption

$$2C + O_2 \rightarrow 2C(O) \quad \Delta H = -395 \frac{kJ}{mol} \tag{5}$$

- Carbon gasification

$$C + O_2 \rightarrow CO_2 \quad \Delta H = -395 \frac{kJ}{mol} \tag{6}$$

- Oxide gasification on the surface of carbon material

$$C(O) + O_2 \rightarrow CO_2 + CO \quad \Delta H = -111 \frac{kJ}{mol} \tag{7}$$

Subsequent porosity development occurs through the interaction of the gaseous activating agent with amorphous carbon, leading to the opening and widening of previously inaccessible pores and the formation of new ones [75]. Additionally, the high temperature and reactive nature of the gases can encourage the formation of various oxygen-containing functional groups. This is connected with the presence of heteroatoms in the precursors of ACs, which can react with the oxidizing agent during the activation step [76, 77].

2.6.2 Chemical activation

Chemical activation comprises the reaction of AC precursor or char with chemical reagents, and then heat treatment at a temperature of 450-900 °C under neutral conditions to produce activated carbons [78]. The two most common chemical activation procedures are a single step approach, known as dry mixing, and a two-step approach called wet impregnation

[79]. The main difference between the two activation procedures is related to the environment for the reactions and the number of required activation steps, as illustrated in **Figure 12**.

Factors that affect the development of the porous structure by chemical activation include the content of organic or synthetic raw material in the precursor, and the conditions for activations such as activation temperature, residence time, heating rate, type of activating agent, and the weight ratio between the AC precursor and the activating agent [80]. The optimal conditions for activation vary mainly depending on the precursor of choice and the used activating agent. However, some general trends have also been observed previously when choosing different activation conditions, such as:

- Increased impregnation ratios (1:2 to 1:4) have often been observed to lead to a deeper and more extensive activation process that creates larger and more numerous pores; this range provides an optimal amount of activating agent.
- Within activation temperatures ranging from 600 °C to 900 °C, the activation temperature intensifies chemical and physical transformations within the carbon structure, thereby promoting a more porous framework.
- Prolonged activation times (2-3 hours) have been noticed to allow for more thorough interaction between the activating agent and the carbon material, leading to increased porosity and a more uniform pore distribution.

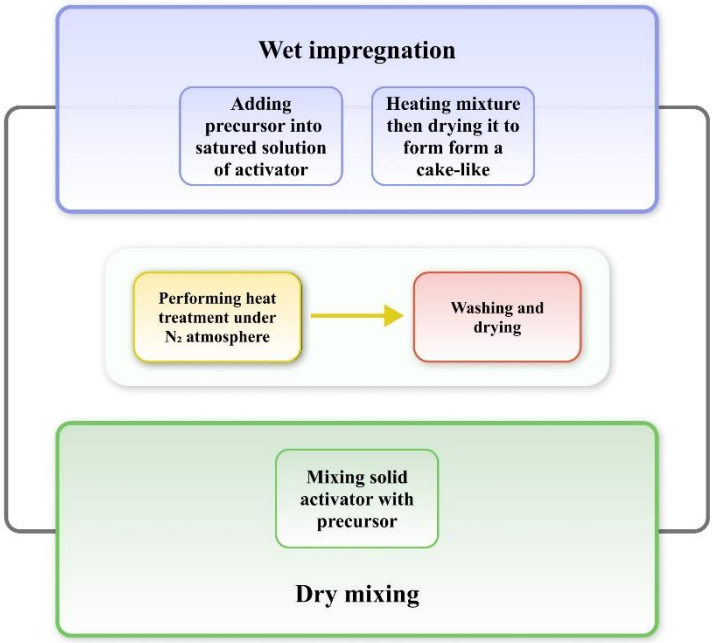

Figure 12. Schematic of two chemical activation methods for activated carbons: dry mixing and wet impregnation of the precursor and activator.

Chemical activation provides a number of benefits over physical activation, such as a reduction in temperature and activation time, higher carbon yield, more porous structure of activated carbon, low energy and operating cost, or easier development of microporosity [81]. It has also been observed that chemically activated chars have higher surface areas than

physically activated ones. On the other hand, chemical activation has several drawbacks, which include an additional rinse step to remove excess chemical agent, which results in a generation of a waste stream and problems with ecological disposal as well as secondary contamination issues connected to impurities in the used chemical agents [82]. Various chemicals have been utilized in the activation of AC precursors, which fall into three main classes, namely alkaline activators (KOH, NaOH, K_2CO_3, Na_2CO_3 and K_3PO_4), which are most commonly used, acidic activators (H_3PO_4, H_2SO_4, HNO_3) and neutral activators ($FeCl_3$, $ZnCl_2$).

Over the past several years, researchers have increasingly turned their attention to utilizing waste materials as precursors for producing activated carbons through chemical activation. Published findings consistently indicate that potassium-containing activators and especially KOH are the preferred chemical activators. The preference for KOH over other activating agents is attributed to its ability to create highly porous structures with large surface areas. KOH's enhanced chemical reactivity allows for a more effective interaction with the precursor, facilitating reactions at lower temperatures and thereby promoting the formation of an increased number of micropores and mesopores [83]. Nevertheless, it's important to note that an excessive use of KOH can lead to pore blockage and a subsequent decrease in surface area [84].

2.7 Applications of ACs in environmental issues

ACs stand out as a highly effective and multifunctional adsorbent, primarily utilized for eliminating color, odor, taste, and various unwanted organic and inorganic pollutants from drinking water. Their uses span multiple areas, including treating industrial wastewater (dyes [85-87], heavy metals [88-90], and phenolic compounds [91-93]), purifying air (H_2S [94-96], SO_2 [97-99], NO_x [100-102], and volatile organic compounds [103-105]), and processing various chemical, food, and pharmaceutical products. Around 80% of all ACs are dedicated to liquid phase applications, highlighting their significance in this area.

The ACs must exhibit specifically defined characteristics and meet technical and economic criteria related to specific adsorption applications, as summarized in **Figure 13**. Unfortunately, fulfilling these requirements is relatively rare. Beyond adsorption capacity, several other essential factors contribute to the effectiveness and efficiency of ACs, including [106, 107]:

- Selectivity, which refers to the ability of ACs to preferentially adsorb specific substances from a mixture.
- Adsorption-desorption kinetics, describing the rate at which substances are adsorbed onto and released from the AC surface, impacting the speed and reversibility of the process.
- Mechanical strength, critical for resisting abrasion and crushing under operational conditions; and pore size distribution, which affects the accessibility of adsorbates and the overall capacity of the ACs.
- Chemical and thermal stability, ensuring that ACs can withstand harsh conditions without degrading.

- Regeneration capacity, the ability of ACs to be reused after adsorption, crucial for cost efficiency.
- Stability across adsorption-desorption cycles, indicating the long-term usability of ACs without loss of performance.
- Production costs, influencing the overall affordability and market viability of ACs.

By evaluating these properties and criteria, one can select an AC that optimally fits the specific requirements of an adsorption application, balancing performance, cost, and operational longevity.

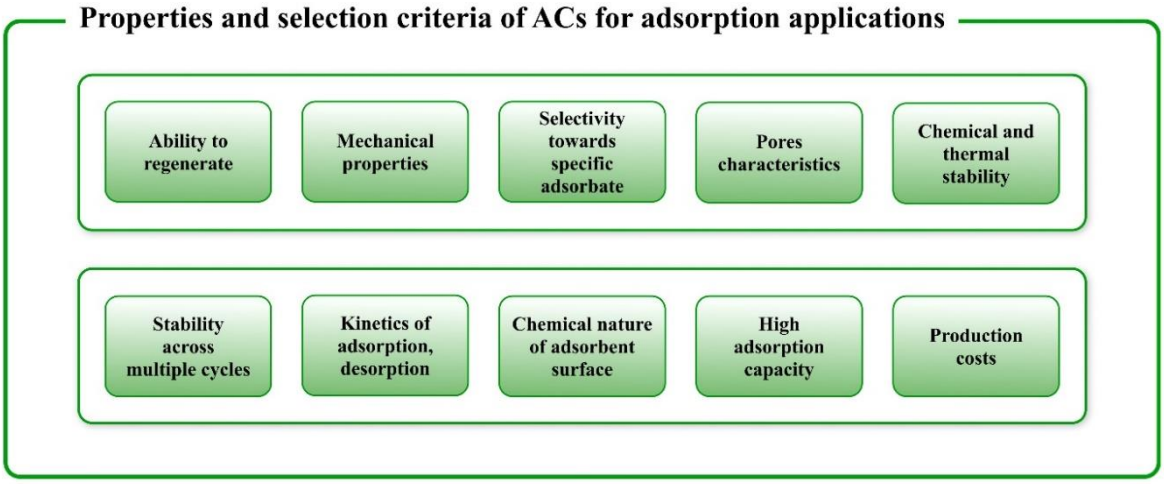

Figure 13. Summary of key properties and criteria of selecting ACs for adsorption applications.

2.8 ACs for CO_2 capture

The CO_2 capture by adsorbent materials is primarily influenced by two factors: the development of the material's porous structure, which includes the pore characteristics, and the size of the specific surface area, as well as its chemical properties. The first factor determines the space available for gas adsorption, while the second influences the interaction forces between CO_2 molecules and the solid surface, ultimately determining the adsorption properties. Additionally, the effectiveness of CO_2 capture materials depends on a variety of other factors that strongly influence the practical application, such as diverse process conditions connected with the specific branch of industry and the composition of the flue gas mixture [108].

In CCUS technology, there are three main capture configuration that allow obtaining a concentrated CO_2 stream from fuel combustion. The CO_2 capture process is expected to account for approximately 70–80% of the total cost of CCUS [109]. Thus, achieving a purified gas stream with the required CO_2 concentration through an efficient process is importance. They are classified into pre-combustion capture, post-combustion capture, and oxy-fuel combustion, varying in CO_2 concentration, pressure and temperature as presented in **Figure 14**. Those variations present unique challenges [110]. In this step, CO_2 is separated from other gaseous media using various existing gas separation technologies integrated into CO_2 capture systems, including adsorption by different types of solid materials. Moreover, this phase of CCUS is

critically important because flue gases may contain additional pollutants such as H_2S, CO, NO_x, CH_4, SO_x, and water vapor. These pollutants can modify the physicochemical properties of solid sorbents, resulting in poor separation performance. Consequently, this can affect the properties of the gas stream, such as its density and the equilibrium limit of vapor-liquid interactions, leading to inefficient storage. In this context, one possible strategy to enhance the CO_2 capture capability of adsorbents, including ACs, is by stabilizing their surfaces and addressing their vulnerability to the impurities present in flue gases. Furthermore, it is essential to address the instability and diminished adsorption capacity of ACs at lower CO_2 concentrations and elevated temperatures [111].

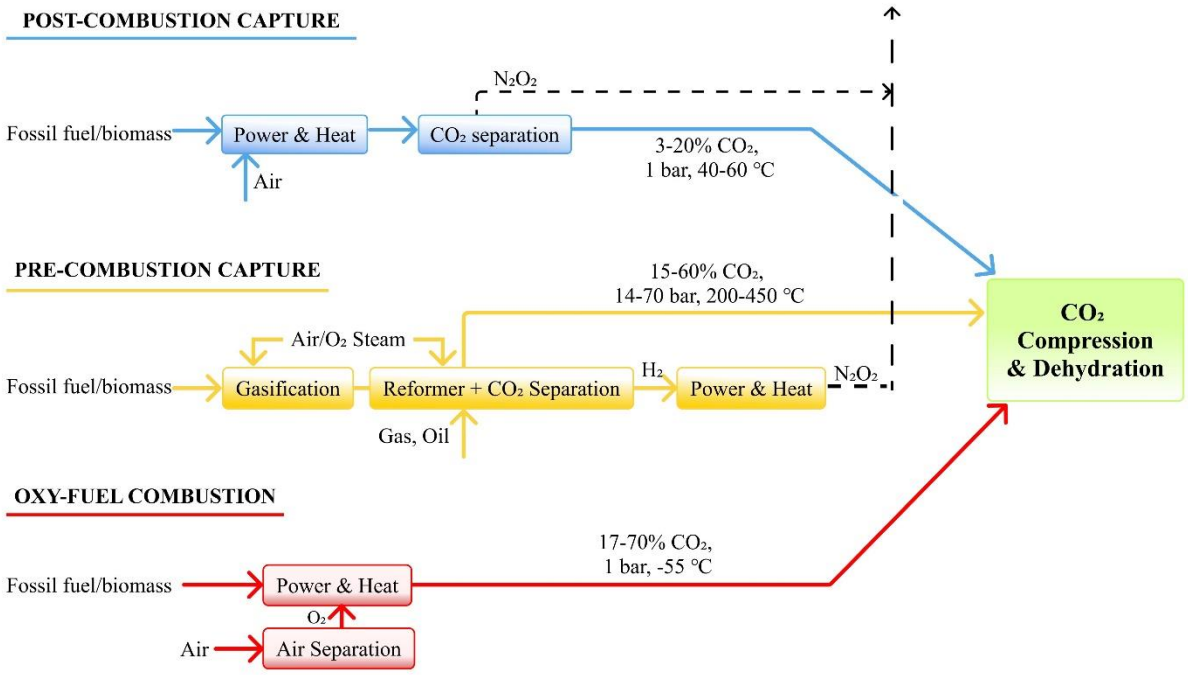

Figure 14. Generic comparison of the existing CO_2 capture system from stationary sources.

Activated carbons are among the most thoroughly researched and exceptionally effective materials for CO_2 capture, alongside zeolites [112]. These carbons exhibit desirable properties such as reversibility and stability in adsorption-desorption cycles, adjustable surface chemistry and pore structure, cost-effectiveness, low temperature required for desorption, straightforward regeneration process, fast CO_2 sorption kinetics, high thermal and chemical stability, and mechanical strength [113, 114, 115]. ACs available on the market typically exhibit limited CO_2 adsorption capabilities, due to their broad pore size distribution and low surface attraction to CO_2 molecules [116]. Therefore, addressing these two issues is considered a focal point for further investigation to overcome the challenges of the aforementioned industrial application.

Previous research has demonstrated that the textural properties of ACs such as specific surface area, total pore volume, and especially micropore volume, are associated with their capacity to adsorb CO_2. Among these, pore filling has been identified as the dominant mechanism for CO_2 adsorption [117, 118]. For enhanced CO_2 capture, it's crucial for AC to

have a substantial share of micropores to offer large surface areas (500 to 2500 m^2/g), and to provide favorable sites for CO_2 molecule adsorption [119, 120]. This pore size configuration, along with the considerable content of mesopores, favors CO_2 diffusion within the materials, thereby making the adsorption kinetics very fast as well. Additionally, it has been observed that micropores with diameter between 0.4-1 mm, enhances CO_2 adsorption performance [121], due to the occurrence of intermolecular interaction of CO_2 in addition to the CO_2-carbon pore interaction [122]. These micropores are well-suited to the kinetic diameter of CO_2 molecules (0.33 nm), which refers to an effective diameter characterizing a molecule's ability to collide with others [123]. However, the appropriate micropore size for CO_2 adsorption is highly dependent on the temperature and pressure.

Surface functional groups on ACs are pivotal in CO_2 capture. Commonly, activated carbon surfaces contain functional groups like carboxyl (-COOH), phenolic (-OH), lactone (-C=O), carbonyl (-C=O), and quinone (-C=O) groups [124], as earlier mentioned in this thesis. These groups emerge primarily during the activation process, with the temperature and duration of this process significantly affecting their distribution and concentration. Particularly, carboxyl groups play a significant role in the CO_2 adsorption, strongly attracting CO_2 molecules through Lewis base interactions [125]. In light of these properties, numerous scientific strategies can be formulated regarding CO_2 adsorption on ACs, which are summarized in **Figure 15**.

Figure 15. Research directions of activated carbons for CO_2 capture applications.

These strategies include: (1) adjusting the synthesis conditions, like thermal conversion or activation processes; (2) conducting surface modifications, including high-temperature ammonia treatment [126, 127] and amine functionalization [128, 129]; (3) creating AC composites by incorporating carbon-based nanomaterials [130], polymers [131, 132, 133], metal oxides or metals [134, 135], zeolites [136-139], and metal-organic frameworks [140, 141]. The combination of the above modification strategies has also been reported in the literature [142, 143].

2.9 Mechanism of CO_2 adsorption at the solid-gas interface

Adsorption is a surface phenomenon that is primarily influenced by the concentration of adsorbate or its partial pressure, which initiates the adsorption process at the solid-gas interface. Consequently, there is a change in the concentration of adsorbate in the interfacial layer. This process involves adhesion that occurs at the contact boundary between two phases, particularly at the solid-gas interface, and is driven by strong interatomic and intermolecular forces [144]. Initially, CO_2 molecules are attracted to the solid surface due to the difference in energy. On the surface of the adsorbent, surface forces attract the adsorbate and cause accumulation, while inside the solid, internal forces are balanced (**Figure 16**) [145]. The surface energy, which appears in the context of this difference, determines the stability of the adsorption complex. It is also influenced by the specific surface area of the solid, its chemical properties, porosity, and the structural arrangement of the adsorbate molecules [146]. Further, as CO_2 molecules continue to accumulate on the surface, a concentration gradient is formed. This gradient acts as a driving force for further adsorption, moving adsorbate from areas of higher concentration in the gas phase to areas of lower concentration on the adsorbent surface. The process progresses until an equilibrium state is reached.

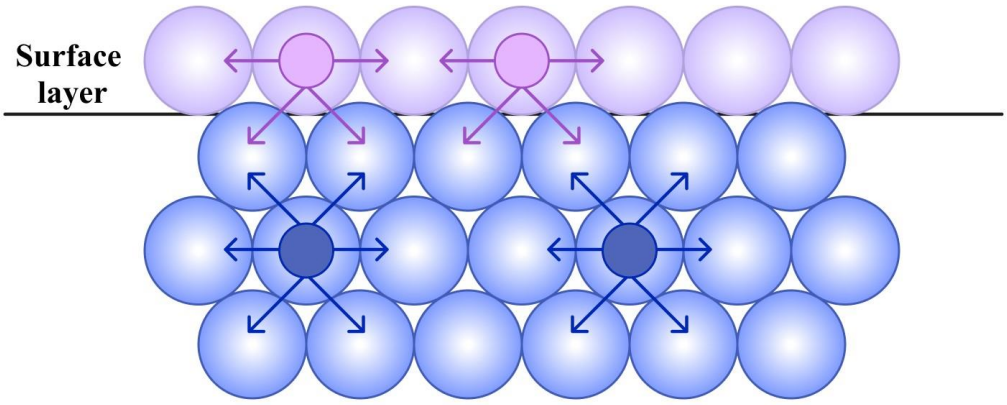

Figure 16. Schematic representation of the force interactions at the solid-gas boundary.

Adsorption is also a kinetic process involving the movement of gas molecules from a gas phase to the surface of an adsorbent, ultimately reaching an equilibrium in specific time [147]. Initially, CO_2 molecules migrate from areas of higher to lower concentration toward the adsorbent surface in a process known as external mass transfer, facilitated by a concentration gradient, as mentioned before. Once near the adsorbent surface, CO_2 molecules must diffuse

through the surface liquid film surrounding the solid particles, a stage known as film diffusion or external diffusion. Upon contacting the porous surface, the adsorbate first undergoes intraparticle diffusion, which involves two primary mechanisms: (1) pore diffusion, influenced by particle porosity and morphology, and (2) surface diffusion, as molecules seek more favorable adsorption sites [148]. Once at the optimal location, the adsorbate adsorbs onto the active sites available within the pores or on the external surface, either through physical or chemical adsorption (as described in subchapter 2.10). In the case of reversible adsorption, one also has to include the desorption of the adsorbate from the adsorbent surface. Over time, the rates of adsorption and desorption, which involve molecules detaching from the surface and returning to the bulk phase, balance each other [149]. This equilibrium state is characterized by an equal number of CO_2 molecules being adsorbed and desorbed in the same unit of time. The amount of adsorbate adsorbed per unit mass of adsorbent (m) depends on the partial pressure of the gas medium (p) and the temperature (T). This relationship can be expressed mathematically as:

$$m = f(p, T) \tag{8}$$

Considering these two parameters, the amount of CO_2 adsorbed at equilibrium decreases with increasing temperature, reflecting the exothermic nature of adsorption. An increase in temperature accelerates diffusion by boosting the energy of gas molecules, which leads to the destabilization of the adsorbed gas on the surface of adsorbent. Consequently, the adsorbed gas molecules gain enough energy to overcome the attractive surface forces and return to the gas phase [150]. Conversely, an increase in the partial pressure, which serves as the driving force for adsorption, intensifies the amount of adsorbate adsorbed. Lower partial pressures, however, can induce desorption by reducing the molecular concentration on the surface.

2.10 The main types of CO_2 sorption process

There are two primary types of sorption process depending upon the nature of interactive forces between the surface and incoming molecules: physisorption and chemisorption [151].

Physisorption, or physical adsorption, occurs when the adsorbate accumulates on the surface of a solid due to weak intermolecular van der Waals interactions [152]. These interactions, arising from dispersion forces or dipole interactions, act perpendicular to the surface and are weaker with a longer range, having lower enthalpy values (20-40 kJ/mol). This allows for the formation of a multilayer adsorbate complex. Because the interactions are not strong, this type of adsorption can be easily reversed. Physisorption is the primary mechanism governing CO_2 capture on ACs, with the gas uptake directly related to their porous texture [153]. The reduction in CO_2 adsorption capacity of ACs at elevated temperatures demonstrates that the process favors lower temperature.

In contrast, chemisorption, or chemical adsorption, occurs when CO_2 molecules form chemical bonds with the surface of an adsorbent [154]. Also known as irreversible adsorption, it involves adsorbate molecules exchanging or sharing electrons with the adsorbent surface, resulting in the formation of covalent or ionic bonds. Chemisorption results in the formation of

chemical bonds, and the heat of adsorption released during this process aligns with the energies typically associated with bond formation, reflecting the strong chemical interactions between the adsorbate and the adsorbent surface (80-240 kJ/mol) [155]. Furthermore, similar to many chemical reactions, chemisorption requires a specific activation energy to initiate and maintain these strong bonds, leading to a new equilibrium state where the adsorbate is firmly attached to the surface [156]. This results in a stable monolayer with adsorbed gas molecules chemically bonded to specific sites on the adsorbent. Regarding practical applications, to enhance the gas selectivity towards CO_2 by ACs, their surfaces are often chemically grafted or coated with basic groups, as mentioned in subchapter 2.8. Those groups effectively interact with the acidic CO_2 molecules, specifically based on the chemisorption mechanism. The chemical interaction, favored at high temperatures, significantly improves the CO_2 capture capacity of the modified physical adsorbents. Typically, CO_2 adsorption at temperatures above 140 °C is predominantly controlled by chemisorption, although both chemisorption and physisorption can occur within the temperature range of 25–140 °C [157].

The comparison of the physical and chemical adsorption mechanisms is schematically shown and summarized in **Figure 17** and **Table 2**.

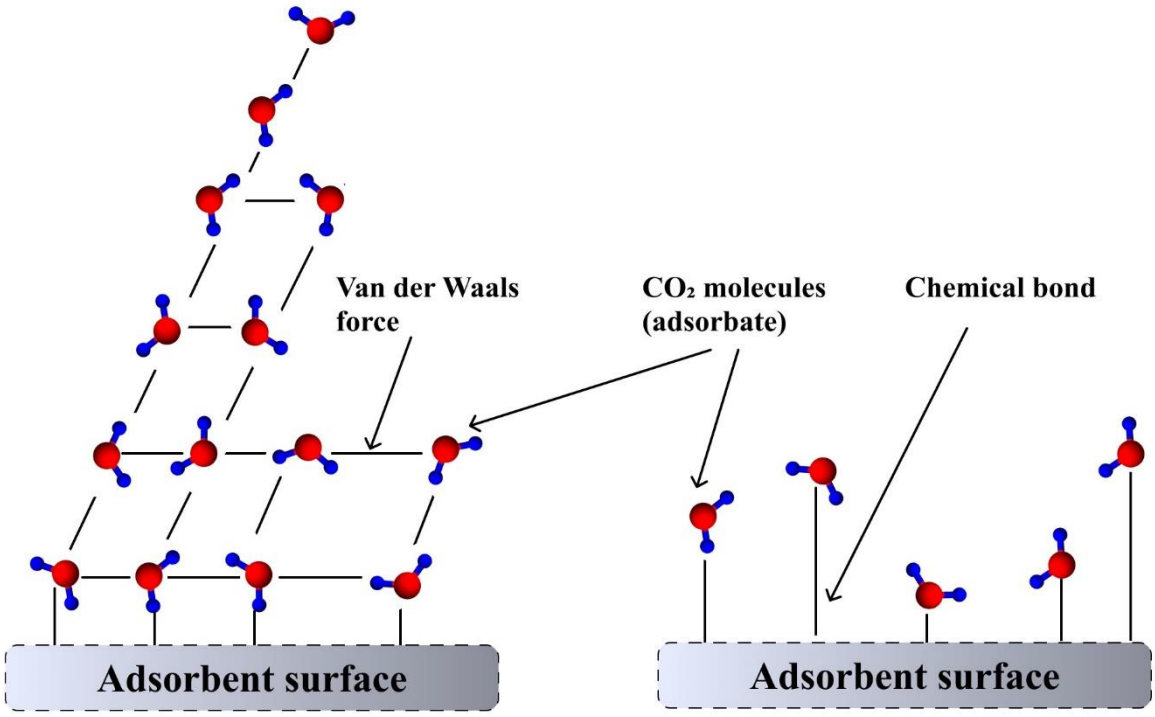

Figure 17. Schematic of the interactions between CO_2 molecules and the adsorbent surface during physisorption (left) and chemisorption (right).

Table 2. Comparison of the physical and chemical adsorption mechanism [158].

Characteristic	Physisorption	Chemisorption
Type of bonding	Van der Waals bonds	Chemical bonds
Thermal effect of the phenomenon	< 40 kJ/mol (low heat of adsorption)	80-240 kJ/mol (large heat of adsorption)
Equilibrium of adsorption and desorption	Complete reversibility	Partial irreversibility
Chemical change of adsorptive	None	Formation of a surface compound
Energy needed to establish an equilibrium	Very low	High energy needed
Course of the phenomenon	It is unbraked even at low temperatures, therefore fast	Only at higher temperatures is it no longer strongly braked
Specificity of adsorbate adsorbent interaction	No outstanding specificity	Outstanding specificity
Covering the surface with a solid as an adsorbent	Possible formation of multimolecular adsorption layers	Establishing the phenomenon with complete monomolecular coverage

3. Experimental section

This section of the thesis details the materials, analytical techniques methods, and methods applied in research, focusing on the use of rCB for producing ACs and their application in CO_2 capture. It outlines the processes involved in transforming ELTs into valuable carbon materials and assesses their effectiveness in environmental remediation. Each subsection is carefully organized to provide a clear and concise overview of the experimental approach, from the initial material recovery to the final application testing.

3.1 Materials

3.1.1 Recovered carbon black (rCB)

Recovered carbon black utilized in this work was sourced from end-of-life tires. rCB was obtained through a series of procedures as depicted in **Figure 18**, involving the industrial pyrolysis of ELTs followed by subsequent purification steps to enhance its quality.

- **Pyrolysis for pyrolytic char production**

Pyrolysis is essentially the thermal decomposition of ELTs materials at high temperatures (>500 ℃) in an oxygen-free atmosphere. This environment is crucial as it prevents

combustion and facilitates the breakdown of the polymers in tires, such as synthetic and natural rubber, which are composed of long molecular chains. The heat in the pyrolysis process breaks these chains apart. Pyrolysis leads to a three-phase product stream that includes: a solid phase in the form of char, an oily liquid phase, and a gaseous phase.

The key output from pyrolysis is char, a carbon-rich solid residue that constitutes approximately 33-40% of the mass exiting the pyrolysis process. The resulting pyrolytic char primarily consists of carbon black (80-90%), along with inorganic substances (10-15%) and other residual additives (1-3%), which are always present in compounds used in the manufacture of tires. The specific composition depends on the tire formula, as stated in subsection 2.1.3.

➢ **Purification steps of pyrolytic char**

When processing pyrolytic char derived from the pyrolysis of ELTs, purification is a crucial step. The main goal of purification is to reduce the high content of impurity elements (such as Zn, Si, Ca, S, Al etc.). This enhances the quality and usability of the pyrolytic char for various applications by benefiting the improvement of active sites, increasing porosity, and boosting the elemental carbon content, thus addressing the main issue that influences its use as a replacement for virgin carbon black.

- **Post-pyrolysis processing**

Following pyrolysis, the pyrolytic char is laden with various contaminants, specifically including residual ash, organic residues, inorganic materials, and potentially partially reacted or unreacted hydrocarbons. Further purification steps can be performed using chemical or physical methods to remove impurity elements that are found in them.

- **Purification steps**

To transform pyrolytic char into commercially viable recovered rCB, several purification steps are undertaken. These may include concentrated pickling, devolatilization, milling, pulverizing, and optionally, pelleting to remove impurities, standardize particle size, and reduce variability in material quality.

Figure 18. Overview of the general steps in rCB production from waste tires.

The rCB used in the present study was with an average particle size of 30 μm and an ash content ranging from 0.5-2%. As shown in **Figure 19**, the rCB contained particles in the 15-100 μm range where the main fraction was in the sizes between 73-80 μm,. The chemical composition of the rCB varied, primarily influenced by the tire composition used in pyrolysis, with carbon being the major element, present in concentrations of 92–99.5%. The content of volatile substances exceeded 0.2% and mineral content of about 0.5-2%, which includes elements like silicon, aluminium, zinc, sulphur, and calcium. The specific chemical composition of rCB is presented in **Paper I** and **Paper II**.

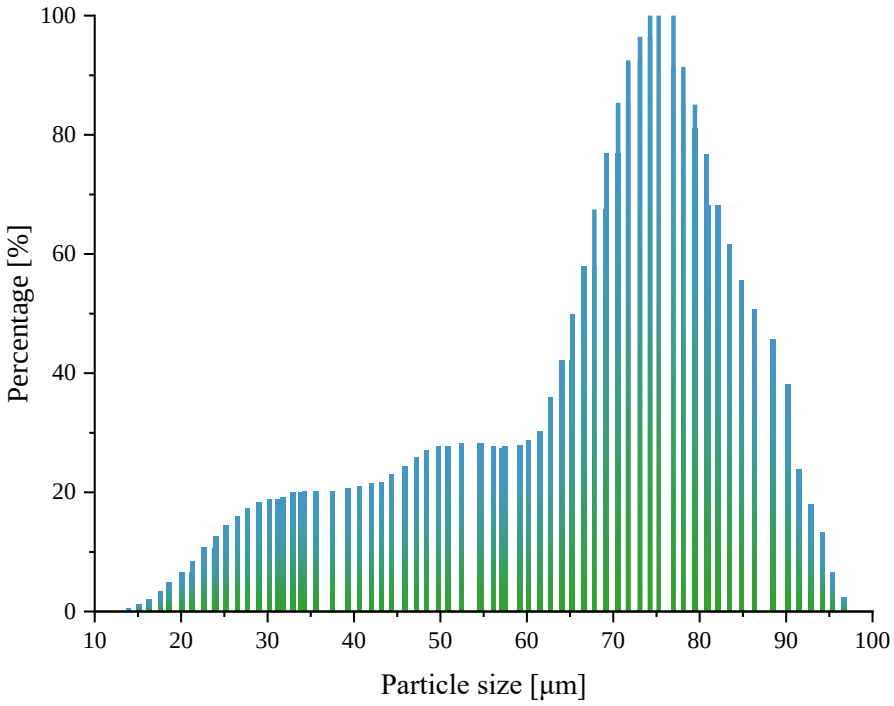

Figure 19. Histogram of particle size distribution for recovered carbon black obtained through pyrolysis of waste tires.

3.2 Analytical techniques

3.2.1 N_2 and CO_2 adsorption-desorption isotherm analysis

Gas adsorption technique is used to characterize the physical characteristics of porous materials, including pore volume, specific surface area, and pore size distribution (PSD). Gas adsorption experiments rely on sophisticated instruments, including a sample chamber to hold the material, a pressure control system, and a gas delivery setup. Successive amounts of the adsorbate are introduced and at each stage, the system is allowed sufficient time to attain equilibrium, which corresponds to a series of single points on the adsorption isotherm. During the experiments, an adsorbate physisorbs on the surface of the material, forming a liquid-like phase at a certain pressure (P), which is lower than the saturation pressure (P_0) [159]. Initially, at low relative pressures (P/P_0) one monolayer of adsorbed gas is formed on the surface of the material. As pressure gradually increases, multi-layers of adsorbed gas are formed until reaching a critical film thickness, causing the molecules to tightly pack and shift into a

thermodynamically lower energy state. This transition is marked by a plateau where the pores become completely filled [160]. Further, when the pressure decreases, the molecules, especially in mesoporous materials, tend not to desorb easily, leading to lower pressures during evaporation than during condensation, creating a hysteresis loop. This loop concludes when only a monolayer film remains on the surface.

According to the IUPAC, six basic types of isotherms can be distinguished, as presented in **Figure 20**. The type I isotherm, corresponding to the Langmuir model, describes adsorption on microporous materials where adsorbate molecules fill available active sites until saturation, shown by an asymptotic approach to a maximum value. Type II isotherms illustrate reversible multilayer adsorption on non-porous or larger pore materials. Initially resembling the Langmuir isotherm at low pressures, they progress through a linear multilayer formation phase after a distinct inflection point, concluding at complete pore filling, defined by the BET model. Type III isotherms occur with weaker adsorbent-adsorbate interactions, leading to increased adsorption with rising relative pressure due to stronger intermolecular forces among the adsorbate molecules. Type IV and V isotherms describe mesoporous adsorbents, featuring a unique desorption path due to capillary condensation. Type IV follows the BET model, starting with monolayer adsorption and transitioning to multilayer adsorption at higher pressures. Type V, similar to types III and I, is commonly observed in the case of homogeneous adsorbent surfaces, where the heat of adsorption does not depend on the degree of surface coverage. Type VI isotherm, typical for uniform nonporous surfaces, shows distinct layer-by-layer adsorption, with each layer's capacity reflected in the step-height influenced by the system and temperature.

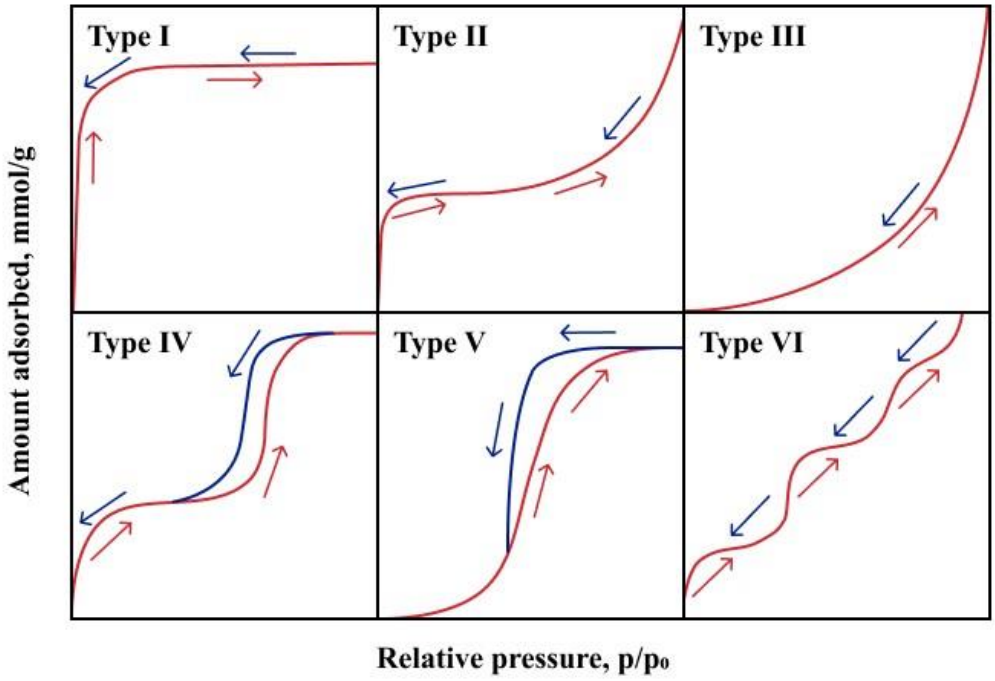

Figure 20. Classification of adsorption-desorption isotherms (red arrows: adsorption course; blue arrows: desorption course).

Regarding calculation of textural properties, the total pore volume and BET surface area are specifically calculated based on the N_2 adsorption method. The total pore volume of material

is calculated from the N_2 amount adsorbed at a relative pressure, p/p_0 = 0.99, often corresponding to the saturation pressure, where the pores are considered to be completely filled [161]. Furthermore, the Brunauer-Emmett-Teller (BET) equation is typically employed to estimate the specific surface area, based on of measurements at a relative pressure of 0.05–0.35. The BET theory assumes that a monolayer of gas molecules is adsorbed onto the surface of the material, followed by multilayer adsorption, with the binding energy decreasing in successive layers [162]. Additionally, CO_2 adsorption measurements is supplemented for a more comprehensive pore analysis. It is instrumental in evaluating the micropores (<1.4 nm) within ACs, providing a complementary analysis to N_2 adsorption, especially at low pressures where N_2 may not penetrate the smallest pores effectively. CO_2 adsorption is particularly valuable for characterizing materials where N_2 adsorption does not fully reveal the narrowest pore structures. Based on the N_2 and CO_2 adsorption measurements, the pore size distribution within specific pore size ranges of 2–50 nm and 0.3-1.4 nm is assessed, respectfully. This analysis is a critical factor in characterizing the porosity of ACs by using the density functional theory (DFT) method. The DFT approach provides detailed insights into the pore structure, enabling accurate calculations of the PSD and determination of pore volumes by considering the effects of pore geometry, like cylinders or slits, and molecular theory models tailored to adsorption phenomena [163].

In this thesis, N_2 adsorption analysis was extensively used to determine the BET surface area, total pore volume, micropore volume (<2 nm) and PSD of rCB/ACs in **Paper I** and **Paper II**. The N_2 adsorption-desorption isotherms were measured at a constant temperature of -196 °C in the relative pressure range of 10^{-6} to 0.99. Complementing the analysis, CO_2 adsorption measurements were also performed in **Paper I** to further assess the small micropore volume with diameters 0.3–1.4 nm. These measurements were conducted by recording CO_2 adsorption isotherms at 0 °C and low relative pressures (10^{-6} to 0.025), which provided additional insight into the finer aspects of micropore analysis, including the PSD.

3.2.2 Fourier-transform infrared spectroscopy (FT-IR)

Fourier-transform infrared spectroscopy (FT-IR) is an analytical technique that combines the principles of infrared spectroscopy with Fourier transforms to achieve high-resolution spectral data (**Figure 21**). This method is particularly effective in identifying organic, polymeric, and, in some cases, inorganic substances through characteristic features evident in produced FT-IR absorption/desorption spectra. The core component of an FT-IR spectrometer is the interferometer. The interferometer uses a beam of infrared light, which is split into two paths (as shown on figure 18): one path is reflected off a stationary mirror and the other off a moving mirror, causing an interference pattern [164]. This pattern is recorded over time, producing an interferogram. The interferogram is a complex signal containing all the spectral information of the sample, which, when subjected to a Fourier transform, yields the spectrum.

In the context of activated carbons, FT-IR spectroscopy is particularly useful for characterizing surface functional groups of these materials. These groups play a crucial role in the adsorption processes of organic molecules, pollutants, and even gases from air or aqueous solutions, as mentioned earlier.

In this work, by applying FT-IR spectroscopy to rCB/ACs, valuable information about the surface chemistry is obtained. FT-IR method was used in **Paper I**.

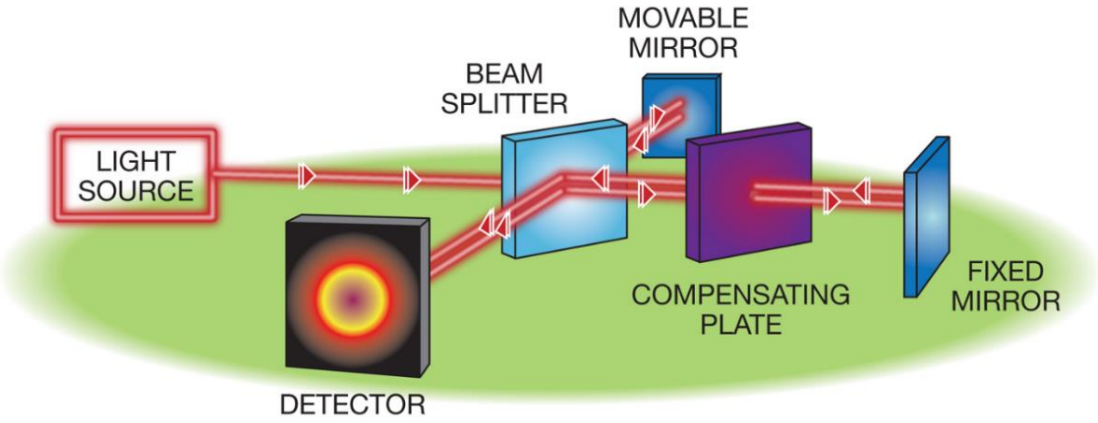

Figure 21. Principle of Fourier-transform infrared spectroscopy.

3.2.3 Raman spectroscopy

Raman spectroscopy is a versatile and non-invasive analytical method that offers insights into the molecular composition, chemical structure, and lattice dynamics of materials. The Raman effect is the phenomenon of inelastic scattering of photons by molecules, resulting in a shift in the energy of the incoming light [165]. This shift corresponds to the vibrational energies of the molecules present in the sample. When light interacts with a substance, the majority of photons undergo elastic scattering, namely Rayleigh scattering, which implies that they maintain their initial energy (**Figure 22**). Nevertheless, a minute proportion of the light (about 1 in 10 million photons) undergoes inelastic scattering, resulting in an alteration of its energy level either upwards or downwards. The energy shift serves as a distinctive characteristic that allows for the identification of molecules.

The key element of a Raman spectrometer is the laser, which functions as the source of light. A laser beam is aimed at the sample, and the light that scatters off is gathered using a lens and passed via a monochromator [166]. The charge-coupled device (CCD) camera detects the resulting spectrum, which generates the Raman spectrum. This spectrum displays the intensity as a function of the Raman shift, typically quantified in wavenumbers (cm^{-1}).

Raman spectroscopy is very advantageous method for analyzing carbon-based compounds, such as activated carbons, graphene, carbon nanotubes, and diamond, as well as other materials including minerals, or polymers.

In this work, Raman spectroscopy provided valuable information about the structural characteristics of rCB/ACs, including the level of graphitization and the presence of defects on the surface, as described in **Paper I**.

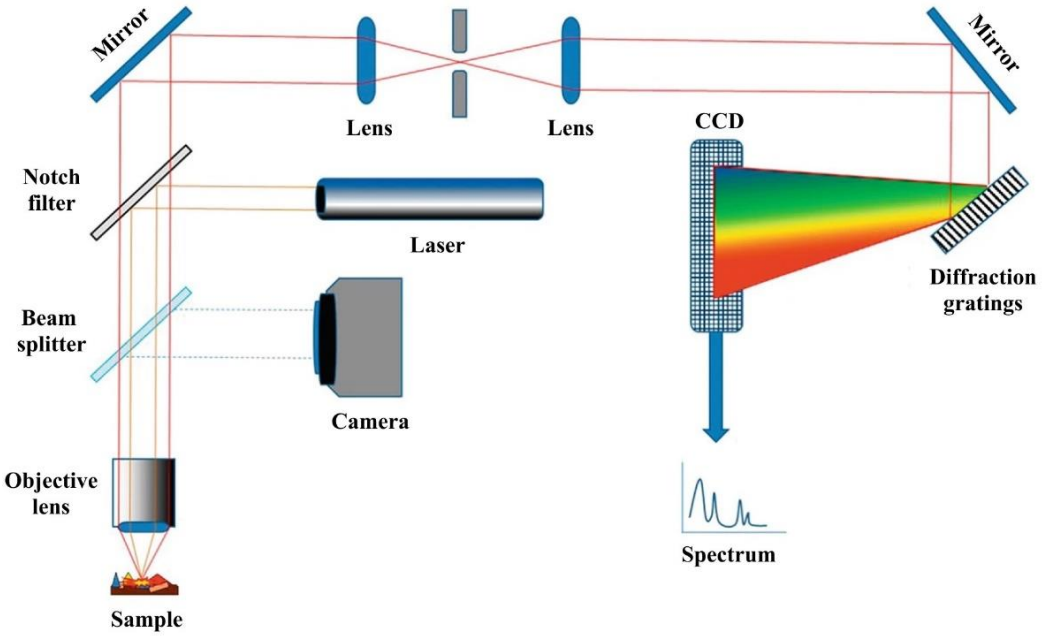

Figure 22. Basic principles of Raman spectroscopy.

3.2.4 Ultimate and proximate analysis

Ultimate analysis is an in-depth study aimed at determining the exact elemental compositions of a material, focusing on important elements like carbon, hydrogen, oxygen, nitrogen, and sulfur [167]. This analysis operates on the "Dumas method" principle, which involves "flash combustion" to oxidize the sample completely and instantly. The combustion products are then separated by chromatography before detection by a thermal conductivity detector (TCD). The TCD produces an output signal corresponding to the concentration of each component in the mixture. Ultimate analysis is crucial for understanding the material's chemical characteristics, energy content, and potential environmental effects.

On the other hand, proximate analysis evaluates the physical constituents of the material, classifying it based on its moisture, volatile matter, fixed carbon, and ash content [168]. It can be performed using a thermogravimetric analyzer, which measures changes in a material's mass as it is heated, thereby providing insights into its composition (described in subsection 3.2.5). Proximate analysis offers valuable information about the material's operational properties, such as combustion efficiency, thermal stability, and material handling characteristics.

These two analytical methods were applied in **Paper I** to rCB/ACs and revealed essential information about the structural composition and physical attributes of rCB/ACs, crucial for optimizing their performance in adsorption applications.

3.2.5 Thermogravimetric analysis (TGA)

Thermogravimetric analysis (TGA) is a method used to quantify the change in mass of a material in relation to temperature or time, as a gas atmosphere is passed over it. The primary purpose of thermogravimetric analysis is to evaluate the thermal stability and composition of materials [169]. Through gradually increasing the temperature of the sample and recording

changes in weight of the sample different processes leading to material changes can be revealed , such as dehydration, breakdown, or oxidation (**Figure 23**).

TGA is a useful technique for evaluating the thermal stability of ACs, which is an important factor in determining their suitability for practical use.

In this work, TGA enabled the measurement of changes in weight of rCB/ACs samples caused by thermal degradation, loss of volatile components, or chemical interactions **(Paper I**). This was achieved by heating the samples in a controlled atmosphere of N_2. This knowledge is essential for establishing the temperature ranges in which rCB/AC materials maintain their structural integrity and performance qualities, particularly for applications that require strong thermal stability.

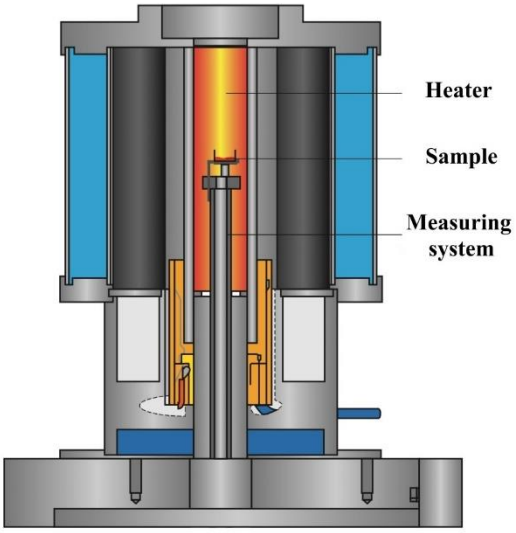

Figure 23. Schematic representation of thermogravimetric analysis apparatus (TGA).

3.2.6 Scanning electron microscopy (SEM) with energy-dispersive X-ray spectroscopy (EDS) analysis

The scanning electron microscopy (SEM) system consists of three primary components: the electron gun, which generates and accelerates the electron beam; the electron column, which employs electromagnetic lenses to manipulate the beam; and the sample chamber, where interactions between the electron beam and the specimen take place [170]. Achieving high-quality SEM images requires the electron beam to be finely focused on the specimen, ensuring a minimal probe size while sustaining a high electron current. This precision is attained through the use of electromagnetic lenses and apertures that guide the accelerated electrons towards the specimen. Key elements in the electron column include the condenser lens, which narrows the electron beam for a small probe size, and the objective lens, which focuses the beam on the specimen. The SEM different signals (**Figure 24)** are formed based on the type of interactions with the specimen surface, notably secondary electrons (SE), backscattered electrons (BSE), and characteristic X-rays, each originating from distinct specimen depths and providing varied spatial resolutions. Surface characterization is achieved through the use of SE and BSE, while the identification of elemental composition is obtained from the X-ray photons via energy-dispersive X-ray spectroscopy (EDS).

Secondary electrons emerge due to inelastic collisions of primary electrons with the specimen's atoms, possessing energy below 50 eV. This low energy limits their escape to a surface depth of under 20 nm, enabling them to provide imaging resolution between 5-20 nm, which is crucial for revealing surface topography.

On the other hand, ***backscattered electrons*** are electrons that bounce back from the specimen, as a result of the elastic interactions with the specimen's atoms. These electrons originate from greater depths within the specimen. Their emission varies with the specimen's atomic mass (or average atomic number), making them valuable for obtaining chemical contrast.

X-ray emissions are unique to each element and occur when primary electrons knock out an electron from an atom's inner shell. The following replacement of the vacancy by an electron from a higher shell results in energy release in the form of an X-ray photon. This unique transition for every element is used to determine the chemical composition of the evaluated specimen.

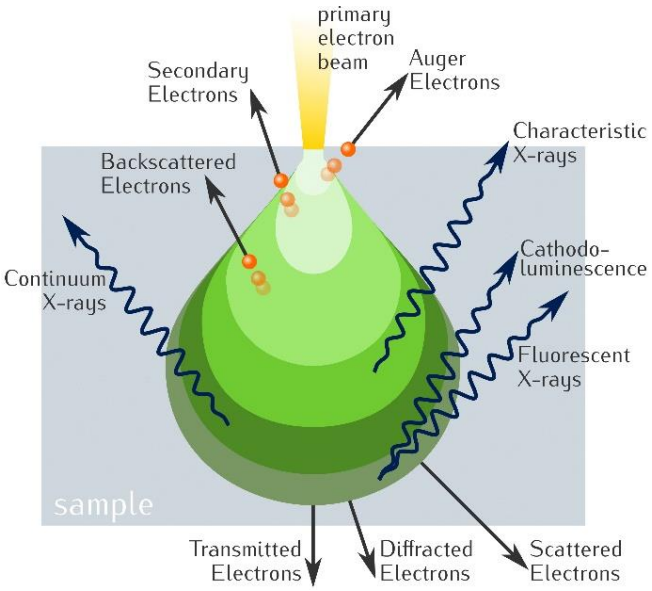

Figure 24. Electron-matter interactions: the different types of signals generated at the beam-surface interface in a SEM chamber.

In this thesis, SEM-EDS was employed to evaluate the morphological characteristics of rCB/ACs and the identification of elements and their distribution post-activation, focusing on the impact of the activator and the content of trace elements from the precursor (**Paper I**). Additionally, in **Paper II**, the technique was used to investigate the distribution of potassium on rCB/ACs after chemical activation using potassium salts.

3.2.7 X-ray diffraction (XRD) analysis

X-ray diffraction (XRD) is both a qualitative and quantitative analytical technique used to gather structural information about a material, including its crystalline phases and crystallinity level. This method operates on the principle of constructive interference between an X-ray beam and a sample [171].

The technique involves generating polychromatic X-rays in a cathode ray tube (usually Cu or Mo), which are then filtered to produce a monochromatic beam. This beam interacts with the lattice planes within the crystalline structure, leading to the elastic scattering of X-rays (**Figure 25**). When constructive interference occurs, the interactions result in a diffraction pattern, a diffractogram.

For the purpose of this thesis, XRD was utilized for the identification of various phases that emerge during the rCB activation process by potassium-containing salts (**Paper II**). This technique played a role in evaluating the underlying mechanisms involved in the activation process. The acquired data was used for understanding how K-activators influence the pore structure and chemical composition of rCB/ACs. The recorded XRD spectra were compared qualitatively to the X-ray diffraction patterns from existing databases (PDF 4+) and also used for semi-quantitative analysis.

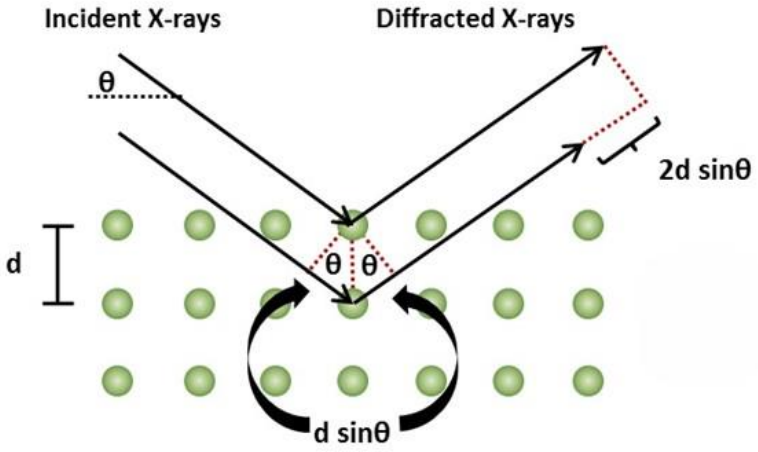

Figure 25. Schematic representation on the working principles of X-ray diffraction.

3.3 Methods

This section outlines the methodologies employed to prepare and characterize rCB/ ACs as well as the subsequent evaluation of their performance in CO_2 adsorption. The section is divided into two primary subsections: preparation methods of rCB/ACs and CO_2 adsorption studies, detailed descriptions of the experimental setups, conditions, and analytical techniques utilized to achieve and verify the research objectives.

3.3.1 Preparation of rCB/ACs

This subsection focuses on the methodologies employed to prepare activated carbons from recovered carbon black using both physical and chemical activation processes, describing the equipment, conditions, and post-treatment procedures.

3.3.1.1 Physical activation

rCB/ACs prepared through the physical method (using air), were investigated in **Paper I**. The overall process is demonstrated in **Figure 26**. Barnstead Thermolyne 47900 muffle furnace was used for the physical activation, where the temperature was varied from 500 to 700

°C. Atmospheric air was used as the reactive medium (a gaseous composition containing 21% O_2 and a balance of N_2) in all the experiments. The conditions were set to a heating rate of 7 °C/min with a holding time of 2 hours. Subsequently, the resultant rCB/AC materials were thoroughly dried in an oven for 24 hours at a temperature of 200 °C.

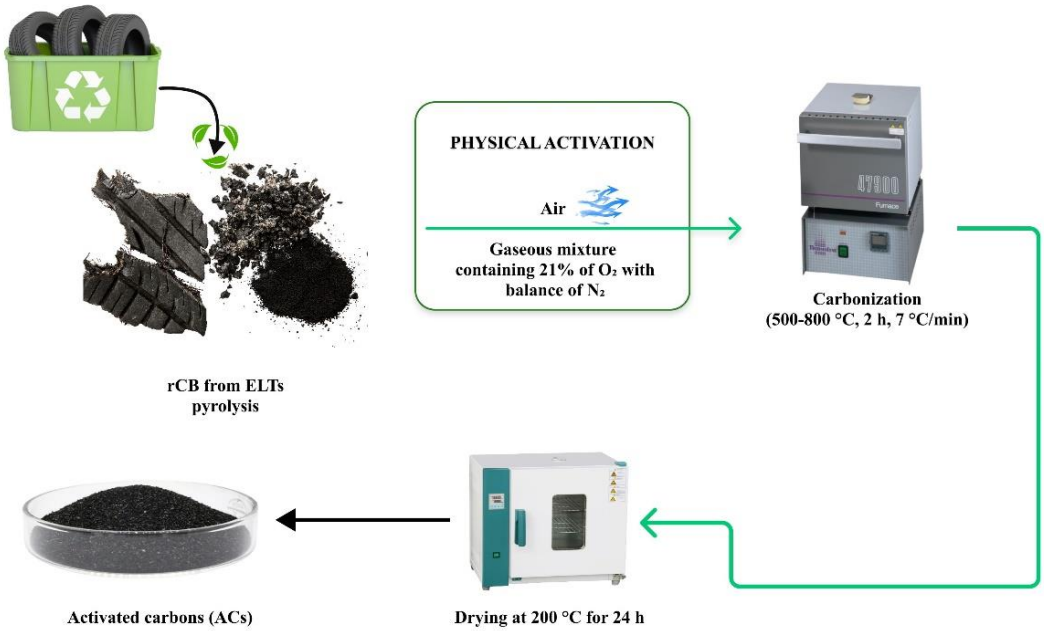

Figure 26. Illustrative diagram of the physical activation process applied for rCB/ACs production.

3.3.1.2 Chemical activation

The rCB was chemically activated using KOH (as described in **Paper I**) and various potassium-based agents, including KOH, K_2CO_3, KCl, CH_3COOK, and $K_2C_2O_4 \cdot H_2O$. Subsequent comparative analysis with NaOH (as mentioned in **Paper II**) through a dry mixing technique was performed. **In Paper I**, the 1:1 mass ratio (rCB:activator) was used as a reference point. The specific description for labeling samples is shown in **Paper I** and **Paper II**.

Within the activation procedure rCB and the potassium activators were evenly blended in a mortar until a uniform solid mixture was achieved. This mixture was placed in alumina crucible and placed in a horizontal tubular furnace with nitrogen atmosphere and a steady gas flow. The activation process was conducted according to the methodologies outlined in Paper I and Paper II, which are summarized in **Table 3**.

Table 3. Experimental conditions for chemical activation processes.

Paper	Heating rate [°C/min]	Temperature [°C]	Activation time [h]	Flow rate of N_2 [cm^3/min]	Cooling rate [°C/min]	rCB:activator ratio
I	7	800-900	2	150	5	1:1
II	5-13	700-900	1-4	200	5	1:3-1:6

The resulting chemically rCB/ACs were repeatedly rinsed with deionized water until the wash water reached a stable pH level of 7. The final step involved drying the produced rCB/ACs in an oven at 200 °C for 24 hours.

Furthermore, the interactions between rCB and activators in different states were examined in Paper II, focusing on solid-solid and gas-solid reactions. Two configurations of designed experiments for studying reactions involving rCB-activators are presented in **Figure 27**. Configuration (a) demonstrates a solid-solid state reaction where the rCB is mixed homogeneously with the activator within a crucible. In contrast, configuration (b) is employed to investigate a gas-solid state reaction. Here, the reactants for the gas-solid reactions were positioned in distinct crucibles, allowing only the gaseous phase of the activator, heated in the furnace, to come into contact with the rCB.

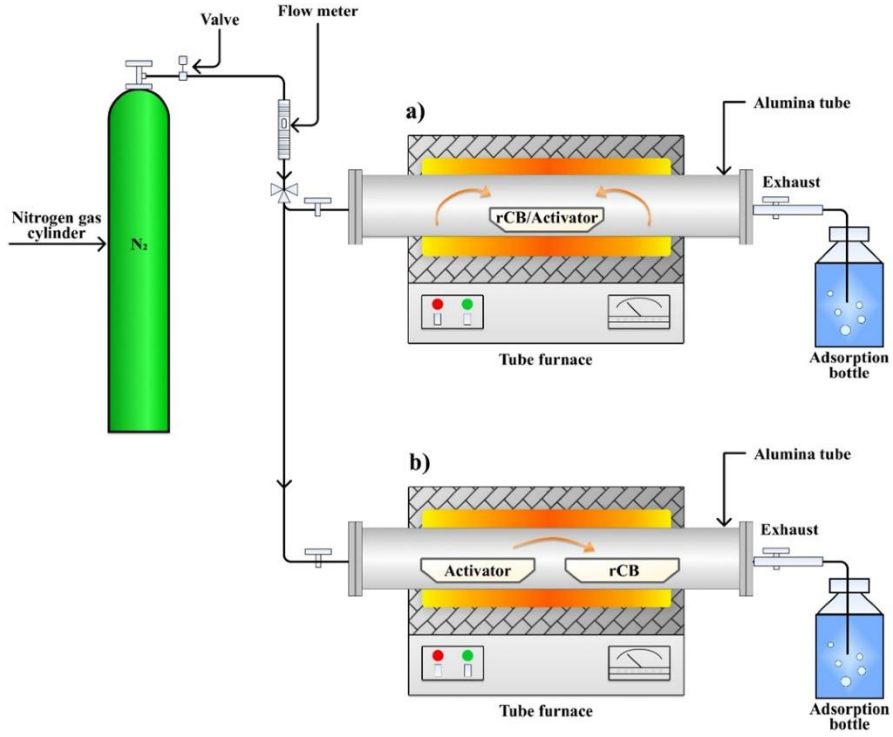

Figure 27. Diagram illustrating the setup of the experimental procedure used for (a) solid-state activation and (b) gas-state activation.

3.3.2 CO_2 adsorption studies

The CO_2 capture performance of rCB/ACs was investigated in **Paper I**. The CO_2 adsorption isotherms were obtained using a Micromeritics ASAP 2020 Plus Sorption Analyzer. The device was calibrated to maintain temperatures of 0, 15, 25, and 30 °C,. The absolute pressure varied from $5 \cdot 10^{-4}$ to 1 bar. Prior to the measurements, the samples underwent a degassing process at 110 °C in a vacuum (10-8 bar) for an hour. Additionally, the ideal adsorption solution theory (IAST) was utilized to calculate the selectivity for CO_2/N_2 adsorption of the ACs, which is considered a critical parameter for CO_2 capture with reference to N_2 sorption data at 25 °C. The selectivity was analyzed for an equimolar CO_2/N_2 mixture and post-combustion capture scenario (15% CO_2 and 85% N_2). Cyclic regeneration stability was

also evaluated for 1, 5, and 10 cycles to assess the durability and reusability of the adsorbents under repeated use conditions.

In **Paper I**, the investigation into the CO_2 adsorption mechanism involved aligning the experimental isotherm data with several isotherm models, conducting thermodynamic analysis, and examining the CO_2 capture dependency on the rCB/ACs textural properties.

The correlation of experimental isotherm data with the five isotherm models, including Toth, Freundlich-Langmuir, Sips, Redlich-Peterson, and Radke-Prausnitz, was achieved using non-linear regression through the quasi-Newton method implemented in Matlab's fmincon function. **Table 4** presents the non-linear versions of these isotherm equations, with their theoretical foundations and parameter descriptions. The assumptions of each model are discussed in **Paper I**.

Table 4. Description of selected adsorption isotherm models.

Isotherm model	Non-linear model equations	Characterization of equations	Ref.
Freundlich-Langmuir	$q_e = \frac{q_m \cdot K_{FL} \cdot P^{n_{FL}}}{1 + K_{FL} \cdot P^{n_{FL}}}$	q_m - maximum adsorption capacity (cm^3/g) K_{FL} - Langmuir-Freundlich constant (bar^{-nFL}) n_{FL} - index of heterogeneity [-]	[172]
Redlich-Peterson	$q_e = \frac{K_{RP} \cdot P}{1 + a_{RP} \cdot P^{\beta_{RP}}}$	K_{RP} - Redlich-Peterson constant ($cm^3 \cdot g^{-1} \cdot bar^{-1}$) a_{RP} - constant ($bar^{-\beta RP}$) β_{RP} - Redlich–Peterson exponent (-)	[173]
Toth	$q_e = \frac{q_m \cdot K_T \cdot P}{[1 + (K_T \cdot P)^{n_T}]^{\frac{1}{n_T}}}$	K_T - Toth constant (bar^{-1}) n_T – heterogeneity factor (-)	[174]
Sips	$q_e = \frac{q_m \cdot (K_S \cdot P)^{\frac{1}{n_S}}}{1 + (K_S \cdot P)^{\frac{1}{n_S}}}$	K_S - Sips constant (bar^{-1}) n_S – Sips exponent (-)	[175]
Radke-Prausnitz	$q_e = \frac{q_m \cdot K_{RPr} \cdot P}{(1 + K_{RPr} \cdot P)^{e_{RPr}}}$	K_{RPr} - Radke–Prausnitz constant (bar^{-1}) e_{RPr} - Radke–Prausnitz exponent (-)	[176]

The effectiveness of the selected theoretical models was evaluated based on the total of the absolute errors (EABS), as described below:

$$EABS = \sum_{i=1}^{n} \left| q_{e,\exp} - q_{e,mod} \right| \quad (9)$$

Where: $q_{e,mod}$ is the predicted amount of adsorbed adsorbate at equilibrium state [cm^3/g], $q_{e,exp}$ is the experimental amount of adsorbed adsorbate at equilibrium state [cm^3/g].

To investigate how adsorption correlates with textural characteristics, the dependency of CO_2 capture on all activated carbons at 0 °C was evaluated. This evaluation involved following the relationship between CO_2 adsorption and different textural properties, such as: the BET surface area, the total pore volume shown, the volume of micropores less than 2 nm in width, and the volume of micropores under 1 nm in width. The coefficient of determination (R^2) was employed as a critical statistical indicator to measure the predictive ability of these textural parameters on the variability of CO_2 adsorption. A high R^2 value indicated a strong correlation, suggesting that these textural parameters significantly influence or predict changes in CO_2 adsorption. Conversely, a low R^2 value proved a weak or negligible correlation, pointing to their limited influence on the variations observed in CO_2 adsorption.

The adsorption thermodynamic parameters were determined through the Van't Hoff and Clausius-Clapeyron equations (**Equation 10** and **Equation 12**), applied to the experimental CO_2 adsorption isotherm data at temperatures of 0, 15, 25, and 30 °C. Those methods are commonly utilized for estimating the Gibbs free energy (ΔG°), standard enthalpy change (ΔH°), standard entropy change (ΔS°), and isosteric heat of adsorption (Q_{st}).

$$ln(K_L) = \frac{\Delta S^\circ}{R} - \frac{\Delta H^\circ}{RT} \tag{10}$$

Where: R is the universal gas constant (8.314 J/mol·K), K_L is the Langmuir adsorption constant that has been utilized as the conventional thermodynamic equilibrium indicator for the computation of thermodynamic parameters (1/bar), and T is absolute temperature (K). Whereas ΔG° was estimated from the below equation by using Langmuir constant:

$$\Delta G^\circ = -RT\, ln(K_L) \tag{11}$$

$$\mathrm{Q_{st}} = -\mathrm{R}\left(\frac{\partial(\ln(\mathrm{P}))}{\partial\left(\frac{1}{\mathrm{T}}\right)}\right)_{\theta} \tag{12}$$

Where: P is the partial pressure of the CO_2 at equilibrium state [bar], Q_{st} denotes isosteric heat of adsorption (J/mol), and θ indicates a specific surface coverage (-).

4. Results and discussion

4.1 Characterization of rCB/AC materials

The rCB/ACs were thoroughly characterized in **Paper I**, using a set of analytical techniques, including FT-IR, SEM-EDS, Raman spectroscopy, TGA, and N_2/CO_2 adsorption isotherms. This characterization was done to understand the morphological, chemical, and particularly structural properties, setting the base for further optimization and evaluation of the activation mechanism by potassium-containing activators in **Paper II**.

4.1.1 Chemical characterization

FT-IR analysis showed a diverse surface chemistry across a spectrum of 450 to 4000 cm^{-1}. Key absorption peaks were found at 3550-3350 cm^{-1} (O-H), 3000-2850 cm^{-1} (C-H), 1700-1600 cm^{-1} (C=C), 1400-1350 cm^{-1} (C-H), and 1100-1000 cm^{-1} (C-O), indicating similar functional groups among the rCB/ACs (**Figure 28**). Specifically, the broad band at 3450 cm^{-1} highlights O-H stretching vibrations, indicative of hydroxyl groups affected by chemical and physical activation and important for intermolecular hydrogen bonding. The presence of strong bands at 3000-2850 and 1380 cm^{-1}, and at 1650 cm^{-1}, corresponds to C-H bending vibrations in alkanes and C=C stretching vibrations in aromatic rings, respectively. Additionally, C-O stretching vibrations were noted between 1100 and 1000 cm^{-1}. The uniform absorption bands suggest a similarity in functional groups across samples.

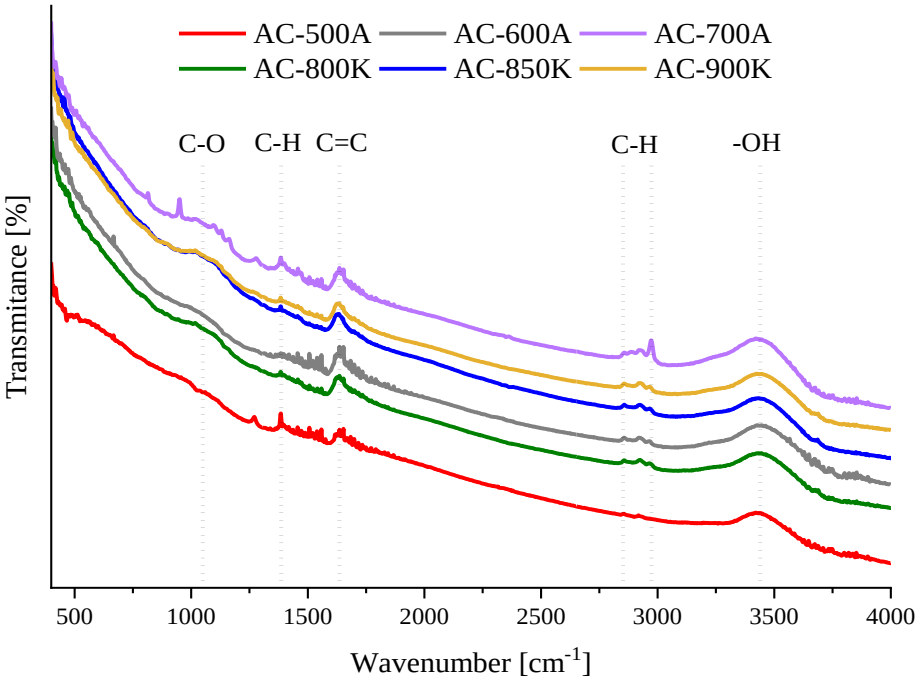

Figure 28. FT-IR spectra of rCB/AC materials.

The ultimate analysis (CHNS/O) was essential in assessing the suitability of rCB/ACs for adsorption uses, with particular emphasis on achieving high carbon content and minimizing non-carbon elements to ensure purity. Results revealed that rCB possessed a high carbon content of 92.53 wt.% and minimal other elements (7.47 wt.%), indicative of its very pure carbon form (**Table 5**). Further analysis showed that rCB/ACs produced with KOH had much higher carbon content (83.76-85.64%) and typically lower oxygen content than those activated with air, suggesting the addition of oxygen-containing groups to the carbon surface. A positive correlation between oxygen content and activation temperature was noted, with AC-900K showing the highest oxygen level at 14.93 wt.%. In contrast, the physically rCB/ACs displayed more diverse elemental variations, with AC-700A showing the most considerable deviation, likely due to oxidation during activation.

Table 5. Ultimate analysis of rCB/ACs.

Sample	Yield content [wt.%]	C [wt.%]	H [wt.%]	N [wt.%]	S [wt.%]	O* [wt.%]
rCB	-	92.53	1.16	0.42	0.71	5.18
AC-800K	91.6	85.64	0.31	0.34	0.31	13.40
AC-850K	86.3	84.62	0.27	0.72	0.28	14.11
AC-900K	77.9	83.76	0.18	0.90	0.23	14.93
AC-500A	55.8	83.46	0.53	0.43	0.80	14.78
AC-600A	42.4	83.54	0.40	0.40	0.74	14.92
AC-700A	35.9	83.81	0.30	0.34	0.53	15.02

* value obtained by calculation.

Furthermore, the yield varied significantly between chemically and physically activated rCB, ranging between 77.9-88.6% and 35.9-55.8%, respectively. This variance highlights the considerable effect of air exposure during the production process on carbon loss. The proximate analysis of the rCB/AC samples demonstrated a composition range of volatile matter (0.90-2.12 wt.%), fixed carbon (86.50-89.90 wt.%), and ash (9.45-12.60 wt.%). These findings highlight the high fixed carbon content in the rCB/AC samples.

The TGA of rCB/ACs up to 950 °C showed weight loss in three distinct phases, indicating different thermal degradation stages, as shown in **Figure 29**. The early stage loss (up to 200 °C) was due to moisture and volatile compound removal (Section A). A significant weight decrease between 200-700 °C indicated the removal of mineral and inorganic residues (Section B). The gradual decline in the later stage, at temperatures of 700-900 °C, signifies the combustion of rCB/AC samples, highlighting their high purity and thermal stability at elevated temperatures (Section C). Lastly, a minor ash residue of post-combustion suggested the presence of inorganic compounds.

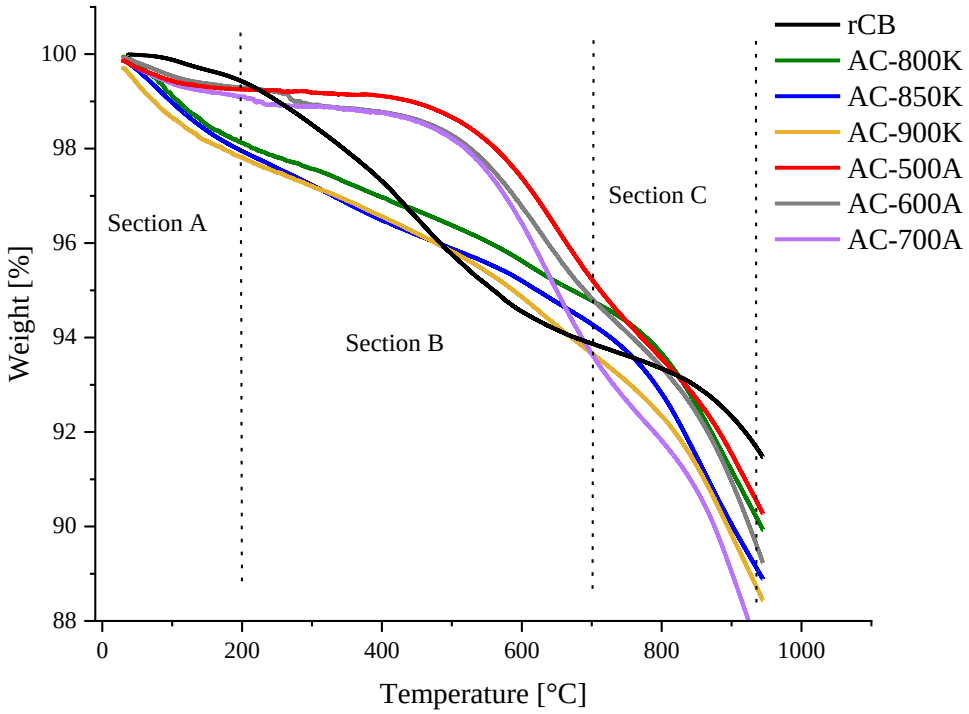

Figure 29. TGA curves of rCB/AC samples: Section A (moisture and volatile compound loss), B (inorganic decomposition), and C (combustion process).

4.1.2 Textural properties

The desired characteristics for rCB/ACs material include a specific size distribution that primarily encompasses micropores along with mesopores, high pore volume, and elongated micropore structures to optimize performance in CO_2 adsorption applications. Considering these objectives, the N_2 isotherms curves rCB/ACs (**Figure 30**) indicated a combination of type I and IV isotherms. At low relative pressures ($P/P_0<0.1$), there was a rapid increase in adsorption, transitioning to a gradual rise as pressure increased, which indicated the presence of respectively microporous (<2 nm) and mesoporous (2 to 50 nm) structures. A distinctive hysteresis loop, characteristic of type IV isotherms, suggested the presence of mesopores filled by capillary condensation. The observed H3-type hysteresis across a wide range of relative pressures ($P/P_0>0.35$) implied a dual porosity system comprising micro- and mesopores, including aggregates forming slit-shaped pores.

Among the studied samples, those activated chemically with KOH at 900 °C displayed superior textural properties compared to the pristine rCB, including the highest values for surface area (328 m^2/g), total pore volume (0.448 cm^3/g), and microporosity (0.1 cm^3/g). This enhancement was more pronounced at activation temperatures between 800 °C to 900 °C. The observed enhancement can be tributed to the increased reactivity of carbon atoms and the diffusion rate of potassium salts.

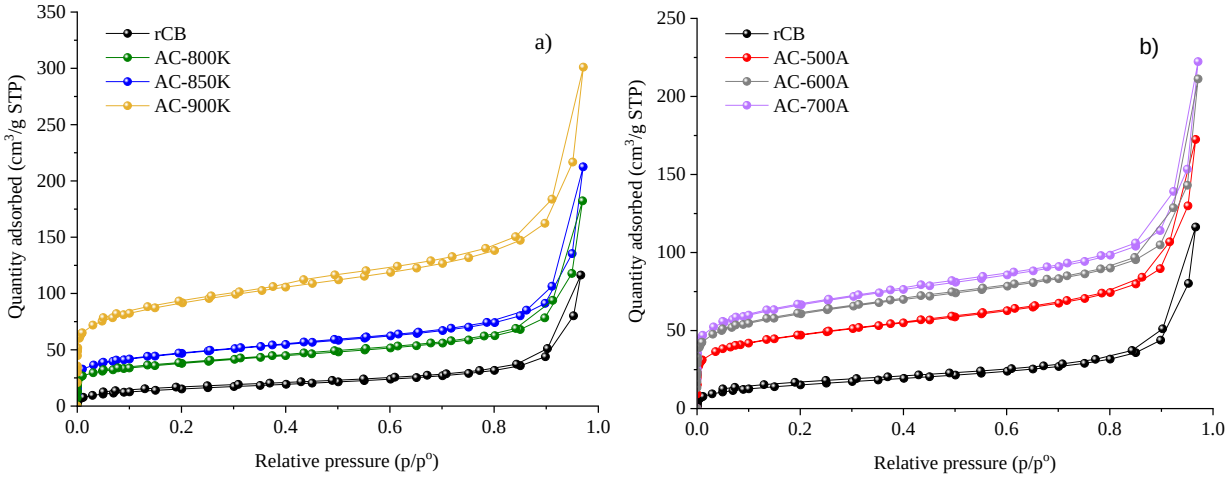

Figure 30. N_2 adsorption-desorption isotherm curves at -196 ℃ of the prepared activated carbons samples by (a) chemical activation, (b) physical activation.

Furthermore, the pore size distribution analysis of the rCB/ACs using N_2 adsorption and evaluation by the DFT method highlighted a broad range of micropores (below 2 nm), primarily between 1.05–1.19 nm and 1.25–1.54 nm, and mesopores (2–50 nm) in the 2.30–3.90 nm, 9.48–10.36 nm, and 12.36–13.50 nm ranges. Additionally, CO_2 adsorption at 0 °C detected the development of supermicropores (0.7-2 nm) and ultramicropores (<0.7 nm), especially in AC-

900K and AC-700A. Formation of smaller submicropores (<0.4 nm) was limited. Regarding CO_2 adsorption applications, this dual porosity of rCB/ACs ensure effective sorption process, with each pore type playing a specific role. In CO_2 adsorption, mesopores aid initial transport to deeper adsorption sites, facilitating access and diffusion. Micropores, especially those sized 0.4 nm to 1 nm, maximize adsorption capacity through optimal surface interactions with CO_2 molecules, enhanced by strong van der Waals forces.

4.1.3 Morphological characterization

SEM-EDS analysis revealed the morphology and elemental composition of rCB/ACs, particularly AC-700A and AC-900K. The rCB/ACs was characterized with high degree of porosity and complex, irregular structures. These properties surpass the simpler structure of rCB, which typically represents an expanding chain or a prolate spheroid-bunch shape. **Figure 31** presents SEM micrographs that illustrate the varied size, shape, and surface features of rCB/ACs, which can be connected to the high activation temperatures. The elevated temperatures likely increase diffusion rates, facilitating the creation of a more extensive network of pores by promoting increased mobility of atoms and accelerating reactions involved in the activation process, such as carbon gasification.

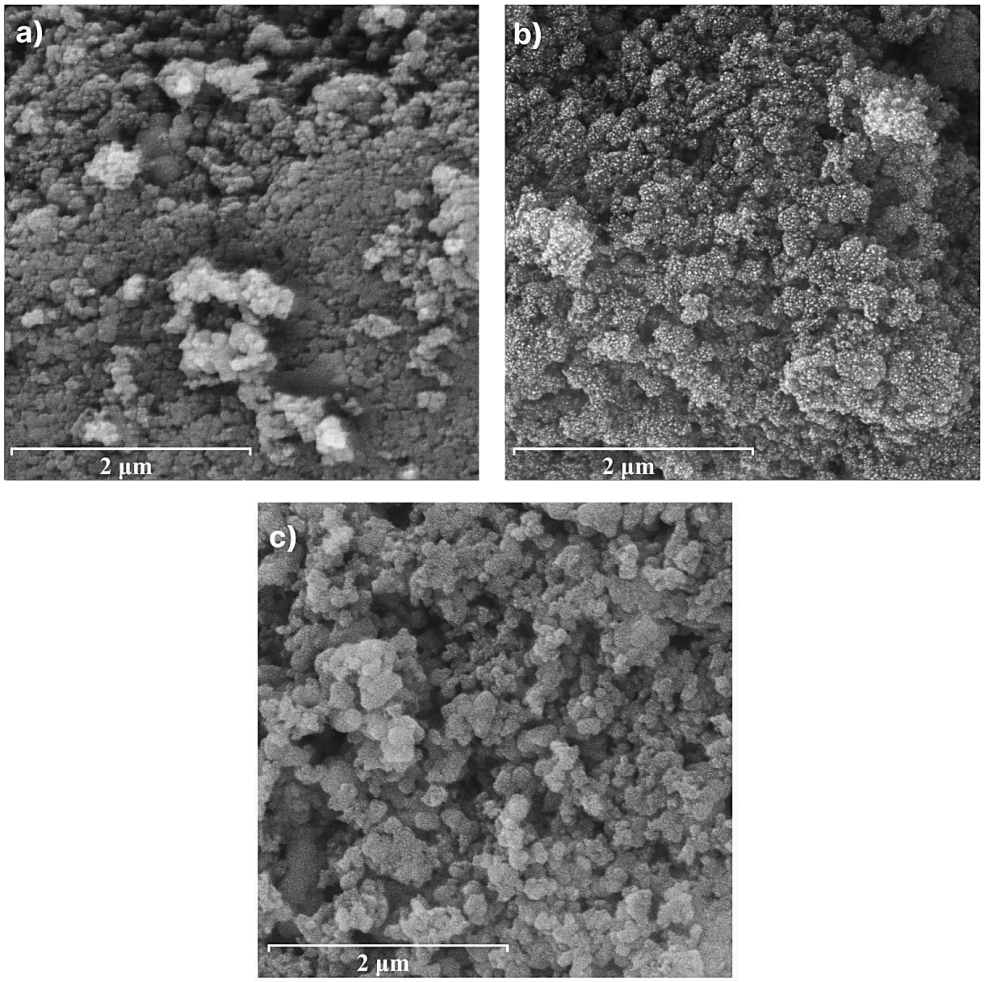

Figure 31. SEM micrographs at a magnification of 2 µm for (a) AC-700A, (b) AC-900K, and (c) recovered carbon black.

Furthermore, particle aggregates and agglomerates in cluster forms are detected, heterogeneously distributed within the rCB/ACs. The formation of these clusters contributes to the overall porosity and surface complexity after the activation process, as depicted in **Figure 32.**

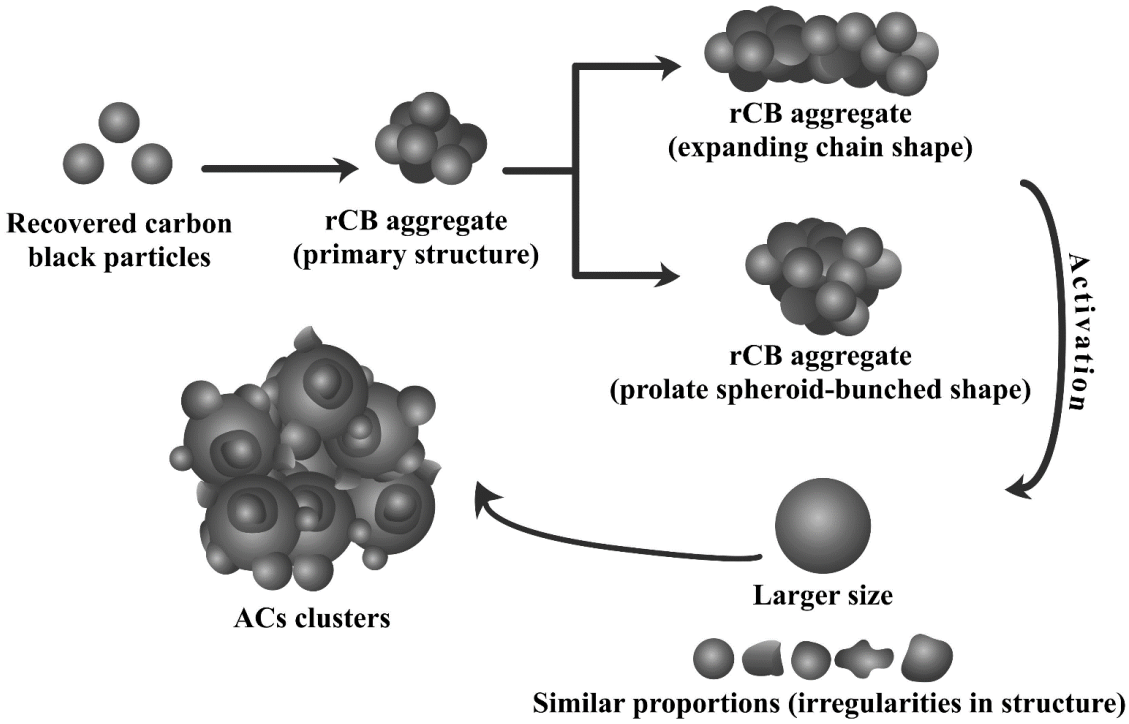

Figure 32. Morphological changes of particles during rCB activation process.

The EDS analysis showed that the AC-900K sample primarily contained carbon, oxygen, and potassium. The presence of potassium compounds suggests that they remained in the ACs after washing, most probably due to the intercalation in the structure. On the other hand, the AC-700A mainly comprised carbon and oxygen, with minor amounts of silicon, aluminum, magnesium, and sulfur. This indicates the pristine rCB might have contained additives, as discussed earlier in this thesis.

The analysis of Raman spectra for rCB/ACs samples showed two primary bands: the D-band around 1330 cm^{-1}, associated with structural defects in carbon materials, and the G-band at 1590 cm^{-1}, indicative of graphitic structures (**Figure 33**). The D-band resulted from the vibrations of sp^3 carbon atoms, proving the presence of structural irregularities, while the G-band reflected the symmetric stretching of sp^2 carbon atoms in a graphite layer. The ratio of the intensity of the D-band (I_D) to the G-band (I_G) served as an indicator of the defect level in the material, with the rCB/ACs showing I_D/I_G ratios between 1.03 and 1.22, which suggest structural irregularities. Generally, defects introduce structural irregularities, increasing the surface area available for adsorption. This provides more active sites for adsorbate molecules to interact with, potentially leading to higher adsorption capacities.

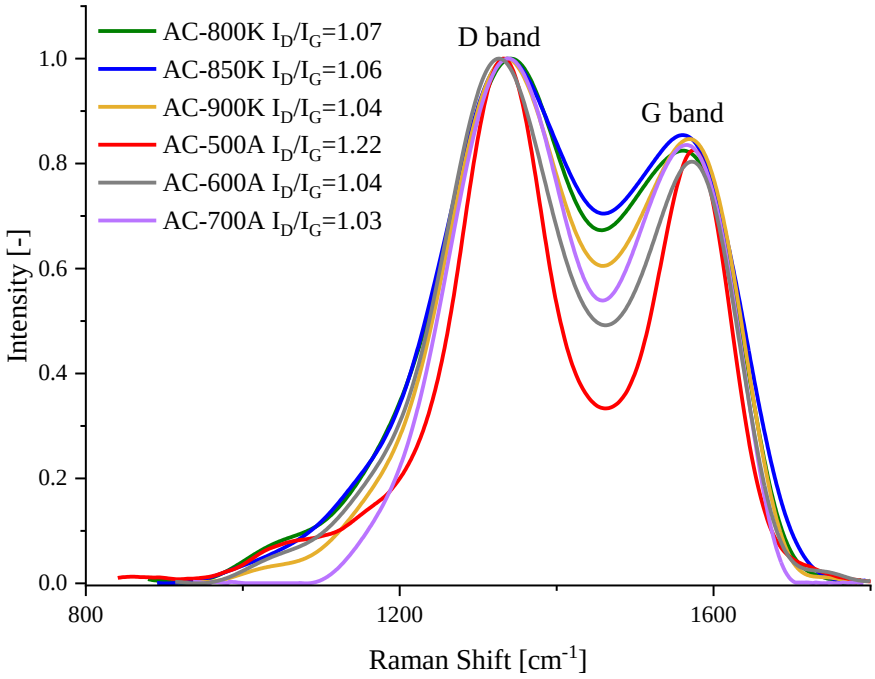

Figure 33. Raman spectra of rCB/AC illustrating D- and G-band for structural characterization.

4.2 Enhancement of rCB/ACs textural properties by potassium-based activators

In **Paper II**, the role of various potassium-based activators was investigated, focusing on their effectiveness in altering the structural characteristics of rCB/ACs. Influence of KOH activation was studied through the change of several experimental parameters such as: the mass ratio of rCB:KOH, activation temperatures, activation duration, and heating rates. Additionally, in **Paper II** comparison between the physical states of KOH (solid/liquid-solid, gas-solid) and their impact in relation to sodium hydroxide (NaOH) was investigated. The goal was to compare the effect of K^+ and Na^+ on the activation process. Furthermore, the effects of various potassium salts, used as activators including KCl, K_2CO_3, CH_3COOK, and $K_2C_2O_4$, were evaluated in comparison to KOH. KOH was chosen as a reference salt as it is considered as the most effective activating agent when it comes to the development of porosity and surface modifications in the resultant rCB/AC.

4.2.1 Exploration of KOH activation impact on structural characteristics of rCB/ACs

In the analysis of N_2 adsorption-desorption isotherms, it was observed that the shape of the curves remained consistent with those reported in **Paper I**. The variation in the activation conditions resulted in different adsorbed quantities of N_2, but the resultant N_2 isotherm curves did not deviate in shape from the baseline,. This consistency in shape of the isotherms suggests a robustness in the rCB/ACs adsorptive properties, irrespective of the alterations in activation parameters. Moreover, the results presented in **Table 6** indicate that within certain ranges of temperature, mass ratio, activation time, and heating rate, using KOH significantly improves the porosity and BET surface area of rCB/ACs, exceeding the outcomes reported in **Paper I**.

Table 6. Textural properties associated to produced rCB/ACs by specific activation parameters.

Sample	BET surface area[a], [m^2/g]	Total pore volume[b], [cm^3/g]	Micropore volume[c], [cm^3/g]	Mesopore volume volume[c], [cm^3/g]	Micropore volume/total pore volume, [%]
rCB	55±0.8	0.170	-	-	-
Effect of temperature					
KOH_1:4_900_3_5	915±2.3	0.854	0.288	0.566	39
KOH_1:4_800_3_5*	945±5.6	0.743	0.303	0.440	36
KOH_1:4_700_3_5	688±1.8	0.605	0.225	0.380	37
Effect of mass ratio between rCB/ACs					
KOH_1:6_800_3_5	1022±3.8	0.837	0.312	0.525	39
KOH_1:5_800_3_5	1025±2.2	0.901	0.327	0.574	35
KOH_1:3_800_3_5	801±1.8	0.651	0.252	0.399	39
Effect of activation time					
KOH_1:4_800_4_5	1028±1.5	0.874	0.332	0.542	38
KOH_1:4_800_2_5	876±3.08	0.727	0.276	0.467	37
KOH_1:4_800_1_5	788±1.3	0.699	0.211	0.488	30
Effect of heating rate					
KOH_1:4_800_3_7	970±1.9	0.884	0.314	0.460	41
KOH_1:4_800_3_10	934±2.0	0.774	0.298	0.452	40
KOH_1:4_800_3_13	900±1.8	0.750	0.289	0.595	32

[a]Brunauer, Emmett & Teller method using the Rouquerol criteria.

[b]V_{TOT} calculated by N_2 adsorption isotherm at a high relative pressure (~0.99).

[c]DFT method by NLDFT model.

*The study's base activation conditions were set at 1:4 ratio, 800 °C, 3 hours, and 5 °C/min.

Under the optimal conditions identified in **Table 8**, a combination of factors was found to significantly impact the activation process. Among these factors, the temperature effect was most evident for the temperature interval between 700 and 800 °C. Temperature in this interval led to increasing the KOH activation and diffusion rates in carbon, which enhances the microporosity of the material (0.225-0.303 cm^3/g) and increase in the BET surface area (688-945 m^2/g). At this range, K^+ ions can better penetrate the carbon surface, increasing micropore volume. The optimal rCB/KOH ratio was found to be 1:5, whereas a ratio of 1:6 was found to have negative effects, likely due to excessive KOH, resulting in the blockage of pores through the deposition of potassium compounds within them. Moreover, an activation time of 4 hours was most beneficial, leading to an improved pore size distribution. Finally, a heating rate of 7 °C/min promoted the optimal heat distribution and kinetics. **Figure 34 (a-d)** presents the pore size distribution in rCB/ACs, indicating the highest enhancement in micropore content under the optimal conditions: 800 °C, a 1:5 rCB:KOH ratio, 7 °C/min heating, and 4 hours duration. Pore sizes were mainly found in three peaks: 0.99-1.09 nm, 1.09-1.30 nm, and 1.43-1.63 nm, consistent across all rCB/ACs samples examined, the same as in **Paper I**.

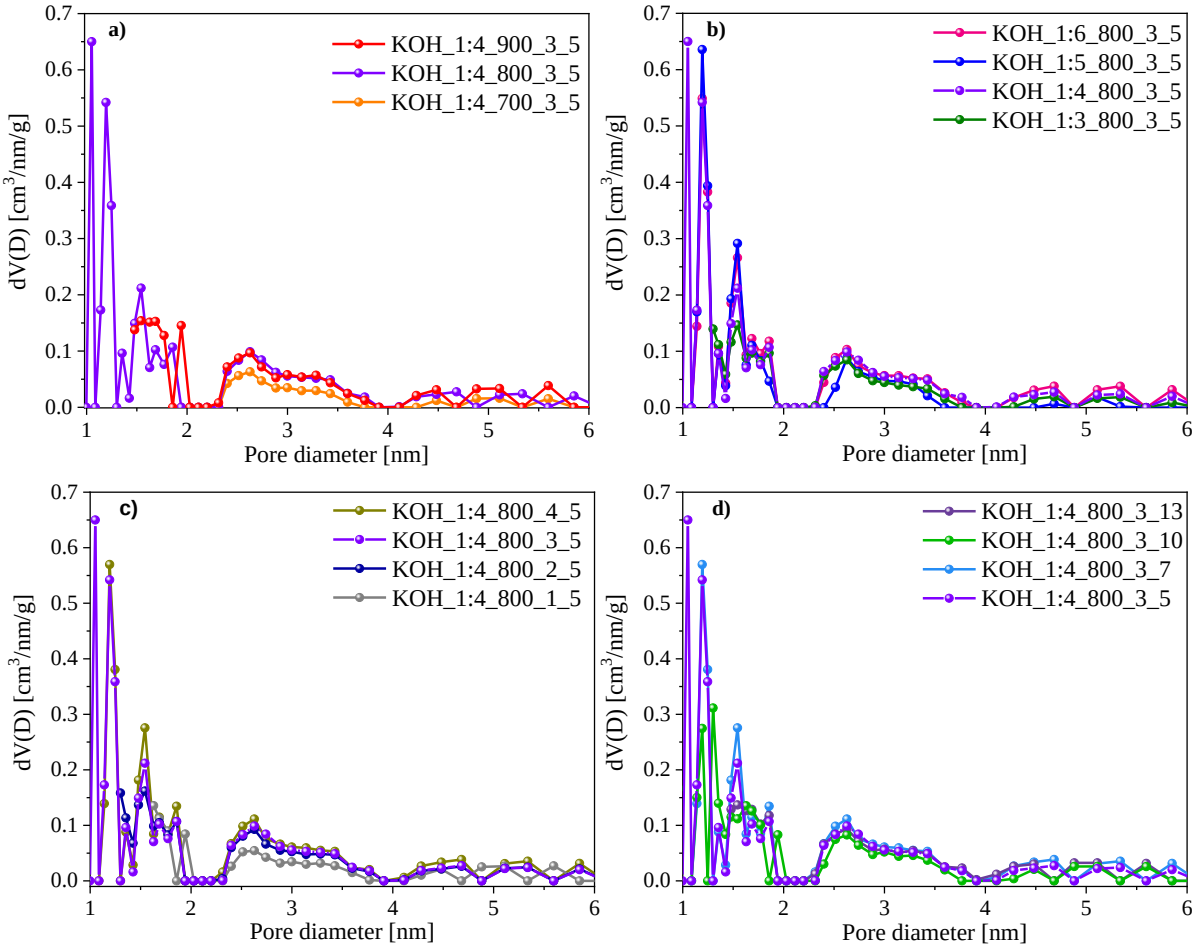

Figure 34. Pore size distribution of the rCB/ACs based on DFT method of N_2 adsorption at 77K on carbon slit pores by NLDFT model in relation to the activation effect of (a) temperature, (b) mass ratio, (c) time, (d) heating rate.

KOH activation pathways were evaluated through, the specific phases formed as a resulted of the addition of KOH. **Figure 5 (a-d)** shows the XRD patterns of rCB/ACs before washing. XRD analysis identified key components like K_2CO_3, $K_2CO_3 \cdot 1.5H_2O$, $K_4(CO_3)_2 \cdot (H_2O)_3$, $KHCO_3$, and K_2O. The results suggest that the chemical evolution in KOH-treated rCB/ACs mainly involves transformation into K_2CO_3 and its hydrated forms, as depicted in **Figure 32**. Theoretically, the process could begin with KOH reacting with carbon at 400 °C, producing K_2CO_3 and K while releasing H_2. This could be followed by pore formation through carbon gasification (below 700 °C), thereby facilitating the formation of K_2CO_3 as well. The hydration of K_2CO_3 into $K_2CO_3 \cdot 1.5H_2O$ likely occurred post-heating, driven by its hygroscopic nature and the absorption of moisture from the surrounding air. Similarly, the synthesis of $K_4(CO_3)_2 \cdot (H_2O)_3$ likely entails a series of reactions among KOH, CO_2, and water vapor, where pivotal factors such as temperature, KOH concentration, and humidity influence the process. After post-thermal treatment at 800-900 °C, K_2O formation was observed, suggesting the decomposition of K_2CO_3 into K_2O and CO_2 at high temperatures, as well as the potential subsequent reaction of K_2O with atmospheric CO_2 to reform K_2CO_3. On the other hand, the presence of $KHCO_3$ was noted, potentially influenced by CO_2 and moisture.

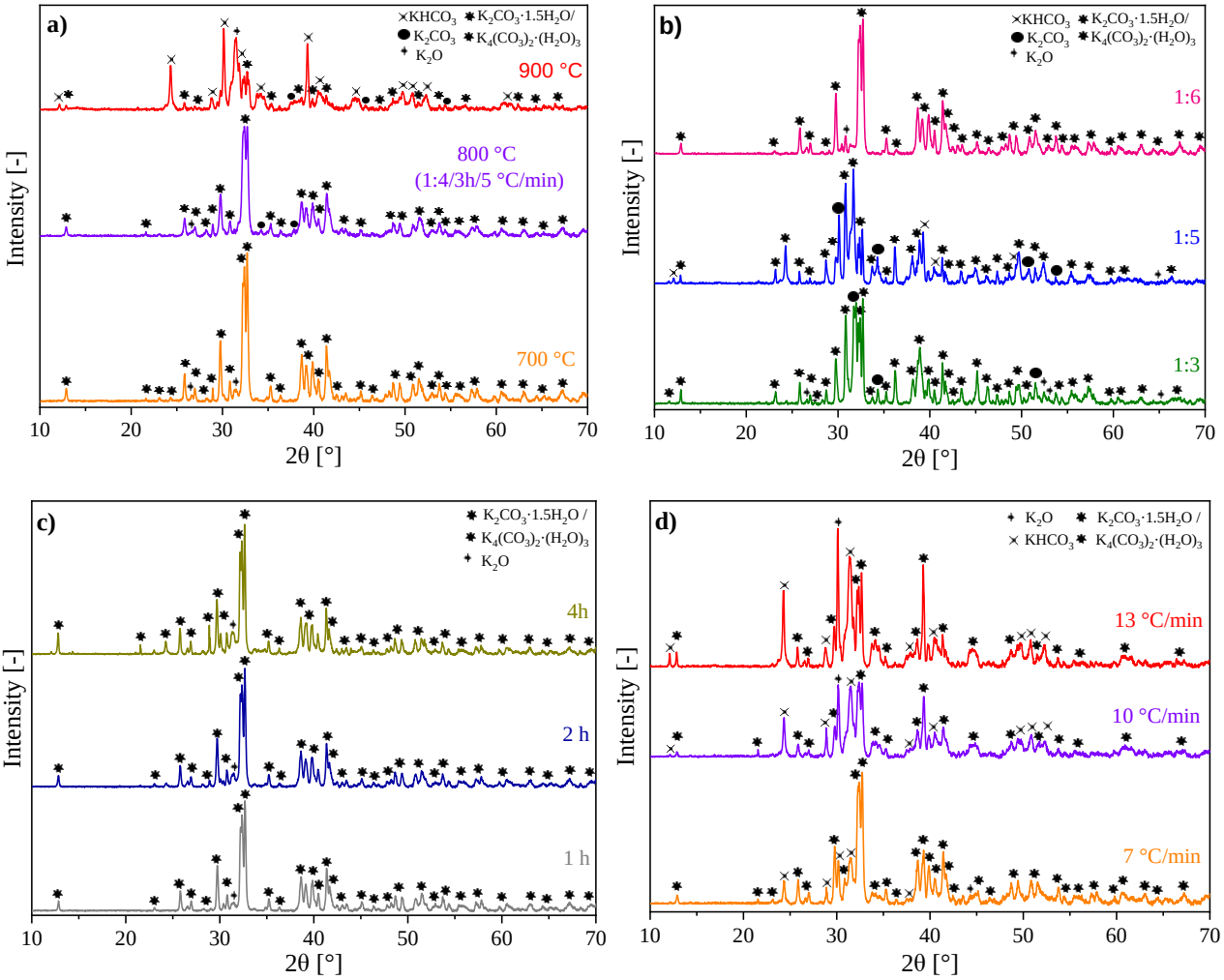

Figure 32. XRD patterns for rCB/ACs before washing treatment and after KOH activation with changed (a) temperature (b) mass ratio, (c) activation time, and (e) heating rate.

The influence of solid-gas reactions during the KOH activation of rCB was further indicated by an increase in total pore volume (from 0.170 to 0.239 cm^3), BET surface area (from 55 to 118 m^2/g), and micropore volume (to 0.033 cm^3/g). The XRD and semi-quantitative analysis of post-reaction rCB/ACs samples revealed the formation of $KHCO_3$ (60 wt.%), K_2O (10 wt.%), and K_2CO_3 (30 wt.%), providing insight into the chemical changes occurring during the reaction process.

Comparison between KOH and NaOH (**Table 7**) indicates that KOH activation of rCB led to a higher BET surface area and pore volumes. The results suggested that the choice between KOH and NaOH depends on the carbon structure of rCB/ACs, which was examined in **Paper I** based on Raman spectroscopy. KOH is favored for more crystalline, graphite-like structures due to its higher ability to integrate with the carbon network. KOH-activated rCB also demonstrated a greater prevalence of potassium (K: 29.5 wt.%) in contrast to sodium (Na: 19.8 wt.%) observed in NaOH-activated rCB, as confirmed by EDS mapping and semi-quantitative analysis. This discrepancy is likely attributed to the distinct properties of potassium and sodium ions. K ions, with their larger ionic radius (152 pm) and higher reactivity compared to Na ions (116 pm), may be more adept at integrating into the carbon structure of rCB.

Table 7. Textural properties associated to rCB/ACs obtained by NaOH activation.

Sample	BET surface area, [m^2/g]	Total pore volume, [cm^3/g]	Micropore volume, [cm^3/g]	Mesopore volume volume, [cm^3/g]	Micropore volume/total pore volume, [%]
KOH_1:4_800_3_5	945±5.6	0.743	0.303	0.440	36
NaOH_1:4_800_3_5	480±0.9	0.523	0.146	0.377	28

4.2.2 The influence of potassium-containing activators on porosity development

Table 8 presents the evolution of textural characteristics in rCB/ACs processed with various potassium salts. The progression of textural properties (BET surface area, total pore volume, micropore volume, and mesopore volume) is arranged in descending order: KOH > $K_2C_2O_4$ > CH_3COOK > K_2CO_3 > KCl. The ranges for BET surface area varied from 57 to 945 m^2/g, total pore volume from 0.189 to 0.743 cm^3/g, micropore volume from 0.011 to 0.303 cm^3/g, and mesopore volume from 0.178 to 0.440 cm^3/g, offering insights into the variation of textural characteristics among different potassium activators.

Table 8. Textural properties associated to rCB/ACs produced via chemical activation with CH_3COOK, $K_2C_2O_4$, K_2CO_3, and KCl.

Sample	BET surface area, [m^2/g]	Total pore volume, [cm^3/g]	Micropore volume, [cm^3/g]	Mesopore volume volume, [cm^3/g]	Micropore volume/total pore volume, [%]
KOH_1:4_800_3_5	945±5.6	0.743	0.303	0.440	36.0
CH_3COOK_1:4_800_3_5	217±2.0	0.240	0.071	0.136	34.3
K_2CO_3_1:4_800_3_5	146±0.3	0.207	0.043	0.197	17.9
$K_2C_2O_4$ _1:4_800_3_5	299±1.1	0.369	0.093	0.276	25.2
KCl_1:4_800_3_5	57±0.08	0.189	0.011	0.178	5.8

The results in **Table 6** highlight the effect of both K^+ and OH^- in enhancing the textural properties of rCB/ACs. KOH's efficiency can be explained with the high mass concentration of K in KOH and its dissociation at high temperatures to K^+ and OH^- ions, typically above 400 °C. Hydroxyl ions possess the capability to chemically break down and weaken the bonds within the carbon substrate, liberating volatile substances. This process effectively transforms the rCB into more porous ACs [177]. The observations were supported through SEM-EDS mapping and EDS semi-quantitative analysis (**Table 9**), confirming both a uniform distribution of potassium from KOH and a consistent interaction of KOH with the surface layer. In contrast, compounds like CH_3COOK, K_2CO_3, and $K_2C_2O_4$ exhibited lower potassium content and partial inhomogeneity in K distribution on the surface, which is associated with less effective porosity enhancement. Further discussion on this topic can be found in **Paper II**. KCl was noted as ineffective due to its high melting point (~770 °C), and consequently low reactivity with rCB.

Table 9. EDS semi-quantitative analysis of rCB/AC samples.

Sample	K [wt.%]	C [wt.%]	O [wt.%]
KOH_1:4_800_3_5	29.5	31.7	38.8
$K_2C_2O_4$ _1:4_800_3_5	27.5	37.9	34.6
CH_3COOK_1:4_800_3_5	20.9	49.8	29.3
K_2CO_3_1:4_800_3_5	13.1	62.0	24.9
KCl_1:4_800_3_5	19.7	76.0	4.4

4.3 CO_2 adsorption performance of rCB/ACs

rCB/ACs were investigated in **Paper I** to follow their CO_2 adsorption capability. The CO2 adsorption capacity was evaluated in terms of mechanism for adsorption, selectivity for CO_2 in a CO_2/N_2 mixture, and stability through multiple adsorption-desorption cycles.

Optimal activation temperatures in **Paper I** were identified as 900°C for KOH-activated and 700°C for air-activated samples, respectively. Those two samples were chosen for further evaluation in this section. The AC-900K showed the highest CO_2 uptake (30.90 cm^3/g at 0 °C) (**Figure 33**), while the AC-700A had CO_2 adsorption capacities ranging from 14.79 to 22.56 cm^3/g across the temperature spectrum at 1 bar. It should be noted that these values are better than the values shown by other industrial by-products, but still lower than that of ACs obtained from biomass waste. Furthermore, considering the importance of real-world conditions, exploring the anticipated performance differences at higher temperatures becomes essential. Further optimization of the textural properties of rCB/ACs was therefore aimed in **Paper II**.

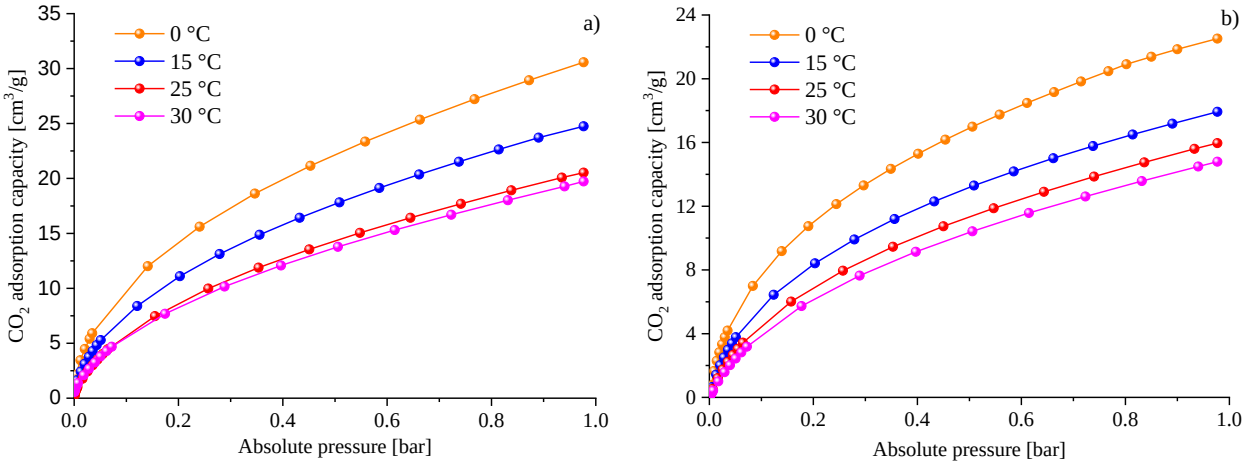

Figure 33. CO_2 adsorption isotherms at temperature of 0 °C, 15 °C, 25 °C, and 30 °C on (a) AC-900K and (b) AC-700A.

4.3.1 CO_2 adsorption mechanism

The exploration of the interplay between textural properties and CO_2 adsorption is essential for optimizing the design and performance of rCB/AC materials. It is crucial to interpret the dependence of the R^2 values, within the range of 0 to 1, on these texture

characteristics. A value closer to 1 indicates a stronger correlation. The investigation into the relationship between CO_2 adsorption and the textural properties of rCB/ACs revealed R^2 values above 0.9, indicating significant associations. This was particularly true for chemical activation methods associated with total pore volume and microporosity (determined by using CO_2 at 0°C), which had R^2 values of 0.946 and 0.940, respectively. For physical activation, the BET surface area and micropore volume (assessed by N_2 adsorption) demonstrated R^2 values of 0.995 and 0.999, indicating a pronounced impact on CO_2 capture. Moreover, the dependency of the R^2 values on cumulative micropore volumes within specific pore diameter ranges was exceptionally high for micropores between 0.4 and 0.9 nm, as given in **Figure 34**. This highlights the significant role of submicropores and ultramicropores in CO_2 capture by rCB/ACs.

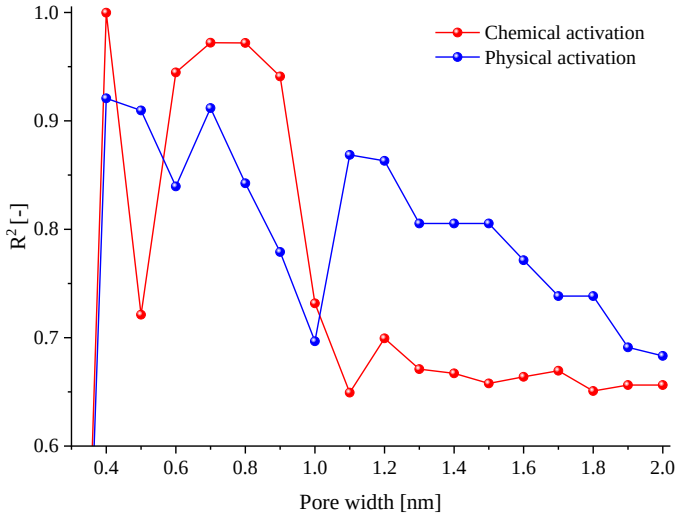

Figure 34. Relationship between the R^2 and cumulative pore volume within the range of 0.3-2 nm, at 0 °C under a pressure of 1 bar.

Based on the isotherm modeling study of CO_2 adsorption isotherms at 0, 5, 25, and 30 °C it was found that the Freundlich-Langmuir equation, which considers both monolayer and multilayer adsorption effects, reliably predicted CO_2 adsorption in AC-900K across all temperatures, with minimal errors (EABS) ranging from 1.3965 to 4.393 (**Figure 35**). This model effectively bridges the gap between purely monolayer-focused and multilayer-oriented adsorption phenomena. For AC-700A, the Redlich-Peterson model, incorporating features of both the Langmuir and Freundlich isotherms, best matched the experimental data, with errors between 0.419 and 0.613. Those two models confirmed the occurrence of multilayer sorption on the heterogeneous surface, indicating the presence of both monolayer and multilayer adsorption effects. Additionally, Toth and Sips equations failed to accurately represent CO_2 sorption rCB/ACs, due to higher error margins. This suggests that these equations may not adequately capture the complexity of the adsorption behavior observed in the studied materials. Further interpretation of models that can explain the on adsorption on the surface of rCB/ACs, can be found in **Paper II**.

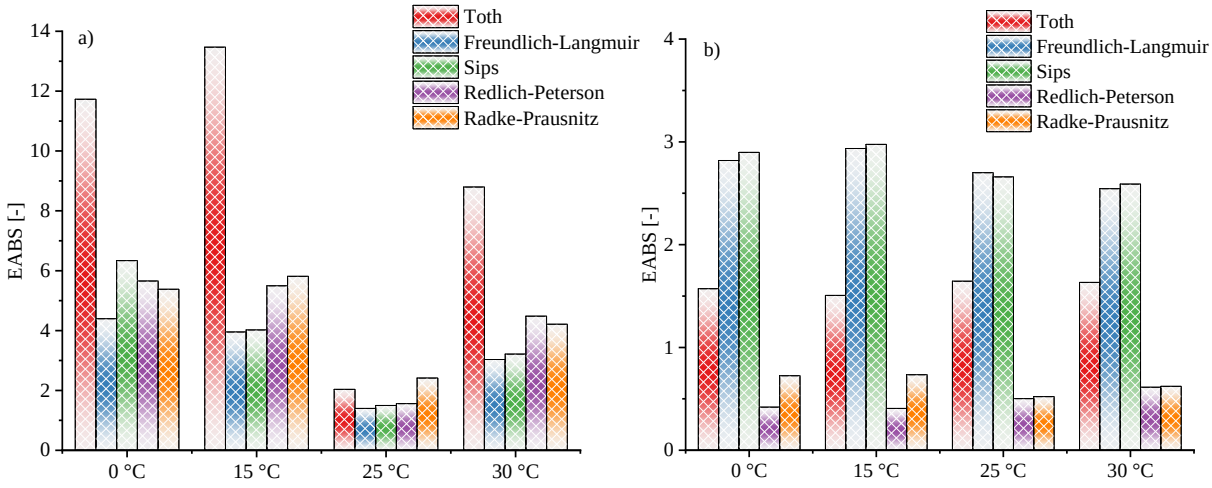

Figure 35. Summary of EABS values derived from fitting selected isotherm models to the data using non-linear regression for (a) AC-900K and (b) AC-700A.

Alongside analyzing isotherms, it is crucial to examine the thermodynamic aspects of the interaction between AC and CO_2. The objective of this study is to gain a comprehensive understanding of the thermodynamic mechanisms involved in the CO_2 adsorption on rCB/ACs under conditions of equilibrium. **Table 10** presents thermodynamic parameters obtained from **Equation 10** and **Equation 11,** with both standard free entropy and enthalpy displaying negative values. This suggests a decrease in disorder and an exothermic adsorption process on the rCB/AC surface. The process was spontaneous, as evidenced by negative ΔG° values, which also revealed that lower temperatures favor CO_2 molecule binding. Comparatively, adsorption was more energetically and entropically favorable for AC-900K than AC-700A.

Table 10. Thermodynamic parameters of CO_2 adsorption.

	AC-900K			**AC-700A**		
T $[°C]$	ΔG^0 $[kJ/mol]$	ΔS^0 $[kJ/mol \cdot K]$	ΔH^0 $[kJ/mol]$	ΔG^0 $[kJ/mol]$	ΔS^0 $[kJ/mol \cdot K]$	ΔH^0 $[kJ/mol]$
0	-2.027	-0.0240	-8.626	-2.534	-0.0365	-12.540
15	-1.772			-2.136		
25	-1.601			-1.736		
30	-1.209			-1.387		

The core aspect of thermodynamic investigation concerning surface phenomena revolves around the isosteric heat of adsorption. This specific parameter serves as a distinct measure of the bond intensity between the adsorbate and the surface of the adsorbent, describing the thermal energy generated during the CO_2 adsorption. Isosteric heat of adsorption for AC-700A and AC-900K ranged from 15.19-27.51 kJ/mol and 22.28-36.81 kJ/mol, respectively, confirming that CO_2 adsorption on rCB/ACs was physical, governed by weak van der Waals forces. Physical adsorption heats vary between 20-40 kJ/mol, in contrast to chemisorption,

which typically fell in the range of 80-200 kJ/mol, evidencing the physical nature of the process [178].

4.3.2 Insights into CO_2/N_2 selectivity and cyclic regeneration stability

When assessing adsorbents for CO_2 removal from flue gas in different industrial sectors, the importance of their ability to preferentially adsorb CO_2 over N_2 is crucial. The IAST was used to determine CO_2/N_2 selectivity of rCB/ACs, comparing data at 25 °C for an equimolar mixture and post-combustion conditions (15% CO_2, 85% N_2). For equimolar mixture, at a very low pressure (0.001 bar), the selectivity ratios were initially high, being 164.80 for AC-700A and 350.91 for AC-900K. However, as pressure increased, these ratios declined, dropping to much lower values of 19.77 for AC-700A and 27.39 for AC-900K at 1 bar, as presented in **Figure 36**. In mixtures with a post-combustion composition of 15% CO_2 and 85% N_2, the selectivity at 1 bar was observed to be 59.70 for AC-900K and 44.51 for AC-700A.

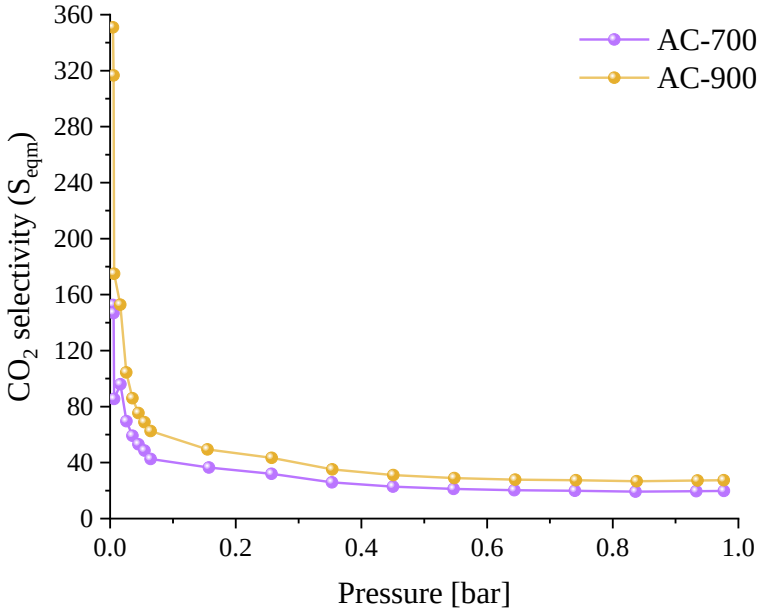

Figure 36. IAST selectivity for CO_2 over N_2 at 25 °C for a CO_2/N_2 binary mixture.

The regenerative ability of ACs also plays a vital role in their effectiveness and cost-efficiency in CO_2 capture, depending on their capacity to recover original adsorption levels after multiple adsorption-desorption cycles. The stability of AC-900K and AC-700A was assessed through the 1st, 5th, and 10th cycles at 0 °C, showing no performance drop in CO_2 uptake after ten cycles with a maximum standard deviation of 0.09, demonstrating their high stability as CO_2 capture material (**Figure 37**).

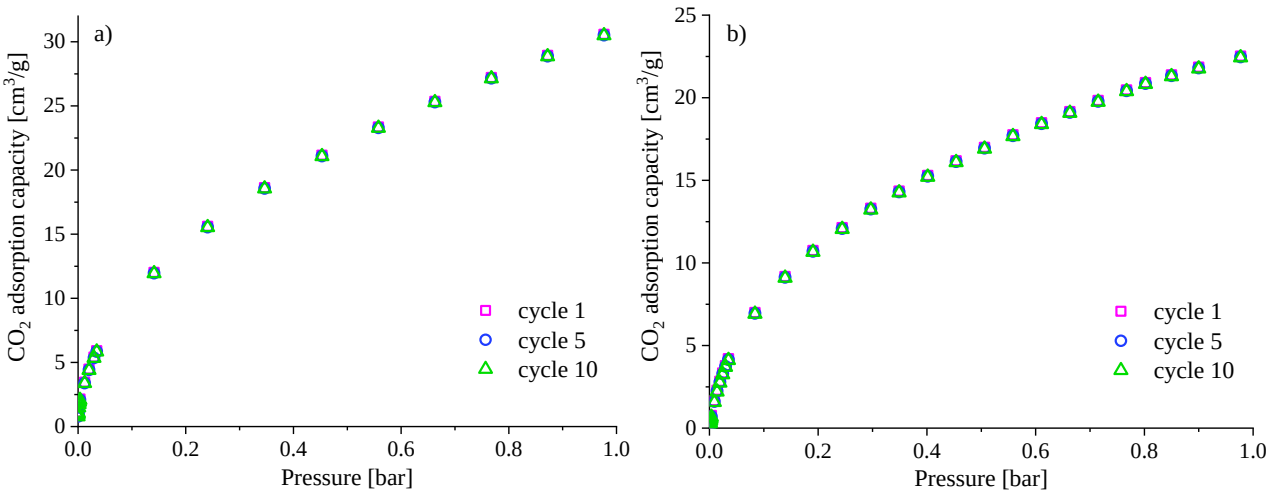

Figure 37. CO_2 capture performance for (a) AC-900K -and (b) AC-700A at 0 °C in 1st, 5th, and 10th adsorption-desorption cycle.

5. Conclusions

This thesis aims to present the utilization of tailor-made rCB from commercial ELTs pyrolysis for high-value-added ACs. It provides characterization of rCB/ACs focusing on chemical, and morphological features development upon potassium activation. It aimed to follow the mechanisms behind rCB activation for sorption processes including CO2 capture. Based on the work and discussion that have been undertaken, the major findings of the present thesis are summarized below.

- **Chemical composition and porosity development**: Ultimate analysis revealed a high carbon content in rCB/ACs. Moreover, well-developed dual porosity of rCB/ACs was observed, consisting mainly of mesopores. Chemical analysis uncovered significant variation in oxygen content due to activation, primarily as oxygen-containing groups (O-H and C-O bonds) (**Paper I**).

- **Morphological features and thermal behavior**: SEM analysis indicated the presence of particle aggregates and agglomerates in cluster forms, which were heterogeneously distributed within the rCB/ACs. Raman spectroscopy confirmed the presence of structural defects and graphitic formations. TGA analysis suggested three distinct thermal degradation stages: the removal of moisture and volatile compounds, the elimination of mineral and inorganic residues, and the combustion of rCB/AC samples (**Paper II**).

- **KOH vs. NaOH activation**: Optimal KOH activation conditions were identified to be a temperature of 800 °C, a rCB:KOH mass ratio of 1:5, an activation time of 4 hours, and a heating rate of 7 °C/min. These conditions yielded the highest increases in BET surface area, total pore volume, and microporosity. KOH proved to have superior activation properties if compared to NaOH. The involvement of solid-gas state reactions during

KOH activation was found to enhance the textural properties of rCB/ACs (Paper II) (Paper II).

- **Comparison of potassium-containing salts as activators**: Among the tested potassium salts (KOH, KCl, K_2CO_3, CH_3COOK, $K_2C_2O_4$), KOH was found to be the most effective in enhancing BET surface area, total pore volume, mesopore and micropore volume. Other salts showed varying degrees of efficiency, this behavior was directly correlated with the potassium content and its distribution on rCB/ACs (**Paper II**).

- **CO_2 capture performance of rCB/ACs:** KOH-activated rCB/ACs (AC-900K) exhibited the highest CO_2 uptake capacity at 0 °C, reaching 30.90 cm^3/g, which was higher compared to air-activated samples (AC-700A). Although their performance was comparable or better that of industrial by-product precursors, rCB/ACs have not exceed the CO_2 capture capabilities of ACs derived from biomass (**Paper I**).

- **Association between textural properties of rCB/ACs and CO_2 adsorption**: Investigations revealed a strong correlation between CO_2 adsorption capacity and microporosity and total pore volume for chemically activated samples, and BET surface area and micropore volume for physically activated samples, highlighting the critical role of submicropores and ultramicropores in enhancing CO_2 capture performance (**Paper I**).

- **CO_2/N_2 selectivity and cyclic stability of rCB/ACs**: The CO_2/N_2 selectivity and the regenerative ability of rCB/ACs, particularly AC-900K, were notable, showing high selectivity ratios and maintaining stable CO_2 uptake across multiple adsorption-desorption cycles, underscoring their potential for efficient CO_2 capture in industrial applications (**Paper I**).

6. Future outlook

The future outlook for rCB/ACs development and their potential in sorption applications, including CO_2 capture, points toward several promising research directions. They can be categorized into material innovation, process optimization, and application expansion.

1. **<u>Material innovation</u>**

- **Advanced and environmentally friendly activation techniques**: Exploring new activation methods to enhance the porosity and surface chemistry of rCB-derived activated carbons. This includes exploring novel and ecofriendly chemical activators, optimizing thermochemical conversion conditions, and employing combined chemical-physical activation methods.

- **Surface functionalization**: Investigating chemical and physical methods to introduce or increase specific functional groups on the surface of rCB/ACs. Research could focus on targeted functionalization techniques that selectively enhance affinity for specific gases, besides aiming to capture significant amount of CO_2. This includes the use of acids, bases, or specific organic compounds in post-treatment processes to alter the surface chemistry of the rCB/ACs.

- **Creation of composite materials**: Creating composites that combine rCB or rCB/ACs with other materials, such as metal-organic frameworks or zeolites, could combine the strengths of each component for improved sorption performance.

2. **Process optimization**

- **Pore structure optimization:** Tailoring the pore structure of rCB/ACs through dual activation or combining different activators could be the focus of further studies, maximizing microporosity or mesoporosity based on the kinetic diameter of the target gaseous adsorbate. This would involve advanced characterization techniques to map pore development and its effects on gas adsorption dynamics.

- **Dynamic adsorption studies**: Conducting dynamic adsorption studies to evaluate the performance of modified rCB-derived activated carbons under conditions that mimic real industrial flue gases. This includes assessing the effects of humidity, temperature fluctuations, and gas composition on the selectivity and capacity of the adsorbents, providing valuable data for scaling up and application in real-world scenarios.

3. **Application expansion**

- **Sorption applications beyond CO_2 capture**: Expanding the application scope of rCB-derived activated carbons to include the adsorption of other gaseous pollutants, and even hazardous substances from water. Research will likely explore the multi-functional capabilities of these materials, assessing their effectiveness in a range of environmental remediation and purification processes.

- **Integration into existing systems**: Investigating into how rCB/ACs can be integrated into existing industrial processes, such as power plants or manufacturing facilities in real world conditions.

- **Sustainable and economical production**: Addressing the scalability of rCB-derived activated carbon production in an environmentally and economically sustainable manner. This involves optimizing manufacturing processes to minimize energy consumption and waste production, utilizing renewable energy sources, and evaluating the life cycle impact of these materials. Integrating life cycle assessment and techno-economic analysis will be crucial in this context.

References

[1] Odunlami, O. A., Vershima, D. A., Oladimeji, T. E., Nkongho, S., Ogunlade, S. K., & Fakinle, B. S. (2022). Advanced techniques for the capturing and separation of CO_2–a review. Results in Engineering, 15, 100512. https://doi.org/10.1016/j.rineng.2022.100512

[2] Ungureanu, N., Vlăduț, V., & Voicu, G. (2020). Water scarcity and wastewater reuse in crop irrigation. Sustainability, 12(21), 9055. https://doi.org/10.3390/su12219055

[3] Moasas, A. M., Amin, M. N., Khan, K., Ahmad, W., Al-Hashem, M. N. A., Deifalla, A. F., & Ahmad, A. (2022). A worldwide development in the accumulation of waste tires and its utilization in concrete as a sustainable construction material: A review. Case Studies in Construction Materials, 17, e01677. https://doi.org/10.1016/j.cscm.2022.e01677

[4] Peres, C. B., Resende, P. M., Nunes, L. J., & Morais, L. C. D. (2022). Advances in Carbon Capture and Use (CCU) Technologies: A Comprehensive Review and CO_2 Mitigation Potential Analysis. Clean technologies, 4(4), 1193-1207. https://doi.org/10.3390/cleantechnol4040073

[5] Lu, K., Yang, X., Gielen, G., Bolan, N., Ok, Y. S., Niazi, N. K., Song, X., Yuan, G., Zhang, X., Liu, D., Song, Z., Liu, X., & Wang, H. (2017). Effect of bamboo and rice straw biochars on the mobility and redistribution of heavy metals (Cd, Cu, Pb and Zn) in contaminated soil. Journal of environmental management, 186, 285-292. https://doi.org/10.1016/j.jenvman.2016.05.068

[6] Li, Y., & Yu, J. (2021). Emerging applications of zeolites in catalysis, separation and host–guest assembly. Nature Reviews Materials, 6(12), 1156-1174. https://doi.org/10.1038/s41578-021-00347-3

[7] Nie, L., Mu, Y., Jin, J., Chen, J., & Mi, J. (2018). Recent developments and consideration issues in solid adsorbents for CO_2 capture from flue gas. Chinese Journal of Chemical Engineering, 26(11), 2303-2317. https://doi.org/10.1016/j.cjche.2018.07.012

[8] Kwiatkowski, M., Gómez-Delgado, E., Nunell, G. V., Bonelli, P. R., & Cukierman, A. L. (2022). Mathematical analysis of the effect of process conditions on the porous structure development of activated carbons derived from Pine cones. Scientific Reports, 12(1), 15301. https://doi.org/10.1038/s41598-022-19383-2

[9] Lopez, G., Alvarez, J., Amutio, M., Mkhize, N. M., Danon, B., Van der Gryp, P., Görgens, J.F., & Olazar, M. (2017). Waste truck-tyre processing by flash pyrolysis in a conical spouted bed reactor. Energy conversion and management, 142, 523-532. https://doi.org/10.1016/j.enconman.2017.03.051

[10] Czajczyńska, D., Czajka, K., Krzyżyńska, R., & Jouhara, H. (2020). Waste tyre pyrolysis–Impact of the process and its products on the environment. Thermal Science and Engineering Progress, 20, 100690. https://doi.org/10.1016/j.tsep.2020.100690

[11] Karaağaç, B., Ercan Kalkan, M., & Deniz, V. (2017). End of life tyre management: Turkey case. Journal of Material Cycles and Waste Management, 19, 577-584. https://doi.org/10.1007/s10163-015-0427-2

[12] Global Tire Recycling Market Analysis 2025: Opportunity, Demand, Growth and Forecast 2017–2025—Edition. (2020). https://www.goldsteinresearch.com/report/global-tire-recycling-industry-market-trends-analysis [Accessed 1 May 2024].

[13] Hoang, A. T., Varbanov, P. S., Nižetić, S., Sirohi, R., Pandey, A., Luque, R., & Ng, K. H. (2022). Perspective review on Municipal Solid Waste-to-energy route: Characteristics, management strategy, and role in circular economy. Journal of Cleaner Production, 131897. https://doi.org/10.1016/j.jclepro.2022.131897

[14] Urrego-Yepes, W., Cardona-Uribe, N., Vargas-Isaza, C. A., & Martínez, J. D. (2021). Incorporating the recovered carbon black produced in an industrial-scale waste tire pyrolysis plant into a natural rubber formulation. Journal of environmental management, 287, 112292. https://doi.org/10.1016/j.jenvman.2021.112292

[15] IEA (2021). Global Energy Review 2021, IEA, Paris. https://www.iea.org/reports/global-energy-review-2021

[16] https://www.climate.gov/news-features/understanding-climate/climate-change-atmospheric-carbon-dioxide [Accessed 1 May 2024].

[17] IEA (2019). Transforming Industry through CCUS, IEA, Paris. https://www.iea.org/reports/transforming-industry-through-ccus

[18] Dziejarski, B., Krzyżyńska, R., & Andersson, K. (2023). Current status of carbon capture, utilization, and storage technologies in the global economy: A survey of technical assessment. Fuel, 342, 127776. https://doi.org/10.1016/j.fuel.2023.127776

[19] Ebner, A. D., & Ritter, J. A. (2009). State-of-the-art adsorption and membrane separation processes for carbon dioxide production from carbon dioxide emitting industries. Separation Science and Technology, 44(6), 1273-1421. https://doi.org/10.1080/01496390902733314

[20] Mmereki, D., Machola, B., & Mokokwe, K. (2019). Status of waste tires and management practice in Botswana. Journal of the Air & Waste Management Association, 69(10), 1230-1246. https://doi.org/10.1080/10962247.2017.1279696

[21] https://canadianrecycler.ca/tire-troubles-research-from-the-recycled-rubber-coalition-estimates-12-percent-increase-in-scrap-tires-with-greater-ev-adoption/ [Accessed 1 May 2024].

[22] Czarna-Juszkiewicz, D., Kunecki, P., Cader, J., & Wdowin, M. (2023). Review in Waste Tire Management—Potential Applications in Mitigating Environmental Pollution. Materials, 16(17), 5771. https://doi.org/10.3390/ma16175771

[23] Landi, D., Marconi, M., Gianvincenzi, M., & Mosconi, E. M. (2023). Technical and environmental assessment of a circular economy scenario for end of life tires fibers used as reinforcement in plastic compounds. International Journal on Interactive Design and Manufacturing (IJIDeM), 1-12. https://doi.org/10.1007/s12008-023-01249-0

[24] Tibor, S. T., & Grande, C. A. (2022). Industrial production of activated carbon using circular bioeconomy principles: Case study from a Romanian company. Cleaner Engineering and Technology, 7, 100443. https://doi.org/10.1016/j.clet.2022.100443

[25] Lin, J. H., & Wang, S. B. (2017). An effective route to transform scrap tire carbons into highly-pure activated carbons with a high adsorption capacity of ethylene blue through thermal and chemical treatments. Environmental Technology & Innovation, 8, 17-27. https://doi.org/10.1016/j.eti.2017.03.004

[26] Paul, S., Rahaman, M., Ghosh, S. K., Katheria, A., Das, T. K., Patel, S., & Das, N. C. (2023). Recycling of waste tire by pyrolysis to recover carbon black: an alternative reinforcing filler. Journal of Material Cycles and Waste Management, 25(3), 1470-1481. https://doi.org/10.1007/s10163-023-01635-6

[27] Saputra, R., Walvekar, R., Khalid, M., Mubarak, N. M., & Sillanpää, M. (2021). Current progress in waste tire rubber devulcanization. Chemosphere, 265, 129033. https://doi.org/10.1016/j.chemosphere.2020.129033

[28] Gao, N., Wang, F., Quan, C., Santamaria, L., Lopez, G., & Williams, P. T. (2022). Tire pyrolysis char: Processes, properties, upgrading and applications. Progress in Energy and Combustion Science, 93, 101022. https://doi.org/10.1016/j.pecs.2022.101022

[29] Singh, R. K., Ruj, B., Jana, A., Mondal, S., Jana, B., Sadhukhan, A. K., & Gupta, P. (2018). Pyrolysis of three different categories of automotive tyre wastes: Product yield analysis and characterization. Journal of Analytical and Applied Pyrolysis, 135, 379-389. https://doi.org/10.1016/j.jaap.2018.08.011

[30] Ucar, S., Karagoz, S., Ozkan, A. R., & Yanik, J. (2005). Evaluation of two different scrap tires as hydrocarbon source by pyrolysis. Fuel, 84(14-15), 1884-1892. https://doi.org/10.1016/j.fuel.2005.04.002

[31] Kyari, M., Cunliffe, A., & Williams, P. T. (2005). Characterization of oils, gases, and char in relation to the pyrolysis of different brands of scrap automotive tires. Energy & Fuels, 19(3), 1165-1173. https://doi.org/10.1021/ef049686x

[32] Wang, M., Zhang, L., Li, A., Irfan, M., Du, Y., & Di, W. (2019). Comparative pyrolysis behaviors of tire tread and side wall from waste tire and characterization of the resulting chars. Journal of Environmental Management, 232, 364-371. https://doi.org/10.1016/j.jenvman.2018.10.091

[33] Chen, G., Sun, B., Li, J., Lin, F., Xiang, L., & Yan, B. (2022). Products distribution and pollutants releasing characteristics during pyrolysis of waste tires under different thermal process. Journal of Hazardous Materials, 424, 127351. https://doi.org/10.1016/j.jhazmat.2021.127351

[34] Tian, X., Zhuang, Q., Han, S., Li, S., Liu, H., Li, L., Zhang, J., Wang, C., & Bian, H. (2021). A novel approach of reapplication of carbon black recovered from waste tyre pyrolysis to rubber composites. Journal of cleaner production, 280, 124460. https://doi.org/10.1016/j.jclepro.2020.124460

[35] Aydın, H., & İlkılıç, C. (2012). Optimization of fuel production from waste vehicle tires by pyrolysis and resembling to diesel fuel by various desulfurization methods. Fuel, 102, 605-612. https://doi.org/10.1016/j.fuel.2012.06.067

[36] Taleb, D. A., Abd Hamid, H., Deris, R. R. R., Zulkifli, M., Khalil, N. A., & Yahaya, A. N. A. (2020). Insights into pyrolysis of waste tire in fixed bed reactor: Thermal behavior. Materials Today: Proceedings, 31, 178-186. https://doi.org/10.1016/j.matpr.2020.01.569

[37] Alhassan, Y., Kumar, N., & Bugaje, I. M. (2016). Catalytic upgrading of waste tire pyrolysis oil via supercritical esterification with deep eutectic solvents (green solvents and catalysts). Journal of the Energy Institute, 89(4), 683-693. https://doi.org/10.1016/j.joei.2015.05.003

[38] Mui, E. L., Cheung, W. H., & McKay, G. (2010). Tyre char preparation from waste tyre rubber for dye removal from effluents. Journal of Hazardous Materials, 175(1-3), 151-158. https://doi.org/10.1016/j.jhazmat.2009.09.142

[39] Danmaliki, G. I., & Saleh, T. A. (2016). Influence of conversion parameters of waste tires to activated carbon on adsorption of dibenzothiophene from model fuels. Journal of Cleaner Production, 117, 50-55. https://doi.org/10.1016/j.jclepro.2016.01.026

[40] Doja, S., Pillari, L. K., & Bichler, L. (2022). Processing and activation of tire-derived char: A review. Renewable and Sustainable Energy Reviews, 155, 111860. https://doi.org/10.1016/j.rser.2021.111860

[41] Alsaleh, A., & Sattler, M. L. (2014). Waste tire pyrolysis: influential parameters and product properties. Current Sustainable/Renewable Energy Reports, 1, 129-135. https://doi.org/10.1007/s40518-014-0019-0

[42] Tan, H., Lee, C. T., Ong, P. Y., Wong, K. Y., Bong, C. P. C., Li, C., & Gao, Y. (2021, February). A review on the comparison between slow pyrolysis and fast pyrolysis on the quality of lignocellulosic and lignin-based biochar. In IOP Conference Series: Materials Science and Engineering (Vol. 1051, No. 1, p. 012075). IOP Publishing. DOI: 10.1088/1757-899X/1051/1/012075

[43] Kurian, V., Gill, M., Dhakal, B., & Kumar, A. (2022). Recent trends in the pyrolysis and gasification of lignocellulosic biomass. In Biofuels and Bioenergy (pp. 511-552). Elsevier. https://doi.org/10.1016/B978-0-323-90040-9.00028-X

[44] Wang, H., Hu, H., Yang, Y., Liu, H., Tang, H., Xu, S., Li, A., & Yao, H. (2020). Effect of high heating rates on products distribution and sulfur transformation during the pyrolysis of waste tires. Waste Management, 118, 9-17. https://doi.org/10.1016/j.wasman.2020.08.015

[45] Lopez, G., Aguado, R., Olazar, M., Arabiourrutia, M., & Bilbao, J. (2009). Kinetics of scrap tyre pyrolysis under vacuum conditions. Waste management, 29(10), 2649-2655. https://doi.org/10.1016/j.wasman.2009.06.005

[46] Sienkiewicz, M., Kucinska-Lipka, J., Janik, H., & Balas, A. (2012). Progress in used tyres management in the European Union: A review. Waste management, 32(10), 1742-1751. https://doi.org/10.1016/j.wasman.2012.05.010

[47] Sun, F., Wu, D., Gao, J., Pei, T., Chen, Y., Wang, K., Yang, H., & Zhao, G. (2020). Graphitic porous carbon with multiple structural merits for high-performance organic supercapacitor. Journal of Power Sources, 477, 228759. https://doi.org/10.1016/j.jpowsour.2020.228759

[48] Pan, F., Chen, T., Cai, M., Wu, F., You, Z., & Li, J. (2021). Fabrication of large-surface-area graphitized carbons by potassium hydroxide-promoted catalytic graphitization. Materials Research Bulletin, 140, 111333. https://doi.org/10.1016/j.materresbull.2021.111333

[49] Rani, M. U., Nanaji, K., Rao, T. N., & Deshpande, A. S. (2020). Corn husk derived activated carbon with enhanced electrochemical performance for high-voltage supercapacitors. Journal of Power Sources, 471, 228387. https://doi.org/10.1016/j.jpowsour.2020.228387

[50] Hassan, M. F., Sabri, M. A., Fazal, H., Hafeez, A., Shezad, N., & Hussain, M. (2020). Recent trends in activated carbon fibers production from various precursors and applications—A comparative review. Journal of Analytical and Applied Pyrolysis, 145, 104715. https://doi.org/10.1016/j.jaap.2019.104715

[51] Ōya, A., & Ōtani, S. (1981). Influences of particle size of metal on catalytic graphitization of non-graphitizing carbons. Carbon, 19(5), 391-400. https://doi.org/10.1016/0008-6223(81)90064-6

[52] Franklin, R. E. (1951). Crystallite growth in graphitizing and non-graphitizing carbons. Proceedings of the Royal Society of London. Series A. Mathematical and Physical Sciences, 209(1097), 196-218. https://doi.org/10.1098/rspa.1951.0197

[53] Yu, S., Wang, J., Zhao, Z., & Cai, W. (2022). Simultaneous coupling of fluidized granular activated carbon (GAC) and powdered activated carbon (PAC) with ultrafiltration process: A promising synergistic alternative for water treatment. Separation and Purification Technology, 282, 120085. https://doi.org/10.1016/j.seppur.2021.120085

[54] Verma, C., & Quraishi, M. A. (Eds.). (2023). Activated Carbon: Progress and Applications. Royal Society of Chemistry. https://doi.org/10.1039/9781839169861

[55] Shi, K., Xu, Z., Wang, Y., Fu, W., & Chen, B. (2024). Study on regeneration characteristics of granular activated carbon using ultrasonic and thermal methods. Environmental Science and Pollution Research, 1-12. https://doi.org/10.1007/s11356-024-32734-y

[56] Sharma, A., Jindal, J., Mittal, A., Kumari, K., Maken, S., & Kumar, N. (2021). Carbon materials as CO2 adsorbents: a review. Environmental Chemistry Letters, 19(2), 875-910. https://doi.org/10.1007/s10311-020-01153-z

[57] Worch, E. (2021). Adsorption technology in water treatment. In Adsorption Technology in Water Treatment. de Gruyter. https://doi.org/10.1515/9783110240238

[58] Sabzehmeidani, M. M., Mahnaee, S., Ghaedi, M., Heidari, H., & Roy, V. A. (2021). Carbon based materials: A review of adsorbents for inorganic and organic compounds. Materials Advances, 2(2), 598-627. DOI: 10.1039/D0MA00087F

[59] Bell, D. A., Towler, B. F., & Fan, M. (2010). Coal gasification and its applications. William Andrew. https://doi.org/10.1016/C2009-0-20067-5

[60] Tan, X. F., Zhu, S. S., Wang, R. P., Chen, Y. D., Show, P. L., Zhang, F. F., & Ho, S. H. (2021). Role of biochar surface characteristics in the adsorption of aromatic compounds: Pore structure and functional groups. Chinese Chemical Letters, 32(10), 2939-2946. https://doi.org/10.1016/j.cclet.2021.04.059

[61] Brunauer, S., Mikhail, R. S., & Bodor, E. E. (1967). Some remarks about capillary condensation and pore structure analysis. Journal of Colloid And Interface Science, 25(3). https://doi.org/10.1016/0021-9797(67)90041-0

[62] Dubinin, M. M., Gregg, S. J., Sing, K. S. W., & Stoeckli, H. F. (1979). Characterization of porous solids. Society of Chemical Industry.

[63] González-García, P. (2018). Activated carbon from lignocellulosics precursors: A review of the synthesis methods, characterization techniques and applications. Renewable and Sustainable Energy Reviews, 82, 1393-1414. https://doi.org/10.1016/j.rser.2017.04.117

[64] Kim, S., Lee, S. E., Baek, S. H., Choi, U., & Bae, H. J. (2023). Preparation of Activated Carbon from Korean Anthracite: Simultaneous Control of Ash Reduction and Pore Development. Processes, 11(10), 2877. https://doi.org/10.3390/pr11102877

[65] Ma, S., Huang, Y., Liu, Y., Liu, H., Chen, Y., Wang, J., & Xu, J. (2023). Big data-driven correlation analysis based on clustering for energy-intensive manufacturing industries. Applied Energy, 349, 121608. https://doi.org/10.1016/j.apenergy.2023.121608

[66] Siddique, I. J., Salema, A. A., Antunes, E., & Vinu, R. (2022). Technical challenges in scaling up the microwave technology for biomass processing. Renewable and Sustainable Energy Reviews, 153, 111767. https://doi.org/10.1016/j.rser.2021.111767

[67] B. Sajjadi, W.Y. Chen, N.O. Egiebor, A comprehensive review on physical activation of biochar for energy and environmental applications, Rev. Chem. Eng. 35 (6) (2019) 735–776. https://doi.org/10.1515/revce-2017-0113.

[68] Molina-Sabio, M., Gonzalez, M. T., Rodriguez-Reinoso, F., & Sepúlveda-Escribano, A. (1996). Effect of steam and carbon dioxide activation in the micropore size distribution of activated carbon. Carbon, 34(4), 505-509. https://doi.org/10.1016/0008-6223(96)00006-1

[69] Sajjadi, B., Chen, W. Y., & Egiebor, N. O. (2019). A comprehensive review on physical activation of biochar for energy and environmental applications. Reviews in Chemical Engineering, 35(6), 735-776. https://doi.org/10.1515/revce-2017-0113

[70] Petrovic, B., Gorbounov, M., & Soltani, S. M. (2021). Influence of surface modification on selective CO_2 adsorption: A technical review on mechanisms and methods. Microporous and mesoporous materials, 312, 110751. https://doi.org/10.1016/j.micromeso.2020.110751

[71] N. Hagemann, K. Spokas, H.P. Schmidt, R. Kägi, M.A. Böhler, T.D. Bucheli, Activated carbon, biochar and charcoal: linkages and synergies across pyrogenic carbon's ABCs, Water 10 (2) (2018) 182. https://doi.org/10.3390/w10020182.

[72] A. Aworn, P. Thiravetyan, W. Nakbanpote, Preparation and characteristics of agricultural waste activated carbon by physical activation having micro-and mesopores, J. Anal. Appl. Pyrol. 82 (2) (2008) 279–285. https://doi.org/10.1016/j.jaap.2008.04.007.

[73] M.S. Tam, M.J. Antal, Preparation of activated carbons from macadamia nut shell and coconut shell by air activation, Ind. Eng. Chem. Res. 38 (11) (1999) 4268–4276. https://doi.org/10.1021/ie990346m.

[74] M.G. Plaza, A.S. González, J.J. Pis, F. Rubiera, C. Pevida, Production of microporous biochars by single-step oxidation: effect of activation conditions on CO_2 capture, Appl. Energy 114 (2014) 551–562. https://doi.org/10.1016/j.apenergy.2013.09.058.

[75] A.K. Dalai, R. Azargohar, Production of activated carbon from biochar using chemical and physical activation: mechanism and modeling, Materials, Chemicals, and Energy from Forest Biomass 29 (2007) 463-476. doi: 10.1021/bk-2007-0954.ch029

[76] B. Petrovic, M. Gorbounov, S.M. Soltani, Impact of surface functional groups and their introduction methods on the mechanisms of CO_2 adsorption on porous carbonaceous adsorbents, Carbon Capture Sci. Technol. (2022) 100045. https://doi.org/10.1016/j.ccst.2022.100045

[77] Phothong, K., Tangsathitkulchai, C., & Lawtae, P. (2021). The analysis of pore development and formation of surface functional groups in bamboo-based activated carbon during CO2 activation. Molecules, 26(18), 5641. https://doi.org/10.3390/molecules26185641

[78] Y. Gao, Q. Yue, B. Gao, A. Li, Insight into activated carbon from different kinds of chemical activating agents: a review, Sci. Total Environ. 746 (2020) 141094. https://doi.org/10.1016/j.scitotenv.2020.141094.

[79] Y. Kan, Q. Yue, B. Gao, Q. Li, Comparative study of dry-mixing and wet-mixing activated carbons prepared from waste printed circuit boards by NaOH activation, RSC Adv. 5 (128) (2015) 105943–105951. https://doi.org/10.1039/C5RA18840G.

[80] Maia, D. A. S., de Oliveira, J. C. A., Nazzarro, M. S., Sapag, K. M., López, R. H., de Lucena, S. M. P., & de Azevedo, D. C. S. (2018). CO_2 gas-adsorption calorimetry applied to the study of chemically activated carbons. Chemical Engineering Research and Design, 136, 753-760. https://doi.org/10.1016/j.cherd.2018.06.034

[81] Venkatachalam, C. D., Sekar, S., Sengottian, M., Ravichandran, S. R., & Bhuvaneshwaran, P. (2023). A critical review of the production, activation, and morphological characteristic study on functionalized biochar. Journal of Energy Storage, 67, 107525. https://doi.org/10.1016/j.est.2023.107525

[82] Rathi, B. S., & Kumar, P. S. (2021). Application of adsorption process for effective removal of emerging contaminants from water and wastewater. Environmental Pollution, 280, 116995. https://doi.org/10.1016/j.envpol.2021.116995

[83] Han, J., Zhang, L., Zhao, B., Qin, L., Wang, Y., & Xing, F. (2019). The N-doped activated carbon derived from sugarcane bagasse for CO_2 adsorption. Industrial Crops and Products, 128, 290-297. https://doi.org/10.1016/j.indcrop.2018.11.028

[84] Rashidi, N. A., & Yusup, S. (2017). A review on recent technological advancement in the activated carbon production from oil palm wastes. Chemical Engineering Journal, 314, 277-290. https://doi.org/10.1016/j.cej.2016.11.059

[85] Azam, K., Shezad, N., Shafiq, I., Akhter, P., Akhtar, F., Jamil, F., Shafigue, S,. Park, Y, K,. & Hussain, M. (2022). A review on activated carbon modifications for the treatment of wastewater containing anionic dyes. Chemosphere, 306, 135566. https://doi.org/10.1016/j.chemosphere.2022.135566

[86] Neolaka, Y. A., Riwu, A. A., Aigbe, U. O., Ukhurebor, K. E., Onyancha, R. B., Darmokoesoemo, H., & Kusuma, H. S. (2023). Potential of activated carbon from various sources as a low-cost adsorbent to remove heavy metals and synthetic dyes. Results in Chemistry, 5, 100711. https://doi.org/10.1016/j.rechem.2022.100711

[87] Nizam, N. U. M., Hanafiah, M. M., Mahmoudi, E., Halim, A. A., & Mohammad, A. W. (2021). The removal of anionic and cationic dyes from an aqueous solution using biomass-

based activated carbon. Scientific Reports, 11(1), 1-17. https://doi.org/10.1038/s41598-021-88084-z

[88] Sultana, M., Rownok, M. H., Sabrin, M., Rahaman, M. H., & Alam, S. N. (2022). A review on experimental chemically modified activated carbon to enhance dye and heavy metals adsorption. Cleaner engineering and technology, 6, 100382. https://doi.org/10.1016/j.clet.2021.100382

[89] Mariana, M., HPS, A. K., Mistar, E. M., Yahya, E. B., Alfatah, T., Danish, M., & Amayreh, M. (2021). Recent advances in activated carbon modification techniques for enhanced heavy metal adsorption. Journal of Water Process Engineering, 43, 102221. https://doi.org/10.1016/j.jwpe.2021.102221

[90] Shahrokhi-Shahraki, R., Benally, C., El-Din, M. G., & Park, J. (2021). High efficiency removal of heavy metals using tire-derived activated carbon vs commercial activated carbon: Insights into the adsorption mechanisms. Chemosphere, 264, 128455. https://doi.org/10.1016/j.chemosphere.2020.128455

[91] Xie, B., Qin, J., Wang, S., Li, X., Sun, H., & Chen, W. (2020). Adsorption of phenol on commercial activated carbons: modelling and interpretation. International Journal of Environmental Research and Public Health, 17(3), 789. https://doi.org/10.3390/ijerph17030789

[92] Reza, M. S., Yun, C. S., Afroze, S., Radenahmad, N., Bakar, M. S. A., Saidur, R., Taweekun, J., & Azad, A. K. (2020). Preparation of activated carbon from biomass and its' applications in water and gas purification, a review. Arab Journal of Basic and Applied Sciences, 27(1), 208-238. https://doi.org/10.1080/25765299.2020.1766799

[93] El-Bery, H. M., Saleh, M., El-Gendy, R. A., Saleh, M. R., & Thabet, S. M. (2022). High adsorption capacity of phenol and methylene blue using activated carbon derived from lignocellulosic agriculture wastes. Scientific reports, 12(1), 5499. https://doi.org/10.1038/s41598-022-09475-4

[94] Sawalha, H., Maghalseh, M., Qutaina, J., Junaidi, K., & Rene, E. R. (2020). Removal of hydrogen sulfide from biogas using activated carbon synthesized from different locally available biomass wastes-a case study from Palestine. Bioengineered, 11(1), 607-618. https://doi.org/10.1080/21655979.2020.1768736

[95] Wang, S., Nam, H., & Nam, H. (2020). Preparation of activated carbon from peanut shell with KOH activation and its application for H_2S adsorption in confined space. Journal of Environmental Chemical Engineering, 8(2), 103683. https://doi.org/10.1016/j.jece.2020.103683

[96] Chan, Y. H., Lock, S. S. M., Wong, M. K., Yiin, C. L., Loy, A. C. M., Cheah, K. W., Chai, S. Y. W., Li, C., How, B. S., Chin, B. L. F., Chan, Z. P., & Lam, S. S. (2022). A state-of-the-art review on capture and separation of hazardous hydrogen sulfide (H_2S): Recent advances,

challenges and outlook. Environmental Pollution, 314, 120219. https://doi.org/10.1016/j.envpol.2022.120219

[97] Hanif, M. A., Ibrahim, N., & Abdul Jalil, A. (2020). Sulfur dioxide removal: An overview of regenerative flue gas desulfurization and factors affecting desulfurization capacity and sorbent regeneration. Environmental Science and Pollution Research, 27(22), 27515-27540. https://doi.org/10.1007/s11356-020-09191-4

[98] Wang, L., Sha, L., Zhang, S., Cao, F., Ren, X., & Levendis, Y. A. (2022). Preparation of activated coke by carbonization, activation, ammonization and thermal treatment of sewage sludge and waste biomass for SO_2 absorption applications. Fuel Processing Technology, 231, 107233. https://doi.org/10.1016/j.fuproc.2022.107233

[99] Jacobs, J. H., Chou, N., Lesage, K. L., Xiao, Y., Hill, J. M., & Marriott, R. A. (2023). Investigating activated carbons for SO_2 adsorption in wet flue gas. Fuel, 353, 129239. https://doi.org/10.1016/j.fuel.2023.129239

[100] Li, Q., Hou, Y., Xiang, N., Liu, Y., & Huang, Z. (2020). A new insight into the promotional effect of nitrogen-doping in activated carbon for selective catalytic reduction of NO_x with NH_3. Science of the Total Environment, 740, 140158. https://doi.org/10.1016/j.scitotenv.2020.140158

[101] Niu, J., Zhang, H., Li, L., & Guo, Y. (2021). Cost-effective activated carbon (AC) production from partial substitution of coal with red mud (RM) as additive for SO_2 and NO_x abatement at low temperature. Fuel, 293, 120448. https://doi.org/10.1016/j.fuel.2021.120448

[102] Park, B., & Choi, Y. C. (2022). Evaluation of NO_x removal performance of foam composites with titanium dioxide and active carbon. Construction and Building Materials, 348, 128646. https://doi.org/10.1016/j.conbuildmat.2022.128646

[103] Ma, X., Yang, L., & Wu, H. (2021). Removal of volatile organic compounds from the coal-fired flue gas by adsorption on activated carbon. Journal of Cleaner Production, 302, 126925. https://doi.org/10.1016/j.jclepro.2021.126925

[104] Li, X., Zhang, L., Yang, Z., Wang, P., Yan, Y., & Ran, J. (2020). Adsorption materials for volatile organic compounds (VOCs) and the key factors for VOCs adsorption process: A review. Separation and Purification Technology, 235, 116213. https://doi.org/10.1016/j.seppur.2019.116213

[105] Isinkaralar, K. (2024). Multi-component volatile organic compounds (VOCs) treatment nexus: High-performance of activated carbon derived from residual agroforestry biomass. International Journal of Environmental Science and Technology, 21(1), 925-938. https://doi.org/10.1007/s13762-023-05202-2

[106] Rouquerol, J., Rouquerol, F., Llewellyn, P., Maurin, G., & Sing, K. (2013). Adsorption by powders and porous solids: principles, methodology and applications. Academic press. https://doi.org/10.1016/C2010-0-66232-8.

[107] Yang, R. T. (1997). Gas separation by adsorption processes (Vol. 1). World Scientific. https://doi.org/10.1142/p037.

[108] Bains, P., Psarras, P., & Wilcox, J. (2017). CO_2 capture from the industry sector. Progress in Energy and Combustion Science, 63, 146-172. https://doi.org/10.1016/j.pecs.2017.07.001

[109] Blomen, E., Hendriks, C., & Neele, F. (2009). Capture technologies: improvements and promising developments. Energy procedia, 1(1), 1505-1512. https://doi.org/10.1016/j.egypro.2009.01.197

[110] Lai, J. Y., Ngu, L. H., & Hashim, S. S. (2021). A review of CO_2 adsorbents performance for different carbon capture technology processes conditions. Greenhouse Gases: Science and Technology, 11(5), 1076-1117. https://doi.org/10.1002/ghg.2112

[111] Querejeta, N., Gil, M. V., Rubiera, F., & Pevida, C. (2023). Prospects of low-temperature solid sorbents in industrial CO_2 capture: A focus on biomass residues as precursor material. Greenhouse Gases: Science and Technology, 13(2), 245-284. https://doi.org/10.1002/ghg.2210

[112] Zhou, J., Li, D., Wang, Y., Tian, Y., Zhang, Z., Wei, L., & Feng, W. (2018). Effect of the feedstock type on the volumetric low-pressure CO_2 capture performance of activated carbons. Energy & fuels, 32(12), 12711-12720. https://doi.org/10.1021/acs.energyfuels.8b02827.

[113] Montagnaro, F., Silvestre-Albero, A., Silvestre-Albero, J., Rodríguez-Reinoso, F., Erto, A., Lancia, A., & Balsamo, M. (2015). Post-combustion CO_2 adsorption on activated carbons with different textural properties. Microporous and Mesoporous Materials, 209, 157-164. https://doi.org/10.1016/j.micromeso.2014.09.037.

[114] Azmi, N. Z. M., Buthiyappan, A., Raman, A. A. A., Patah, M. F. A., & Sufian, S. (2022). Recent advances in biomass based activated carbon for carbon dioxide capture–A review. Journal of Industrial and Engineering Chemistry, 116, 1-20. https://doi.org/10.1016/j.jiec.2022.08.021

[115] Zaker, A., ben Hammouda, S., Sun, J., Wang, X., Li, X., & Chen, Z. (2023). Carbon-based materials for CO_2 capture: their production, modification and performance. Journal of Environmental Chemical Engineering, 109741. https://doi.org/10.1016/j.jece.2023.109741

[116] Drage, T. C., Blackman, J. M., Pevida, C., & Snape, C. E. (2009). Evaluation of activated carbon adsorbents for CO_2 capture in gasification. Energy & fuels, 23(5), 2790-2796. https://doi.org/10.1021/ef8010614

[117] Rodriguez-Reinoso, F., Molina-Sabio, M., & González, M. T. (1995). The use of steam and CO_2 as activating agents in the preparation of activated carbons. Carbon, 33(1), 15-23. https://doi.org/10.1016/0008-6223(94)00100-E

[118] Presser, V., McDonough, J., Yeon, S. H., & Gogotsi, Y. (2011). Effect of pore size on carbon dioxide sorption by carbide derived carbon. Energy and Environmental Science, 4(8). https://doi.org/10.1039/c1ee01176f

[119] Zhang, Z., Zhou, J., Xing, W., Xue, Q., Yan, Z., Zhuo, S., & Qiao, S. Z. (2013). Critical role of small micropores in high CO_2 uptake. Physical chemistry chemical physics, 15(7), 2523-2529. DOI: 10.1039/C2CP44436D

[120] Abd, A. A., Othman, M. R., & Kim, J. (2021). A review on application of activated carbons for carbon dioxide capture: present performance, preparation, and surface modification for further improvement. Environmental Science and Pollution Research, 28(32), 43329-43364. https://doi.org/10.1007/s11356-021-15121-9

[121] Serafin, J., Narkiewicz, U., Morawski, A. W., Wróbel, R. J., & Michalkiewicz, B. (2017). Highly microporous activated carbons from biomass for CO_2 capture and effective micropores at different conditions. Journal of CO_2 Utilization, 18, 73-79. https://doi.org/10.1016/j.jcou.2017.01.006

[122] Mochizuki, Y., Bud, J., Byambajav, E., & Tsubouchi, N. (2024). Pore properties and CO_2 adsorption performance of activated carbon prepared from various carbonaceous materials. Carbon Resources Conversion, 100237. https://doi.org/10.1016/j.crcon.2024.100237

[123] Zhao, M., Ban, Y., Yang, K., Zhou, Y., Cao, N., Wang, Y., & Yang, W. (2021). A highly selective supramolecule array membrane made of zero-dimensional molecules for gas separation. Angewandte Chemie, 133(38), 21145-21151. https://doi.org/10.1002/ange.202108185

[124] Li, B. (2012). Charaterization of Pore Structure and Surface Chemistry of Activated Carbons–A Review. Fourier Transform-Materials Analysis. Primera. Shanghai: InTech, 165-90. DOI: 10.5772/37460

[125] Song, X., Wang, L. A., Gong, J., Zhan, X., & Zeng, Y. (2020). Exploring a new method to study the effects of surface functional groups on adsorption of CO_2 and CH_4 on activated carbons. Langmuir, 36(14), 3862-3870. https://doi.org/10.1021/acs.langmuir.9b03475

[126] Plaza, M. G., Pevida, C., Arias, B., Casal, M. D., Martín, C. F., Fermoso, J., Rubiera, F., & Pis, J. J. (2009). Different approaches for the development of low-cost CO_2 adsorbents. Journal of Environmental Engineering, 135(6), 426-432. https://doi.org/10.1061/(ASCE)EE.1943-7870.0000009

[127] Shafeeyan, M. S., Daud, W. M. A. W., Houshmand, A., & Arami-Niya, A. (2011). Ammonia modification of activated carbon to enhance carbon dioxide adsorption: effect of pre-

oxidation. Applied Surface Science, 257(9), 3936-3942. https://doi.org/10.1016/j.apsusc.2010.11.127.

[128] Mehrvarz, E., Ghoreyshi, A. A., & Jahanshahi, M. (2017). Surface modification of broom sorghum-based activated carbon via functionalization with triethylenetetramine and urea for CO_2 capture enhancement. Frontiers of Chemical Science and Engineering, 11, 252-265. https://doi.org/10.1007/s11705-017-1630-6.

[129] Boonpoke, A., Chiarakorn, S., Laosiripojana, N., Towprayoon, S., & Chidthaisong, A. (2012). Investigation of CO_2 adsorption by bagasse-based activated carbon. Korean Journal of Chemical Engineering, 29, 89-94. https://doi.org/10.1007/s11814-011-0143-0.

[130] Jin, Y., Huynh, C. P., Hawkins, S. C., & Su, S. (2015). Expanded graphite/phenolic resin-based carbon composite adsorbents for post-combustion CO_2 capture. RSC Advances, 5(77), 62604-62610. https://doi.org/10.1039/C5RA09853J.

[131] Park, J., Cho, S. Y., Jung, M., Lee, K., Nah, Y. C., Attia, N. F., & Oh, H. (2021). Efficient synthetic approach for nanoporous adsorbents capable of pre-and post-combustion CO_2 capture and selective gas separation. Journal of CO_2 Utilization, 45, 101404. https://doi.org/10.1016/j.jcou.2020.101404.

[132] Liang, W., Liu, Z., Peng, J., Zhou, X., Wang, X., & Li, Z. (2018). Enhanced CO_2 adsorption and $CO_2/N_2/CH_4$ selectivity of novel carbon composites CPDA@ A-Cs. Energy & Fuels, 33(1), 493-502. https://doi.org/10.1021/acs.energyfuels.8b03637.

[133] Chen, H., Zhang, Y. J., He, P. Y., Li, C. J., & Liu, L. C. (2020). Novel activated carbon route to low-cost geopolymer based porous composite with high mechanical resistance and enhanced CO_2 capacity. Microporous and Mesoporous Materials, 305, 110282. https://doi.org/10.1016/j.micromeso.2020.110282.

[134] Przepiórski, J., Czyżewski, A., Pietrzak, R., & Tryba, B. (2013). MgO/CaO-loaded porous carbons for carbon dioxide capture: effects accompanying regeneration process. Journal of thermal analysis and calorimetry, 111, 357-364. https://doi.org/10.1007/s10973-012-2354-y.

[135] Shahkarami, S., Dalai, A. K., & Soltan, J. (2016). Enhanced CO_2 adsorption using MgO-impregnated activated carbon: impact of preparation techniques. Industrial & Engineering Chemistry Research, 55(20), 5955-5964. https://doi.org/10.1021/acs.iecr.5b04824.

[136] Rostami, M., Mofarahi, M., Karimzadeh, R., & Abedi, D. (2016). Preparation and characterization of activated carbon–zeolite composite for gas adsorption separation of CO_2/N_2 system. Journal of Chemical & Engineering Data, 61(7), 2638-2646. https://doi.org/10.1021/acs.jced.6b00374.

[137] Okutani, T., Utsumi, T., & Ohnishi, M. (2012). Synthesis of conjunctive zeolite-activated carbon composite adsorbent from rice hulls for simultaneous adsorption of CO_2 and H_2O. In

42nd International Conference on Environmental Systems (p. 3429). https://doi.org/10.2514/6.2012-3429

[138] Regufe, M. J., Ferreira, A. F., Loureiro, J. M., Shi, Y., Rodrigues, A., & Ribeiro, A. M. (2018). New hybrid composite honeycomb monolith with 13X zeolite and activated carbon for CO_2 capture. Adsorption, 24(3), 249-265. https://doi.org/10.1007/s10450-018-9938-1.

[139] Li, H., Zheng, F., Wang, J., Zhou, J., Huang, X., Chen, L., Hu, P., Gao, J., Zhen, Q., Bashir, S., & Liu, J. L. (2020). Facile preparation of zeolite-activated carbon composite from coal gangue with enhanced adsorption performance. Chemical Engineering Journal, 390, 124513. https://doi.org/10.1016/j.cej.2020.124513.

[140] Zeng, G., Yu, Z., Du, M., Ai, N., Chen, W., Gu, Z., & Chen, B. (2018). Enhanced CO_2 Adsorption on Activated Carbon-Modified HKUST-1 Composites. ChemistrySelect, 3(41), 11601-11605. https://doi.org/10.1002/slct.201802443.

[141] Adhikari, A. K., & Lin, K. S. (2016). Improving CO_2 adsorption capacities and CO_2/N_2 separation efficiencies of MOF-74 (Ni, Co) by doping palladium-containing activated carbon. Chemical Engineering Journal, 284, 1348-1360. https://doi.org/10.1016/j.cej.2015.09.086.

[142] Zhang, C., Song, W., Ma, Q., Xie, L., Zhang, X., & Guo, H. (2016). Enhancement of CO_2 capture on biomass-based carbon from black locust by KOH activation and ammonia modification. Energy & Fuels, 30(5), 4181-4190. https://doi.org/10.1021/acs.energyfuels.5b02764.

[143] Liu, X., Sun, C., Liu, H., Tan, W. H., Wang, W., & Snape, C. (2019). Developing hierarchically ultra-micro/mesoporous biocarbons for highly selective carbon dioxide adsorption. Chemical Engineering Journal, 361, 199-208. https://doi.org/10.1016/j.cej.2018.11.062.

[144] Rozas, S., Gutiérrez, A., Atilhan, M., Bol, A., & Aparicio, S. (2024). Understanding the CO_2 capture potential of tetrapropylammonium-based multifunctional deep eutectic solvent via molecular simulation. Journal of Molecular Liquids, 393, 123416. https://doi.org/10.1016/j.molliq.2023.123416

[145] Phele, M. J., Ejidike, I. P., & Mtunzi, F. M. (2019). Adsorption efficiency of activated macadamia nutshell for the removal Organochlorine pesticides: Endrin and 4, 4-DDT from aqueous solution. Journal of Pharmaceutical Sciences and Research, 11(1), 258-262.

[146] Freund, H. J. (1997). Adsorption of gases on complex solid surfaces. Angewandte chemie international edition in english, 36(5), 452-475. https://doi.org/10.1002/anie.199704521

[147] Pourhakkak, P., Taghizadeh, A., Taghizadeh, M., Ghaedi, M., & Haghdoust, S. (2021). Fundamentals of adsorption technology. In Interface science and technology (Vol. 33, pp. 1-70). Elsevier. https://doi.org/10.1016/B978-0-12-818805-7.00001-1

[148] Al-Jubouri, S. M., Al-Jendeel, H. A., Rashid, S. A., & Al-Batty, S. (2022). Antibiotics adsorption from contaminated water by composites of ZSM-5 zeolite nanocrystals coated carbon. Journal of Water Process Engineering, 47, 102745. https://doi.org/10.1016/j.jwpe.2022.102745

[149] Auerbach, D. J., Tully, J. C., & Wodtke, A. M. (2021). Chemical dynamics from the gas-phase to surfaces. Natural Sciences, 1(1), e10005. https://doi.org/10.1002/ntls.10006

[150] Fowkes, F. M. (1964). Attractive forces at interfaces. Industrial & Engineering Chemistry, 56(12), 40-52. http://dx.doi.org/10.1021/ie50660a008

[151] Chen, X., Hossain, M. F., Duan, C., Lu, J., Tsang, Y. F., Islam, M. S., & Zhou, Y. (2022). Isotherm models for adsorption of heavy metals from water-A review. Chemosphere, 307, 135545. https://doi.org/10.1016/j.chemosphere.2022.135545

[152] Ghaedi, M. (Ed.). (2021). Adsorption: Fundamental Processes and Applications. Academic Press. https://doi.org/10.1016/B978-0-12-818805-7.00001-1

[153] Raganati, F., Miccio, F., & Ammendola, P. (2021). Adsorption of carbon dioxide for post-combustion capture: a review. Energy & Fuels, 35(16), 12845-12868. https://doi.org/10.1021/acs.energyfuels.1c01618

[154] Abd, A. A., Naji, S. Z., Hashim, A. S., & Othman, M. R. (2020). Carbon dioxide removal through physical adsorption using carbonaceous and non-carbonaceous adsorbents: a review. Journal of Environmental Chemical Engineering, 8(5), 104142. https://doi.org/10.1016/j.jece.2020.104142

[155] Dagdag, O., Haldhar, R., Kim, S., Berdimurodov, E., Ebenso, E., & Kaya, S. (2022). Natural corrosion inhibitors: adsorption mechanism. Corrosion Mitigation: Biomass and Other Natural Products, 51-60. https://doi.org/10.1515/9783110760583-003

[156] Song, Z., Zhang, Z., Du, A., Dong, S., Li, G., & Cui, G. (2021). Uniform magnesium electrodeposition via synergistic coupling of current homogenization, geometric confinement, and chemisorption effect. Advanced Materials, 33(26), 2100224. https://doi.org/10.1002/adma.202100224

[157] Vinodh, R., Babu, C. M., Abidov, A., Palanichamy, M., & Jang, H. T. (2019). Facile synthesis of amine modified silica/reduced graphene oxide composite sorbent for CO_2 adsorption. Materials Letters, 247, 44-47. https://doi.org/10.1016/j.matlet.2019.03.082

[158] Jaffrezic-Renault, N., Poirier-Andrade, H., & Trang, D. H. (1980). Models for the adsorption of uranium on titanium dioxide. Journal of Chromatography A, 201, 187-192. https://doi.org/10.1016/S0021-9673(00)83873-X

[159] Cychosz, K. A., & Thommes, M. (2018). Progress in the physisorption characterization of nanoporous gas storage materials. Engineering, 4(4), 559-566. https://doi.org/10.1016/j.eng.2018.06.001

[160] Thommes, M., Morlay, C., Ahmad, R., & Joly, J. P. (2011). Assessing surface chemistry and pore structure of active carbons by a combination of physisorption (H_2O, Ar, N_2, CO_2), XPS and TPD-MS. Adsorption, 17(3), 653-661. https://doi.org/10.1007/s10450-011-9360-4

[161] Wang, Y., Hu, X., Guo, T., Hao, J., Si, C., & Guo, Q. (2021). Efficient CO_2 adsorption and mechanism on nitrogen-doped porous carbons. Frontiers of Chemical Science and Engineering, 15, 493-504. https://doi.org/10.1007/s11705-020-1967-0

[162] Dombrowski, R. J., Hyduke, D. R., & Lastoskie, C. M. (2000). Pore size analysis of activated carbons from argon and nitrogen porosimetry using density functional theory. Langmuir, 16(11), 5041-5050. https://doi.org/10.1021/la990827a

[163] Song, Z. Z., Abula, A., Zhao, J. Y., Liu, G. D., Li, M. R., Yang, D. L., & Wang, Y. L. (2022). A novel hybrid thermodynamic model for pore size distribution characterisation for shale. Petroleum Science, 19(3), 963-978. https://doi.org/10.1016/j.petsci.2021.12.015

[164] Bhargava, R., & Levin, I. W. (2005). Fourier Transform Mid-infrared Spectroscopic Imaging: Microspectroscopy with Multichannel Detectors. Spectrochemical Analysis Using Infrared Multichannel Detectors, 1-24. DOI:10.1002/9780470988541

[165] Peticolas, W. L. (1972). Inelastic light scattering and the Raman effect. Annual Review of Physical Chemistry, 23(1), 93-116. https://doi.org/10.1146/annurev.pc.23.100172.000521

[166] Smith, E., & Dent, G. (2019). Modern Raman spectroscopy: a practical approach. John Wiley & Sons. DOI:10.1002/0470011831

[167] García–Nieto, P. J., García–Gonzalo, E., & Paredes–Sánchez, J. P. (2024). Estimation of the coal higher heating value for energy systems relied on ultimate analysis with machine learning techniques. Fuel, 357, 130037. https://doi.org/10.1016/j.fuel.2023.130037

[168] Ali, B. F., Ibraheem, F. H., Jassim, A. M., & Jassim, H. M. (2020). The Proximate Analysis method for the Composition Determination of Different Coal Types. In 2020 6th International Engineering Conference “Sustainable Technology and Development"(IEC) (pp. 91-96). IEEE. DOI: 10.1109/IEC49899.2020.9122917

[169] Zhu, J., Uhl, F. M., Morgan, A. B., & Wilkie, C. A. (2001). Studies on the mechanism by which the formation of nanocomposites enhances thermal stability. Chemistry of Materials, 13(12), 4649-4654. https://doi.org/10.1021/cm010451y

[170] Zhou, W., Apkarian, R., Wang, Z. L., & Joy, D. (2007). Fundamentals of scanning electron microscopy (SEM). Scanning microscopy for nanotechnology: techniques and applications, 1-40. https://doi.org/10.1007/978-0-387-39620-0

[171] Bunaciu, A. A., UdriŞTioiu, E. G., & Aboul-Enein, H. Y. (2015). X-ray diffraction: instrumentation and applications. Critical reviews in analytical chemistry, 45(4), 289-299. https://doi.org/10.1080/10408347.2014.949616

[172] Nuhnen, A., & Janiak, C. (2020). A practical guide to calculate the isosteric heat/enthalpy of adsorption via adsorption isotherms in metal–organic frameworks, MOFs. Dalton Transactions, 49(30), 10295-10307. https://doi.org/10.1039/D0DT01784A

[173] Cai, K., Liu, P., Zhao, T., Su, K., Yang, Y., & Tao, D. J. (2022). Construction of hyper-crosslinked ionic polymers with high surface areas for effective CO_2 capture and conversion. Microporous and Mesoporous Materials, 343, 112135. https://doi.org/10.1016/j.micromeso.2022.112135

[174] Aniruddha, R., Sreedhar, I., & Reddy, B. M. (2020). MOFs in carbon capture-past, present and future. Journal of CO_2 Utilization, 42, 101297. https://doi.org/10.1016/j.jcou.2020.101297

[175] Mukherjee, S., & Samanta, A. N. (2019). Amine-impregnated MCM-41 in post-combustion CO_2 capture: Synthesis, characterization, isotherm modelling. Advanced Powder Technology, 30(12), 3231-3240. https://doi.org/10.1016/j.apt.2019.09.032

[176] Khoshraftar, Z., & Ghaemi, A. (2023). Evaluation of CaO derived from Cerastoderma glaucum of Caspian beach as a natural sorbent for CO_2 capture. Current Research in Green and Sustainable Chemistry, 6, 100360. https://doi.org/10.1016/j.crgsc.2023.100360

[177] Chen, S., Chen, G., Chen, H., Sun, Y., Yu, X., Su, Y., & Tang, S. (2019). Preparation of porous carbon-based material from corn straw via mixed alkali and its application for removal of dye. Colloids and Surfaces A: Physicochemical and Engineering Aspects, 568, 173-183. https://doi.org/10.1016/j.colsurfa.2019.02.008

[178] Bastos-Neto, M., Patzschke, C., Lange, M., Möllmer, J., Möller, A., Fichtner, S., ... & Gläser, R. (2012). Assessment of hydrogen storage by physisorption in porous materials. Energy & Environmental Science, 5(8), 8294-8303. https://doi.org/10.1039/C2EE22037G